

# Effect of additives, heat treatment and mechanical deformations on hydrogen storage properties of BCC alloys

*Submitted in partial fulfilment of the requirements  
of the degree of*

**Doctor of Philosophy**

*by*

**Amol Kamble**  
(Roll No. 144178001)

Under the guidance of

**Prof. Pratibha Sharma**  
(Supervisor)

&

**Prof. Jacques Huot**  
(Co-supervisor)



**UQTR**



Université du Québec  
à Trois-Rivières

Department of Energy Science and Engineering  
Indian Institute of Technology Bombay  
Mumbai

**2019**

Université du Québec à Trois-Rivières

Service de la bibliothèque

Avertissement

L'auteur de ce mémoire ou de cette thèse a autorisé l'Université du Québec à Trois-Rivières à diffuser, à des fins non lucratives, une copie de son mémoire ou de sa thèse.

Cette diffusion n'entraîne pas une renonciation de la part de l'auteur à ses droits de propriété intellectuelle, incluant le droit d'auteur, sur ce mémoire ou cette thèse. Notamment, la reproduction ou la publication de la totalité ou d'une partie importante de ce mémoire ou de cette thèse requiert son autorisation.

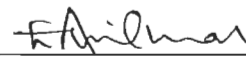
**Dedicated**

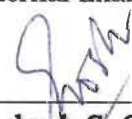
To my Father

## **Thesis Approval**

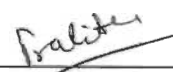
This thesis entitled “Effect of additives, heat treatment and mechanical deformations on hydrogen storage properties of BCC alloys” by Mr. Amol Kamble is approved for the degree of Doctor of Philosophy.

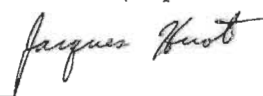
### **Examiners**

1.   
**Prof. Anil Kumar Emadabathuni**  
(External Examiner)

2.   
**Prof. Prakash C. Ghosh**  
(Internal Examiner)

 15/03/2019  
**Prof. P. Vellaisamy**  
(Chair-Person)

  
**Prof. Pratibha Sharma**  
(Supervisor)

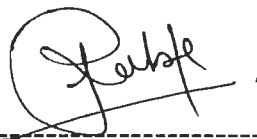
  
**Prof. Jacques Huot**  
(Co-Supervisor)

Date: 15<sup>th</sup> March 2019

Place: IIT Bombay

### **Declaration**

I declare that this written submission represents my ideas in my own words and where others' ideas or words have been included, I have adequately cited and referenced the original sources. I also declare that I have adhered to all principles of academic honesty and integrity and have not misrepresented or fabricated or falsified any idea/data/fact/source in my submission. I understand that any violation of the above will be cause for disciplinary action by the Institute and can also evoke penal action from the sources which have thus not been properly cited or from whom proper permission has not been taken when needed.



Amol Kamble  
Roll No.: 144178001

**Date:** 03/04/2019

## **Abstract**

The BCC 52Ti-12V-36Cr alloy has high gravimetric hydrogen capacity at room temperature under low hydrogen pressure (2 MPa), but it has long incubation time during first hydrogenation. The effects of additives, heat treatment, ball milling and particle size on first hydrogenation were analysed to find suitable additive and synthesizing technique with optimized first hydrogenation.

The impacts of zirconium and nickel as individual additives with respect to additive  $Zr_7Ni_{10}$  on first hydrogenation were investigated. All additives resulted in reduction in the incubation time by at least two orders of magnitude, probable reason could be presence of Zr-Ni rich secondary phase. Fast intrinsic kinetics (slope of hydrogenation curve at mid-capacity) is observed in presence of zirconium while high hydrogen capacity 3.78wt% is achieved in presence of nickel. The  $Zr_7Ni_{10}$  was found to be the most effective additive among the studied additives with optimized absorption properties.

The BCC 52Ti-12V-36Cr alloy with different additives was further processed for heat treatment of 1-week at 1273K. The effect of heat treatment on crystal structure, microstructure and first hydrogenation has been studied. The unwanted incubation time got eliminated but it adversely reduced hydrogen capacity by 30%. The elimination of incubation time is observed probably due to change in phase compositions and their abundance. The loss of hydrogen capacity may be due to reduced BCC phase abundance after heat treatment.

The effect of ball milling on BCC 52Ti-12V-36Cr alloy casted with additive (4wt% of zirconium used as additive) was studied. Ball milling although reduced the crystallite size to a large extent but was observed to have adverse effect in terms of reduced intrinsic kinetics, total and reversible hydrogen capacity. The behaviour of hydrogenation still remained unexplainable.

When the zirconium was added to pre-cast of BCC52Ti-12V-36Cr alloy mechanically using ball milling for durations of 30 and 60 minutes, no absorption was observed. Ball milling for 15 minutes shows heterogeneous layering of zirconium over BCC particles which affects stability of hydride phase and increases desorption plateau pressure. There is loss of reversible hydrogen capacity and intrinsic kinetics. The additional decrease of intrinsic

kinetics probably originated due to change in bulk composition and Zr-rich heterogeneous surface morphology.

The relative importance of particle size and additive was studied for cast of BCC 52Ti-12V-36Cr without/with additive (4wt% of zirconium) for selected ranges of particle size: less than 0.5 mm, between 0.5-1.0 mm and greater than 1.0 mm. The additive has stronger impact than particle size on both the incubation time and intrinsic kinetics. The alloys have monolithic hydrogenation curves.

In short, the  $Zr_7Ni_{10}$  is most effective additive and just melting together with additive could be considered as optimized synthesizing technique for BCC alloys.

## **Acknowledgments**

I take this opportunity to express a bottomless sense of gratitude towards my guide **Prof. Pratibha Sharma** and **Prof. Jacques Huot** for providing excellent guidance, inspiration and encouragement throughout the journey with IIT Bombay and UQTR Canada in order to fulfilment of my doctoral studies. I thanks to both of them for creating good working environment by knowledgeable discussions, sticking to planned schedule and providing excellent laboratory facilities.

I am heartily thankful to my research progress committee member, **Prof. P. C. Ghosh** and **Prof. Srinivas Seethamraju** for their valuable suggestions and queries, which help me to improve my thesis and the research works a lot.

I am extremely thankful to **Prof. R. Banerjee**, HOD of Department of Energy Science & Engineering at IIT Bombay and **Prof. Richard Chahine**, Director, Institute of Hydrogen Research at University du Quebec Trois-Rivieres, QC, Canada for accepting me as doctoral research scholar, approving my student exchange program and helping me during pursue of the doctoral degree.

I express my special thanks to faculty advisor **Prof. Chetan Solanki** and other professors **Prof. Sankara Sarma V Tatiparti**, **Prof. Suneet Singh** and **Prof. Sandip Kumar Saha** for their valuable guidance and support during my course work at IIT Bombay.

How could I forget the team which offered funding through **Queen Elizabeth II Diamond Jubilee Fellowship during my stay at UQTR, Canada**. I appreciate their the most valuable unconditional financial support for my journey with UQTR. I am grateful to fellowship coordinator **Ms. Genevieve Cote** for taking care of continuous funding required for research and trainings.



I am very glad to appreciate the professional support from the managements of **Mahatma Education Society's Pillai HOC college of Engineering & Technology, Rasayani (PHCET-Rasayani)** and **D Y Patil School of Engineering Academy, Ambi (DYPSOEA, Ambi)** for allowing me to complete doctoral studies while working with their institutions. I am very grateful for time to time guidance, suggestions and continuation of support provided by **Mr. Vilas Nitnaware, Principal, DYPSOEA, Ambi.**

I appreciate the technical support of Ms. Marie-Eve Marchand in various mechanical and heat treatments and Ms. Lejeune Agnes in Scanning Electron Microscopy(SEM) plus Energy Dispersive Spectroscopy(EDS). I am also thankful for professional coordination and valuable suggestions during experimentation from my lab mates **Ms. Salma Sleiman, Ms. Viney Dixit, Ms. Volatiana Razak, Mr. Abhishek Patel, Mr. Joydev Manna, Mr. Meraj Alam,** and **Mr. Peng Lv.** I also grateful to Hydrogen & Photovoltaic research group members Mahavas, Saurabh, and Animesh.

Lastly but most important, I would like to acknowledge my family for altogether their love and encouragement. I want to thank my parents **Late Mr. Gulabrao Kamble** and **Mrs. Anjana Kamble**, who worked hard and did whatever possible to make me successful and who never stopped cheering me. I am also thankful to my brother **Prashant** and sister **Kanchan**, for their love and belief in me. And most of all, I am gratified to my sweet heart **Anjali** and my daughter **Priyadarshini**, for their love, support, encourage and patience during this four-year's journey and gladly accepting the pain of living far away from me during my stay at UQTR, Canada.

## **Table of Content**

<b>Abstract.....</b>	<b>v</b>
<b>Acknowledgements.....</b>	<b>vii</b>
<b>Table of Content.....</b>	<b>ix</b>
<b>List of Figures.....</b>	<b>xii</b>
<b>List of Tables.....</b>	<b>xiv</b>
<b>Nomenclature.....</b>	<b>xvi</b>
<b>1. INTRODUCTION</b>	<b>1</b>
1.1 Background.....	2
1.2 Energy carrier-Hydrogen.....	3
1.3 Why BCC solid solution?.....	7
1.4 Choice of alloy composition.....	7
1.5 Research aim and objectives.....	9
1.6 Significance of study-Industrial applications.....	9
1.7 Thesis Structure.....	10
<b>2. LITERATURE REVIEW</b>	<b>11</b>
2.1 Overview.....	12
2.2 Hydrogen Storage Properties.....	12
2.2.1 Storage Capacity.....	12
2.2.2 Hydrogen Absorption Kinetics.....	13
2.2.3 First Hydrogenation.....	15
2.3 Factors affecting first hydrogenation.....	16
2.3.1 Effect of additives on hydrogen sorption properties.....	16
2.3.2 Effect of mechanical deformations on hydrogen sorption properties.....	19
2.3.3 Effect of heat treatment on hydrogen sorption properties.....	22
2.4 Ti-V-Cr Ternary Phase Diagram.....	26
<b>3. MATERIAL SYNTHESIS &amp; CHARACTERIZATION</b>	<b>29</b>
3.1 Overview.....	30
3.2 Weight % & atomic %.....	30
3.3 Raw materials.....	32
3.4 Arc melting.....	33
3.5 Ball milling.....	34
3.6 Heat treatment.....	35
3.7 X-ray Diffraction (XRD).....	36
3.8 Scanning Electron Microscopy (SEM).....	38
3.9 Energy Dispersive X-ray Spectroscopy (EDS).....	39
3.10 Hydrogenation Characterization.....	40

<b>4. EFFECT OF ADDITION OF Zr, Ni AND Zr-Ni IN 52Ti-12V-36Cr ALLOY</b>	<b>46</b>
4.1 Overview.....	47
4.2 Choice of Additive.....	47
4.3 Experimental Procedures.....	47
4.4 Results & Discussion.....	48
4.4.1 Microstructure of as-cast BCC 52Ti-12V-36Cr with/without additive.....	48
4.4.2 Energy Dispersive X-ray Spectroscopy (EDS).....	51
4.4.3 X-ray diffraction(XRD) of as cast alloys.....	54
4.4.4 First hydrogenation.....	55
4.4.5 X-ray diffraction(XRD) after hydrogenation.....	57
4.5 Conclusion.....	58
<b>5. EFFECT OF ANNEALING ON 52Ti-12V-36Cr WITH ADDITIVES</b>	<b>59</b>
5.1 Overview.....	60
5.2 Experimental Procedures.....	60
5.3 Results & Discussion.....	61
5.3.1 Microstructural study.....	61
5.3.2 Energy Dispersive X-ray Spectroscopy (EDS).....	63
5.3.3 Crystal Structure before hydrogenation.....	66
5.3.4 First hydrogenation.....	68
5.3.5 Crystal Structure after hydrogenation.....	69
5.4 Conclusion.....	71
<b>6. EFFECT OF MECHANICAL DEFORMATION ON BCC ALLOY 52Ti-12V-36Cr</b>	<b>73</b>
6.1 Overview.....	74
6.2 Experimental Procedures.....	74
6.3 Results & Discussion.....	75
6.3.1 XRD of ball milled of as cast BCC 52Ti-12V-36Cr + 4wt%Zr.....	75
6.3.2 First hydrogenation.....	77
6.3.3 Scanning Electron Microscopy (SEM).....	78
6.3.4 Energy Dispersive X-ray Spectroscopy (EDS).....	79
6.3.5 Pressure-Concentration Isotherms.....	82
6.4 Conclusion.....	83
<b>7. EFFECT OF PARTICLE SIZE IN 52Ti-12V-36Cr ALLOY WITH AND WITHOUT ADDITIVE</b>	<b>84</b>
7.1 Overview.....	85
7.2 Experimental Procedures.....	85
7.3 Results & Discussion.....	86
7.3.1 Particle size analysis.....	86
7.3.2 First hydrogenation.....	87
7.4 Conclusion.....	91

<b>Conclusion.....</b>	<b>93</b>
<b>References.....</b>	<b>96</b>
<b>Appendix A – Publications.....</b>	<b>103</b>

## **List of Figures**

<i>Figure 1.1</i>	The trends of contributions by energy sources	2
<i>Figure 1.2</i>	Schematics of (a) high pressure gaseous and (b) liquid hydrogen storage.	5
<i>Figure 1.3</i>	Schematics for hydrogen storage in advanced materials: (a) surface adsorption, (b) metal hydrides, (c) complex hydrides and (d) chemical hydrides.	6
<i>Figure 1.4</i>	Summary of the work.	9
<i>Figure 2.1</i>	PC isotherms of TiV0.8Cr1.2 at 297 K and of the composite TiV0.8Cr1.2 + 4 wt.% Zr7Ni10 at 288 K	13
<i>Figure 2.2</i>	Isothermal sections through Ti-V-Cr system at 1273 K	27
<i>Figure 3.1</i>	Titanium	32
<i>Figure 3.2</i>	Vanadium	32
<i>Figure 3.3</i>	Chromium	32
<i>Figure 3.4</i>	Zirconium	32
<i>Figure 3.5</i>	Nickel	32
<i>Figure 3.6</i>	Arc Melter (Centorr Associates Inc, USA).	33
<i>Figure 3.7</i>	Ball miller Spex 8000M.	34
<i>Figure 3.8</i>	Heat treatment set-up with Tube furnace (Branstead thermolyne).	35
<i>Figure 3.9</i>	D8 Focus BRUKER X-ray Powder Diffractometer.	36
<i>Figure 3.10</i>	Schematic of Scanning Electron microscope	38
<i>Figure 3.11</i>	JSM-5500 with master and slave installed with Oxford Instruments software.	39
<i>Figure 3.12</i>	Hydrogen Titration System.	40
<i>Figure 3.13</i>	PCT Sample Holder.	40
<i>Figure 3.14</i>	GUI Hydrogene Home page.	41
<i>Figure 3.15</i>	Operation manual Interface.	42
<i>Figure 3.16</i>	Kinetics measurement parameters	44
<i>Figure 4.1</i>	Flow chart of synthesis & characterization of BCC 52Ti-12V-36Cr alloy with and without additive.	48
<i>Figure 4.2</i>	Backscattering electrons (BSE) SEM micrographs of the as-cast BCC 52Ti-12V-36Cr (a)without additives and with (b)4wt% Zr7Ni10, (c)4wt%Zr, (d)2.2wt%Zr and (e)4wt%Ni additives.	49
<i>Figure 4.3</i>	ImageJ analysis of as-cast BCC 52Ti-12V-36Cr (a)without additives and with (b)4wt% Zr7Ni10, (c)4wt%Zr, (d)2.2wt%Zr and (e)4wt%Ni additives.	50
<i>Figure 4.4</i>	Point mapping on micrographs of the as-cast BCC 52Ti-12V-36Cr (a)without additives and with (b)4wt% Zr7Ni10, (c)4wt%Zr, (d)2.2wt%Zr and (e)4wt%Ni additives.	52
<i>Figure 4.5</i>	XRD patterns of as-cast BCC 52Ti-12V-36Cr alloys with and without additives.	54
<i>Figure 4.6</i>	First hydrogenation of as-cast BCC 52Ti-12V-36Cr alloys with and without additives.	56
<i>Figure 4.7</i>	XRD patterns of hydrogenated BCC 52Ti-12V-36Cr alloy with and without additives.	57
<i>Figure 5.1</i>	Flow chart of the synthesis process, heat treatment and characterization.	60

<i>Figure 5.2</i>	Backscattering electrons (BSE) SEM micrographs of the as cast(Left) and heat treated(Right) BCC 52Ti-12V-36Cr with (a,b) 4wt% Zr <sub>7</sub> Ni <sub>10</sub> , (c,d) 4wt%Zr, (e,f) 2.2wt%Zr and (g,h) 4wt%Ni additives.	61
<i>Figure 5.3</i>	Point mapping of dark phase (1), black phase (2) and bright phase (3) on micrographs of as cast (left) and annealed (right) BCC 52Ti-12V-36Cr with (a,b)4wt% Zr <sub>7</sub> Ni <sub>10</sub> , (c,d)4wt%Zr, (e,f)2.2wt%Zr and (g,h)4wt%Ni additives.	64
<i>Figure 5.4</i>	XRD patterns of annealed BCC 52Ti-12V-36Cr with/without additive.	66
<i>Figure 5.5</i>	First hydrogenation curves for heat treated BCC 52Ti-12V-36Cr with additive.	68
<i>Figure 5.6</i>	XRD patterns of hydrogenated heat-treated BCC 52Ti-12V-36Cr with/without additive.	69
<i>Figure 6.1</i>	Synthesis and characterization melted and ball milled BCC 52Ti-12V-36Cr with Zr.	74
<i>Figure 6.2</i>	XRD patterns of (a) cast BCC 52Ti-12V-36Cr+4wt%Zr milled for (b) 15 min, (c) 30 min, (d) 60 min.	75
<i>Figure 6.3</i>	XRD patterns of cast BCC 52Ti-12V-36Cr milled with 4wt%Zr for (a)15 min, (b)30 min, (c)60 min.	76
<i>Figure 6.4</i>	First hydrogenation curves of (a)as cast BCC 52Ti-12V-36Cr+4wt%Zr milled for (b)15 min, (d)30 min, (f)60 min and cast BCC 52Ti-12V-36Cr milled with 4wt%Zr for (c)15 min, (e)30 min, (g)60 min.	77
<i>Figure 6.5</i>	BSE of (a)as milled cast of BCC 52Ti-12V-36Cr+4wt%Zr and (b)cast BCC 52Ti-12V-36Cr milled with 4wt%Zr for 15 min.	79
<i>Figure 6.6</i>	Elemental mapping of (a) milled of as casted (BCC 52Ti-12V-36Cr+4wt%Zr) and (b) cast of BCC 52Ti-12V-36Cr milled with 4wt%Zr for 15 minutes.	80
<i>Figure 6.7</i>	PCT desorption curves at 483K of (a) BCC 52Ti-12V-36Cr+4wt%Zr, (b) ball milled (BCC 52Ti-12V-36Cr+4wt%Zr) for 15 min and (c)cast BCC52Ti-12V-36Cr ball milled with 4wt%Zr for 15 min.	82
<i>Figure 7.1</i>	Flow chart for synthesis and characterization of sieved BCC 52Ti-12V-36Cr with and without Zr.	85
<i>Figure 7.2</i>	Particle size distribution of 52Ti-12V-36Cr + 4wt%Zr powder.	86
<i>Figure 7.3</i>	Secondary Electron Images of 52Ti-12V-36Cr + 4wt%Zr alloy. (a) PS<0.5mm, (b) 0.5<PS<1.0mm, (c) PS>1.0mm and (d) as-crushed.	87
<i>Figure 7.4</i>	First hydrogenation curves of 52Ti-12V-36Cr doped with 4%Zr for different particle size and for the as-crushed sample.	88
<i>Figure 7.5</i>	First hydrogenation curves of 52Ti-12V-36Cr alloy for different particle size for the as-crushed sample.	89

## **List of Tables**

<i>Table 2.1</i>	Rate limiting step model equations	14
<i>Table 2.2</i>	Effects of additives/substitutes over hydrogen sorption.	18
<i>Table 2.3</i>	Effects of mechanical deformations over hydrogen sorption.	21
<i>Table 2.4</i>	Effects of heat treatment over hydrogen sorption	25
<i>Table 2.5</i>	Crystallographic data of Ti-V-Cr system	28
<i>Table 3.1</i>	Atomic percent, weight percent and weights of each element	31
<i>Table 3.2</i>	Raw elements.	32
<i>Table 3.3</i>	Melting points of Ti, V, Cr, Zr and Ni	33
<i>Table 4.1</i>	Fraction of area (in %) occupied by each phase in as cast 52Ti-12V-36Cr alloys with and without additives. Uncertainty on each measurement is $\pm 1\%$	50
<i>Table 4.2</i>	Element abundances as measured from EDS for bulk compositions of as cast 52Ti-12V-36Cr alloys with and without additives. Uncertainties on measured composition are $\pm 1$ at%.	51
<i>Table 4.3</i>	Composition of dark phases in as-cast BCC 52Ti-12V-36Cr alloys with and without additives.	53
<i>Table 4.4</i>	Composition of black phases in as-cast BCC 52Ti-12V-36Cr alloys with and without additives.	53
<i>Table 4.5</i>	Composition of bright phases in as-cast BCC 52Ti-12V-36Cr alloys with and without additives.	54
<i>Table 4.6</i>	Crystal structure parameters as determined by Rietveld refinement of 52Ti-12V-36Cr with and without additive. The number in parentheses is the error on the last significant digit.	55
<i>Table 4.7</i>	Hydrogenation characteristics of BCC 52Ti-12V-36Cr with and without additive.	56
<i>Table 4.8</i>	Rietveld refinement of BCC 52Ti-12V-36Cr with and without additive.	57
<i>Table 5.1</i>	Fraction area (in %) occupied by each phase in as-cast and heat treated BCC 52Ti-12V-36Cr with additive. Uncertainty on each measurement is $\pm 1\%$	62
<i>Table 5.2</i>	Element abundances as measured for bulk compositions of heat treated 52Ti-12V-36Cr alloys with additives. Uncertainties on measured composition are $\pm$	63
<i>Table 5.3</i>	Chemical composition of dark phases in 52Ti-12V-36Cr alloys with additives. Uncertainties on measured composition are $\pm 1$ at%.	65
<i>Table 5.4</i>	Chemical composition of bright phases in 52Ti-12V-36Cr alloys with additives. Uncertainties on measured composition are $\pm 1$ at%.	65
<i>Table 5.5</i>	Chemical composition of black phases in 52Ti-12V-36Cr alloys with additives. Uncertainties on measured composition are $\pm 1$ at%.	65
<i>Table 5.6</i>	Crystal structure parameters as determined by Rietveld refinement of heat treated 52Ti-12V-36Cr with additive. The number in parentheses is the error on the last significant digit.	67
<i>Table 5.7</i>	Hydrogen storage properties of heat treated BCC 52Ti-12V-36Cr with additive.	69
<i>Table 5.8</i>	Rietveld refinement of hydrogenated heat treated BCC 52Ti-12V-36Cr with additive.	70

<i>Table 5.9</i>	Change in unit cell volume of phases other than BCC due to hydrogenation of BCC 52Ti-12V-36Cr with additive.	71
<i>Table 6.1</i>	Refinement of cast BCC 52Ti-12V-36Cr+4wt%Zr milled for 15 min, 30 min, 60 min.	76
<i>Table 6.2</i>	Hydrogen sorption properties of ball milled samples	78
<i>Table 6.3</i>	EDS of ball milled BCC 52Ti-12V-36Cr+4wt%Zr for 15, 30 and 60 min. The uncertainty measured on each measurement is $\pm 1$ at%.	80
<i>Table 6.4</i>	EDS of cast of BCC 52Ti-12V-36Cr milled with 4wt%Zr for 15, 30 and 60 min. The uncertainty measured on each measurement is $\pm 1$ at%.	81
<i>Table 7.1</i>	Average Particle Size of sample powder ( $\mu\text{m}$ ) for the alloy 52Ti-12V-36Cr + 4wt%Zr.	87
<i>Table 7.2</i>	Incubation of with ( $t_w$ ) and without ( $t_{w/o}$ ) additive samples.	89
<i>Table 7.3</i>	Ratio of incubation time of with and without additive samples with the same particle size.	90
<i>Table 7.4</i>	Effect of particle size on incubation.	90
<i>Table 7.5</i>	Intrinsic kinetics of with and without additive samples.	91



## **Nomenclature**

### **List of symbols**

at%	Atomic percentage
wt%	Weight percentage
X	Concentration factor
t	Instantaneous time during reaction of hydrogen absorption.
k	Slope
$\beta$ -phase	Mono-hydride phase
$\gamma$ -phase	Di-hydride phase
wt% <sub>i</sub>	Weight percentage of element 'i'
at% <sub>i</sub>	Atomic percentage of element 'i'
wt% <sub>j</sub>	Weight percentage of element 'j'
at% <sub>j</sub>	Atomic percentage of element 'j'
W <sub>i</sub>	Atomic weight of element 'i'
W <sub>j</sub>	Atomic weight of element 'j'
ij	Elements in alloy
$\phi$	Raw element size
$B/p$	Ball to Powder weight ratio in milling vial
$\lambda$	Wavelength of X-ray radiation
hkl	Miller Indices of Bragg's plane
$\theta_{hkl}$	Bragg's angle
$d_{hkl}$	Interatomic planer distance between Bragg's plane hkl.
a,c	Lattice parameters
P1	Representative location of EDS measurement for dark phase on micrographs.
P2	Representative location of EDS measurement for black phase on micrographs.
P3	Representative location of EDS measurement for bright phase on micrographs.
H%	Hydrogen storage gravimetric capacity.
t <sub>w</sub>	Incubation time for BCC alloy with additive.
t <sub>w/o</sub>	Incubation time for BCC alloy without additive.
t <sub>0.5</sub>	Incubation time for particles with size less than 0.5 mm.

$t_{0.5-1.0}$	Incubation time for particles with size between 0.5-1.0 mm.
$t_{+1.0}$	Incubation time for particles with size greater than 1.0 mm.

### List of acronyms

US	United States
HD	Hydrogen Decrepitation
BCC	Body Centered Cubic
LHV	Lower Heat Value
JMA	Johnson-Mehl-Avrami
2D	2-Dimensional
3D	3-Dimensional
CV	Contracting Volume
SPL	Surface Passivation Layer
XRD	X-ray Diffraction
HPT	High Pressure Torsion
EACP	Equal Angle Channel Pressure
SS	Stainless Steel
TEM	Transmission Electron Microscopy
PCT	Pressure-Concentration-Temperature
SEM	Scanning Electron Microscopy
BSE	Back Scattered Electron
SE	Secondary Electron
EDS	Energy Dispersive Spectroscopy
GUI	Graphics User Interface
SG	Space Group
FCC	Face Centered Cubic
a.u.	Arbitrary Unit
ECD	Equivalent Circular Diameter
PS	Particle Size

# **Chapter I**

## **INTRODUCTION**

## 1.1 Background

The energy is the driving force of economic and societal development. Currently, the energy market is highly dominated by conventional fuels like gasoline, diesel, natural gas and coal. But, these carry issues such as localized supply source (mostly middle east producers), uncertain source amount creating uncertainty over price, less efficient and associated pollution (air and environmental), as well global warming. Some of these key factors encouraging the development of new and renewable energy technologies. As such the renewables share in world energy consumption is growing.

The **Figure 1.1** shows the world energy consumption by energy sources till 2040 analysed by US energy information administration [1-2].

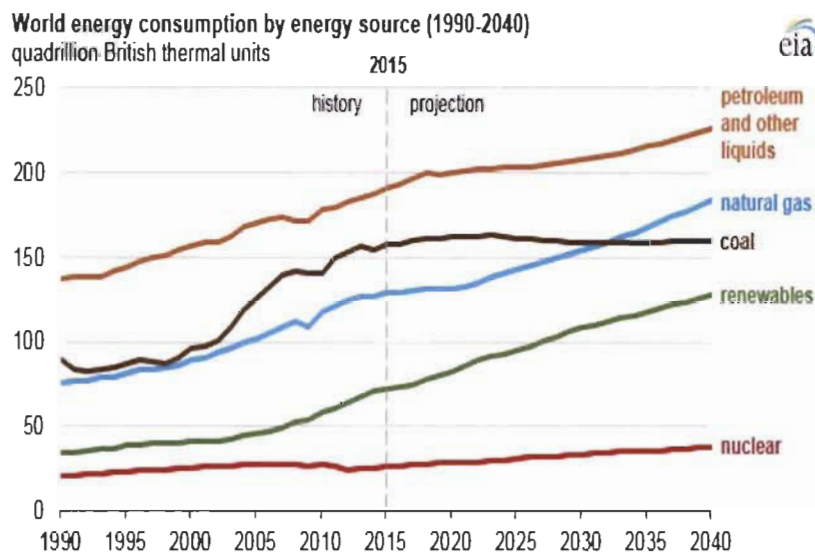


**Figure 1.1- The trends of contributions by energy sources [1-2].**

While significant, the development of renewable sources globally excluding hydro power have been at a slower pace than expected. Thus, with the increase in utilization of renewable energy, the use of fossil fuels could also accelerate in order to achieve increasing demand. According to unique explorative scenario presented by World Energy Council in 2014, by 2050, the energy demand will be doubled and increasing with faster rate than the primary energy supply from fossil fuels. The energy consumption from renewable energy sources showed more significant increase during 2005-2010. The council mentioned that the solar energy could be listed as fastest rising unconventional source and will share about 20-30% share of energy supply. But the share of fossil fuels for energy supply will increase with current trend and remain dominating. This is

threatening notice from World Energy Council. This could increase the global warming emission gases double/triple by 2050 compared to 1990 levels with the potential to turn energy infrastructure to disasters. The energy prices and high volatility will become more critical with the absence of clear path for the taxes on CO<sub>2</sub> emissions. The faster change in policies, scientific innovations and consumer's outlooks are creating energy market increasingly complex. However, the energy efficiency remains as priority but requires a long-term approach. Thus, we need to increase our efforts to access energy for the world's growing population. Otherwise, according to World Energy Council analysis reported in 2014, 530 million people could still lack access to even basic forms of energy in 2050. Thus, it is time to think about policies and, scientific innovations that could deliver tomorrow's sustainable energy. Let's hope for some suitable solutions and cheap sustainable energy could be found by addressing energy trilemma, the triple challenge of providing secured, affordable and environmentally sensitive energy. That concludes the research direction towards clean renewable energy sources and energy storages that are scalable to combat fossil fuels.

These alternative renewable sources could hold the key to combat issues raised during the use of conventional fuels. A renewable energy sources are found environment friendly and do not produce greenhouse gas emissions [3-4]. Though the initial cost of technology and infrastructure is quite high, these are cheaper for long run [3-4]. With advancements in technologies renewable energy is getting more accessible, affordable and efficient. However, the major challenges with renewables are related to scalability and intermittency. Storage need to be an integral component for large scale deployment of renewables.

## **1.2 Energy carrier-Hydrogen**

Hydrogen like electricity is an energy carrier and has several advantages. Hydrogen has highest abundance and energy content about 120.7 MJ/kg which is almost triple that of gasoline and diesel. Probably in future, hydrogen will be a potential candidate to be used as a raw material and as an energy carrier, hence becoming a feasible alternative to fossil fuel [5]. Hydrogen has been acknowledged for a wide variety of applications: the hydrogen decrepitating (HD) process has been applied to successfully produce SmCo<sub>5</sub>, Sm<sub>2</sub>(Co, Fe, Cu, Zr)<sub>17</sub> and Nd<sub>2</sub>Fe<sub>14</sub>B-type magnets [6]. Other kinds of applications reported use of hydrogen are food industries, semiconductor industry, manufacturing

industries, petroleum and chemical processes, aviation industry, and in a limited capacity, as clean fuel and power [7]. The exhaust from combustion of hydrogen or hydrogen operated fuel cells is  $H_2O$ , which is environmentally friendly, contrasting radioactive waste from redundant nuclear power plants or global warming gas emissions from fossil fuels. But the use of hydrogen is limited due to its low density (Gaseous  $H_2$ -0.0899 g/L @1 atm.) [8] and high flammability. The low density of hydrogen creates the need of bulky storage volume which makes the design bulky, otherwise reduce driving range/amount of total energy. Hydrogen is smallest element on the earth with high diffusivity as such it is highly liable for leak. Besides it has a wide flammability limit, which makes the use of all safety procedures essential while producing, storing, transporting or using hydrogen.

To make use of hydrogen as a fuel like petrol and diesel, while you run the application, it must be stored so that it can be used as-you-go [9]. However, safe storage facility will be one of the major bottleneck of using hydrogen. For various stationary/mobile applications, hydrogen storage will be required at stationary power sites, hydrogen production sites, hydrogen-refuelling stations and on-board in vehicles. Developing safe, reliable, compact and cost-effective hydrogen storage technologies are technically challenging barriers to its widespread use as an energy carrier. Hydrogen can be stored in three forms [10] as:

- a. Gaseous hydrogen
  - b. Liquid hydrogen
  - c. Advanced materials
- a. Gaseous hydrogen storage- The hydrogen is stored in tanks in its compressed gaseous form at high pressure between 17.5-70 MPa [10]. **Figure 1.2** shows the comparative schematic of gaseous and liquified hydrogen storage. The density of hydrogen is increased using compression, however energy goes in compressing hydrogen to high pressures. There are four types of tanks based on the tank material, the weight of tank and the pressure they can withstand. However, highly pressurized tanks are suspicious for leak which raises the safety issue. Totally of 341 hydrogen coincidences happened since 2007 because of usage and storage, where ~208 were related to failure in dispensing station, piping fittings and valves [11].

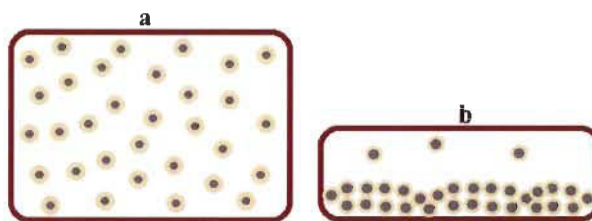


**Figure 1.2 Schematics of (a) high pressure gaseous and (b) liquid hydrogen storage.**

- b. Liquid hydrogen storage- Liquid hydrogen has density of  $0.07099 \times 10^3$  g/L, i.e. required approximately 1000 times smaller volume compared with gaseous storage. But, it requires cryogenic liquefaction process at 20.28 K, the process is highly energy intensive and can consume upto 40% energy out of total energy available with hydrogen [12]. As well, these storages need a special kind of storage facility with the refrigeration unit to maintain hydrogen in cryogenic state. For any mobile application, the entire refrigeration system to maintain the temperature of liquid hydrogen need to be carried on board.
- c. Advanced materials- It has been observed that, hydrogen is getting adsorbed or absorbed on reacting with some of the advanced materials [10]. Due to shortcomings with gaseous and liquid hydrogen storage methods, the researchers are aiming at light weight, safe and cost effective composite materials that reduce the weight and volume of storage system. It has been found that the hydrogen can be stored in advanced materials safely and cost effectively [10]. Some of the materials like activated carbon/ carbon nanotubes has been reported for storage in which hydrogen stored by adsorption. These materials have high specific surface area. In adsorption, the molecules or atoms of hydrogen are bonded with the surface as shown in **Figure 1.3(a)**. By increasing specific surface area, the storage capacity can be improved for these materials. But, the bonding is weak van der waals and lead to dissociation of hydrogen easily.

Secondly, the hydrogen could be dissociated at the surface of metals/alloys and get absorbed inside the solid lattice framework as shown in **Figure 1.3(b)**. These kinds of storage materials are popularly called metal hydrides. Thus, absorption of hydrogen could be achieved in relatively smaller volume at room temperature under low pressure.

Some more types of advanced materials such as complex hydrides and chemical hydrides, in which hydrogen is strongly bonded with molecular structures. It forms a chemical compound containing hydrogen atoms as shown in **Figure 1.3(c-d)**. These are reported to have high hydrogen capacity but has less reversibility due to strong chemical bond with hydrogen.

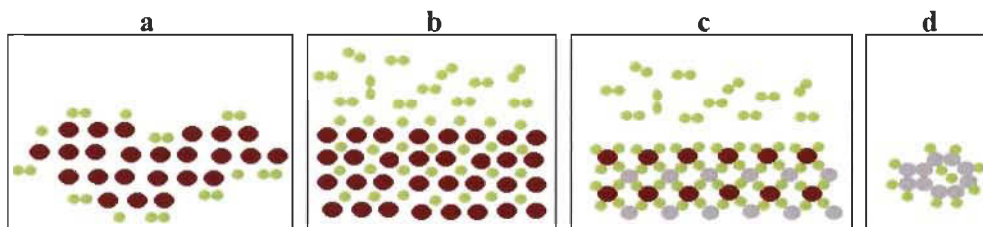


**Figure 1.3 Schematics for hydrogen storage in advanced materials: (a) surface adsorption, (b) metal hydrides, (c) complex hydrides and (d) chemical hydrides.**

The US Department of Energy (DOE) [13] reported an enduring vision for hydrogen-storage applications suitable for operational, economic and environmental parameters. The projected least hydrogen-storage capacity should be 6.5 wt% and 65 g/L hydrogen available, at the decomposition temperature between 60 and 120°C for commercial capability. The magnesium-based metal hydrides reported hydrogen-storage density of 6.5 H atoms/cm<sup>3</sup> higher than 0.99 H atoms/cm<sup>3</sup> of hydrogen gas or 4.2 H atoms/cm<sup>3</sup> of liquid hydrogen [14]. Hence, metal hydride-based storage is a volume-efficient method for on-board vehicular applications. Metal hydrides are popularly classified as Mg-based, Intermetallic and Body Centred Cubic(BCC) solid solution.

Mg-based metal hydrides are well-known for their high theoretical hydrogen capacity of 7.6wt%, high reversibility and low cost. The reported effective hydrogen capacity for Mg-based metal hydrides is about 6wt% which is much closer to targeted value by US-DOE [13]. Due to stable hydride formation, desorption enthalpy is very high with slow desorption kinetics. The corresponding unfavourable desorption temperature for MgH<sub>2</sub> is 573 K at 0.1 MPa of hydrogen. The efforts have been taken to destabilize Mg-hydride phase using nanosizing and heat treatments.

Intermetallic alloys are composed by mixing of A (an alkali earth metal) and B (transition metal) in fixed ratio. These are mainly categorised based on their crystal structure as AB-type, AB<sub>2</sub>-type Laves phases, AB<sub>5</sub>-type. The research on intermetallic has been attempted more than 25 years. The use of LaNi<sub>5</sub> and TiFe for hydrogen absorption opened new possibilities for industrial applications. They can be



hydrogenated and dehydrogenated at room temperature under relative low pressure of hydrogen. But, the hydrogen capacity reported are <1.4wt% and <1.8wt% respectively [10]. These capacities are much below the target of 6.5wt% set by US-DOE.

BCC solid solution is composed of two or more hydrogen absorbing elements at different mixing ratios. These alloys have been reported to possess hydrogen capacity close to 3.8wt% [10]. BCC alloys reported hydrogen absorption at room temperature under low hydrogen pressure (1-2 MPa). Ti-V-Cr and Ti-V-Mn are the most preferred BCC solid solutions. However, these suffer with slow first hydrogenation so called activation, stable hydride phase and sloping plateau of absorption and desorption.

### 1.3 Why BCC solid solution?

- BCC solid solutions can absorb at room temperature under low pressure of hydrogen.
- The reported hydrogen storage capacity for BCC solid solutions is almost 2-3 times higher than traditional intermetallic FeTi and LaNi<sub>5</sub> [10].
- BCC solid solutions have working temperature and pressure (Room temperature/1-2 MPa) much less compared with Mg-based metal hydrides (623 K/5-7 MPa) [10].
- BCC crystal structure has low packing factor (0.68) and more interstitial sites compared with FCC crystal structure (0.74) [15].
- Ti-V based Laves phase BCC solid solutions have been intensively investigated for wide variety of applications like batteries, hydrogen storages and Fuel cell application [16].
- BCC solid solutions are mainly based on V and Ti BCC solid solution with small amount of Laves phases (preferably C14-phase) [5]. These Laves phases probably observed as not only hydrogen absorber but also as catalysts for hydrogenation.

### 1.4 Choice of alloy composition

Based on the literature reports it was found that the Ti-V-Cr BCC solid solution system has high hydrogen capacity, room temperature hydrogen absorption under low hydrogen pressure of 1-2 MPa. The main problems identified with this system was activation and less reversibility.

Recently, Miraglia et al. showed that a dramatic improvement of activation kinetics could be achieved by first casting a BCC alloy of composition 33Ti-30V-37Cr, adding 4wt% of  $Zr_7Ni_{10}$  and recasting the mixture [17]. Later, Bibienne et al studied the BCC alloy 52Ti-12V-36Cr melted together with 4 wt%  $Zr_7Ni_{10}$  [18] and reported short incubation time prior to activation. These results point out that the presence of small proportion of secondary phases are favourable for hydrogen absorption properties of metal hydrides [17-20]. The content of Vanadium is also one of the parameter considered while selecting alloy composition to industrial scale due to its cost of 2400 USD/kg. Thus, there is need to consider an alloy composition with lower vanadium content. A composition region for 52Ti-12V-36Cr was identified in the Ti-V-Cr phase diagram as having a high hydrogen uptake region. Thus, 52Ti-12V-36Cr was chosen as main composition. The research gaps identified from these literature reports includes: absence of study on the individual impact of zirconium and nickel as an additive and effect of mechanical deformations and heat treatment was not studied so far. The 4wt% amount of additive has been reported as optimized amount to get improved hydrogenation [17-18]. Thus, additives Zr and Ni were decided to be added at 4wt%. Additional additive 2.2wt%Zr was chosen on the basis that it is part of Zirconium in 4wt%  $Zr_7Ni_{10}$  (2.2wt% Zr + 1.8% Ni).

Ball milling is a simple way to get reduced crystallinity and particle size, which could increase surface area available for hydrogenation and surface defects for hydride phase initiation. This can in turn facilitate the activation. Ball milling is also used for mechanical alloying. The possibility of change in surface morphology using ball milling for improvement in hydrogenation, change in phase distribution and their compositions could be considered as other ways for change in hydrogenation behaviour. Further heat treatment is one of the way to modify crystal structure, phase chemical composition, catalytic properties and phase abundance [21-23]. Ball milling and heat treatment are simple and easy to adapt at industrial scale. Thus, selected composition was processed with different synthesizing techniques as shown in **Figure 1.4** to get of the different alloy powders. The characterization of these powders gave in depth information on the relevance between phase system, phase compositions, crystallinity and corresponding hydrogen storage mechanism. Finally, the effective additive and synthesizing technique was selected for optimized storage behaviour.

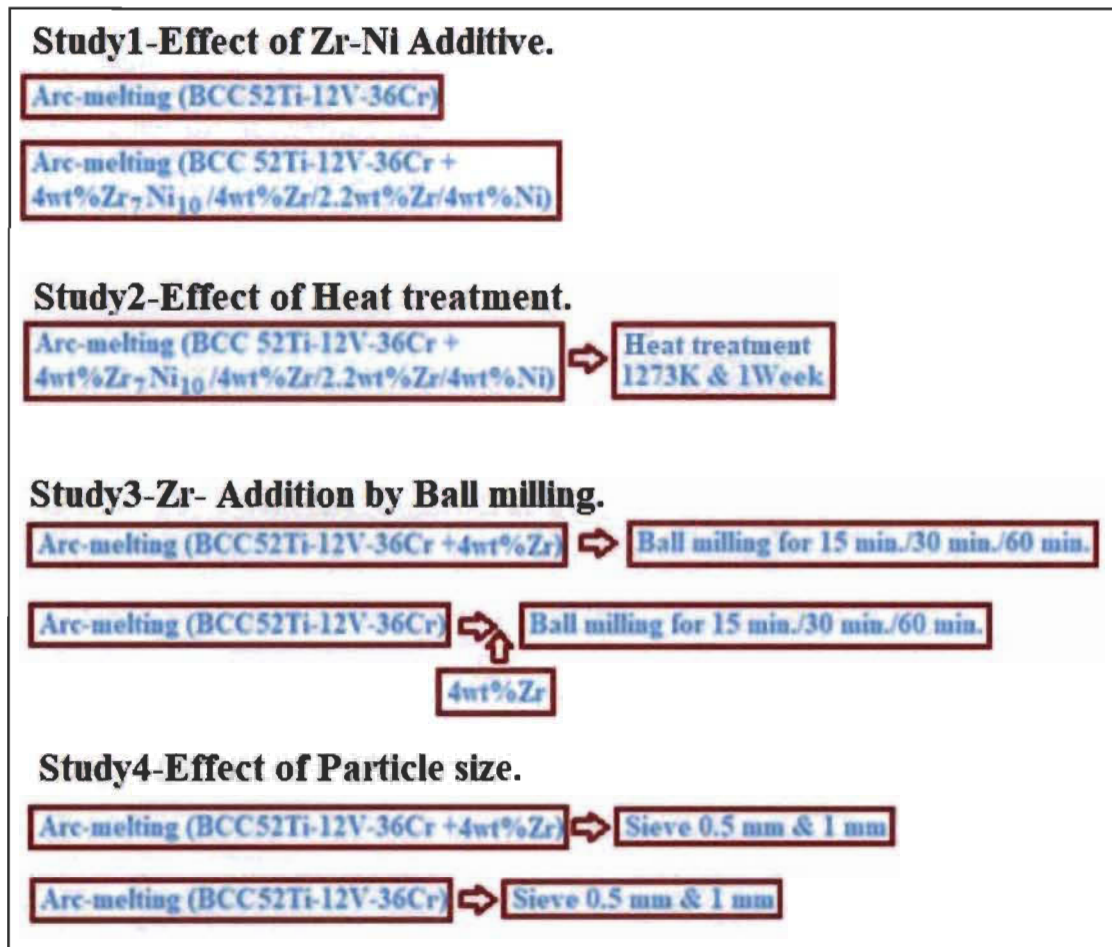


Figure 1.4- Summary of the work

### 1.5 Research aim and objectives

The purpose of the research is to explore the hydrogenation mechanism of BCC 52Ti-12V-36Cr alloy with transition elements as Zr-Ni additives processed by melting, mechanical milling and heat treatment. The ultimate aim is to find suitable additive and synthesizing technique to eliminate the activation step. This investigation will also help to understand the relative importance of particle size and additives on hydrogen absorption properties of BCC alloys. In summary the objective is to relate the variation of hydrogen storage properties with change of microstructure and crystallinity due to mechanical and annealing treatments.

### 1.6 Significance of study-Industrial applications

Activation is one of the major bottleneck while first hydrogenation of BCC solid solutions, thus an obstacle towards use of BCC solid solutions for various applications [17-20]. Thus, understanding the hydrogenation mechanism is very important. It will help to

implement possible ways like mechanical deformations and annealing to improve activation and reduce time required for hydrogenation to full capacity.

### **1.7 Thesis structure**

Chapter 2 introduces Ti-V-Cr BCC alloys and reviewed literature. The brief description about equipment and technical specifications are given in chapter 3. The effect of addition of 4wt%Zr<sub>7</sub>Ni<sub>10</sub>, 4wt%Zr, 2.2wt%Zr and 4wt%Ni as additive on first hydrogenation of BCC 52Ti-12V-36Cr is described in chapter 4. The effect of heat treatment on same alloys with additive is presented in chapter 5. Addition of zirconium by mechanical alloying compared to melting is reported in chapter 6. Chapter 7 reports the relative importance of particle size and additive on hydrogen absorption.

## **Chapter II**

# **LITERATURE REVIEW**

## 2.1 Outline

A brief summary of literature reports on the hydrogen storage properties of alloys is included, mainly with respect to hydrogen capacity, kinetics of hydrogenation and ease of activation. The literature reports on effect of change in chemical composition, mechanical deformation and heat treatment on the first hydrogenation (activation) kinetics are discussed in the current chapter. A focused study of isotherm Ti-V-Cr system has been included towards the end of the chapter.

## 2.2 Hydrogen Storage Properties

The physical and chemical properties of materials related with safety and design of hydrogen storage system decides its suitability for prevalent use as hydrogen store. The cost of material, synthesizing processes, raw elements and their abundance are vital practical considerations. However, the primary scientific aspects related to hydrogen sorption characteristics of alloy are,

- a. Storage capacity (gravimetric, volumetric, reversible)
- b. Thermodynamic properties (Enthalpy of adsorption, absorption and decomposition)
- c. Kinetics (hydrogen absorption, desorption)
- d. Ease of activation
- e. Cyclic performance
- f. Gaseous impurity resistance

Based on literature review, the following important aspects are discussed in detail. For hydrogen storage, it is essential to study various storage capacities, the absorption kinetics and the behaviour when first time exposed to hydrogen. The necessity of activation could be decided from behaviour of storage material when first time exposed to hydrogen storage.

### 2.2.1 Storage capacity

#### *Gravimetric storage capacity*

The gravimetric capacity is the weight percentage of amount of hydrogen absorbed in metal. The theoretical gravimetric capacity of BCC alloys is around 4 wt%. The BCC alloys have much less hydrogen capacity compared to the Mg based hydrides (7.6 wt.%) and complex hydrides (more than 10wt.%) [10]. The light weight metals like Sodium,

Lithium and Beryllium are also hydrogen absorbing metals. This class of hydrides is popularly known as chemical hydrides. The well-known complex hydride  $\text{LiBH}_4$  has capacity of 18wt% [10]. Though the gravimetric capacities of Mg based and light weight metal hydrides have been reported on higher side compared with BCC alloys, they have kinetics and thermodynamics limitations. They decompose at high temperature and are difficult to dehydrogenate. The BCC alloys can usually absorb hydrogen at room temperature under relatively low pressure of 1-2 MPa [17-19].

### *Reversible storage capacity*

The reversible hydrogen capacity is an amount of hydrogen desorbed out of hydrogen absorbed in metal system during repetitive cycles of absorption and desorption under normal conditions. It is measured with in terms of reversibility of the system. The reversibility is defined as percentage amount of desorbed hydrogen out of absorbed hydrogen. This is also one of the important parameters evaluated for hydrogen storage systems. Miraglia et. al. reported reversible capacity of 2wt% in case of Ti-V-Cr system at 288K as shown in **Figure 2.1** [17]. The hydrogen was desorbed by reducing the pressure from 1 MPa to 0.02 MPa step by step. Okada et al. reported the reversible hydrogen capacity of 2.2 wt% for as cast Ti-35V-xCr(x=37,43) at 313 K [22].

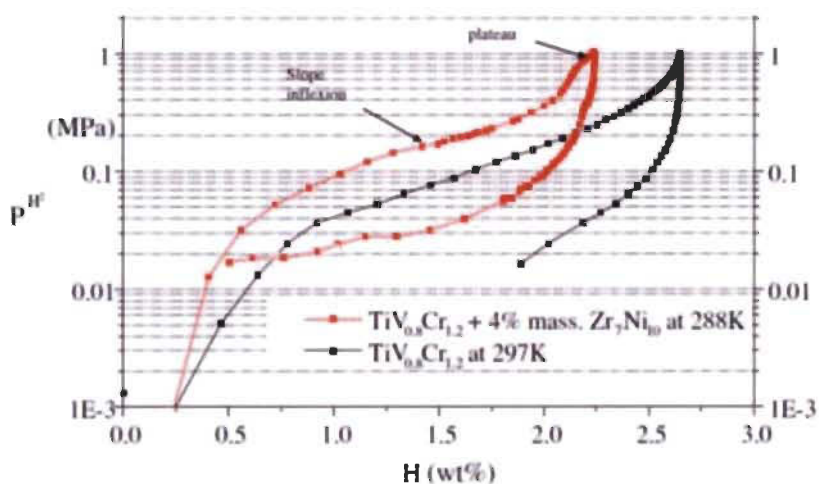


**Figure 2.1** PC isotherms of  $\text{TiV}_{0.8}\text{Cr}_{1.2}$  at 297 K and of the composite  $\text{TiV}_{0.8}\text{Cr}_{1.2} + 4$  wt.%  $\text{Zr}_7\text{Ni}_{10}$  at 288 K [17].

### **2.2.2 Kinetics**

The kinetics of hydrogen absorption and desorption is a result of the way in which overall transition from metal to metal hydride take place. For metal hydrides, the hydrogenation

process takes place in four steps physisorption, chemisorption, nuclei formation and growth.

- a. **Physisorption:** When hydrogen molecules become weakly immobilized on a metal surface, due to Van-der-Waals or dipole interactions, they are said to be physically adsorbed, or physisorbed. The enthalpies of physisorption are typically less than 0-5 kJ/mole [24].
- b. **Chemisorption:** Chemisorption starts with breaking of bond between hydrogen atoms in molecules and forming strong bond between hydrogen and alloy atoms. In this way hydrogen atoms get absorbed inside metal/alloy with initiation of hydride phase. The range of energy involved in chemical absorption is reported to be around 20-150 kJ/mole [24] of H<sub>2</sub> which is very high as compared with physisorption.
- c. **Nuclei formation and growth:** The initiation of metal hydride phase is called Nuclei formation. The nucleation is usually at the surface defects/strain fields/grain boundaries. Nuclei start to grow on metal surface or inside metal/alloy [24].

These all steps collectively determine the kinetics of hydrogen absorption. The step with slowest kinetics limits the overall kinetics of phase transformation. The slower step is known as the rate limiting step. It is a crucial part of study to find out the rate limiting step, which can further help to find out the ways to overcome the rate limiting step.

Rate limiting step is mathematically modelled and reported in literature. It is based upon concentration fraction(X) and time(t). The various rate limiting step model equations found by Mintz et al. and Avrami are summarized in **Table 2.1** with respective explanations [25]. Fitting into these models can give us information about the rate limiting step.

**Table 2.1 Rate limiting step model equations [25]**

Name of the Model	Mathematical Equation	Description
Chemisorption	$X=kt$	Surface Controlled
JMA2D	$[-\ln(1-X)]^{1/2} = kt$	2D growth of existing nuclei with constant interface velocity
JMA3D	$[-\ln(1-X)]^{1/3} = kt$	3D growth of existing nuclei with constant interface velocity.



Contracting Volume (CV) 2D	$1-(1-X)^{1/2} = kt$	2D growth with constant interface velocity.
Contracting Volume (CV) 3D	$1-(1-X)^{1/3} = kt$	3D growth with constant interface velocity.
Diffusion	$1-(2X/3)-(1-X)^{2/3}=kt$	3D growth, diffusion controlled with decreasing interface velocity.

### 2.2.3 First hydrogenation

Some environmental adsorbates surrounding external surfaces of solid [26] could contaminate the fresh and clean surfaces exposed to environment before hydrogenation. It forms a layer of oxides/ corrosion/ hydroxyl. This layer passivates the surfaces for hydrogenation and acts as a barrier for hydrogen to be absorbed within the metal, is called a Surface Passivation Layer (SPL) [27]. The hydrogen absorption/desorption processes are delayed due to SPL originated from contaminants and remnants of solvents in alloys produced using wet chemistry [27-28]. The waiting duration before start of hydrogen absorption is known as incubation time. The incubation could be of few minutes, few hours or few days. The longer incubations are detrimental; thus, a pre-treatment is needed. Generally, the contaminants and remnants are extracted by keeping the sample under vacuum at high temperatures [29]. Samples can also be cleaned with purging of an inert gas used to remove pre-adsorbed species [29]. This removal process is popularly known as degassing and can be supervised by weight loss during degassing (gravimetric system) or decrease in the pressure (volumetric system) [30].

The presence of SPL mostly affects the first hydrogenation and once SPL removed the hydrogenation cycles carried out after first hydrogenation shows quicker absorption. Thus, an activation process is required to remove SPL. Activation is the process of breaking SPL barrier to absorb hydrogen quickly in metal host using high temperature and/or pressure by exposing it to hydrogen first time [27]. For industrial applications and for on-board hydrogen storages, working at high temperature and pressure is not desirable. The high temperature and pressure could raise the safety issues. The limits for working temperature and pressure are set by US DOE as 353 K – 393 K and 2 MPa - 4 MPa respectively [31]. It indicates that activation is additional time-consuming process at additional cost. Thus, avoiding activation is beneficial and many researchers have been working on reduction in incubation time as well as first hydrogenation at reduced temperature and pressure. In the current work, we have developed understanding about the parameters affecting the

activation and its mechanism and have worked towards complete elimination of activation or achieving the first hydrogenation at room temperature under low pressure.

Generally, the mechanism of activation could be explained as follow,

- When alloy exposed to hydrogen first time, hydrogen faces difficulty for physisorption due to surface passivation layer on alloy particles. In order to reach alloy surface, hydrogen molecules supposed to break the passivation layer and then get adsorbed. First time the task of physisorption may be more difficult than for the further cycles.
- Chemisorption could proceed after a physisorption of  $H_2$  molecules over the surface of metal host mostly at cracks/surface defects/grain boundaries. This may initiate the formation of metal hydride phase.
- The growth of hydride phase could create un-uniform strain fields in metal particles.
- High stress and strain fields may be developed at concentrated areas like cracks/surface defects/grain boundaries which leads to fragmentation of metal particles.
- The fragmentation of metal particles may lead to exposure of fresh and clean metal host surface for hydrogenation. The available surface area for hydrogenation also increased with reduced particle size due to fragmentation.
- The enlarged fresh and clean metal host surface could absorb hydrogen quickly. An instantaneous change in kinetics of hydrogen absorption may end up with absorption to full hydrogen capacity.

### **2.3 Factors affecting first hydrogenation**

The variations in crystallite size, particle size, chemical composition and microstructure could be achieved with chemical, mechanical and heat treatment. A vast literature has been reported by researchers on effects of chemical, mechanical and heat treatments over hydrogen sorption of host metals/alloys.

#### **2.3.1 Effect of additives on hydrogen sorption properties**

In the current work we have considered, the main way to improve activation has been the addition of an element or an alloy during melting in order to obtain a multiphase alloy. It

has been noticed from literature reports that, formation of multiphase alloy through inclusion of additive could result in a faster activation kinetics [17-19]. With the objective of not to change the thermodynamics and hydrogen capacity of the parent alloy, this additive must be chosen such as it only minimally substituted with elements of the parent alloy and instead makes a separated phase that will act as a gateway for hydrogen [17-19].

The co-melt procedure for addition of  $Zr_7Ni_{10}$  in BCC alloy was prescribed by Charbonnier et al. in their US patent [32]. The process of co-melt has been reported by various investigators for addition of additives, but the phenomenon is quite complicated [32].

S. Miraglia et al. showed that a dramatic improvement of activation kinetics could be achieved by casting 4wt%  $Zr_7Ni_{10}$  to previously cast BCC 33Ti-30V-37Cr alloy [17]. The conventional microstructure for BCC along with network of Zr-Ni rich intergranular phase was observed. The ease of activation observed is due to presence of secondary phase.

Bibienne et al. studied 52Ti-12V-36Cr and 42Ti-21V-37Cr BCC solid solutions with additive 4wt%  $Zr_7Ni_{10}$  [18-19]. The BCC crystal structure remained intact after addition of  $Zr_7Ni_{10}$ . The single-phase BCC microstructure changed to BCC with network of intergranular secondary phase which was found to be rich in Zr and Ni. The secondary phase was reported to be responsible for short incubation and fast intrinsic hydrogen absorption. The hydrogen capacity was slightly lowered due to reduced BCC phase. These effects of additive on crystal structure, microstructure and hydrogen absorption of BCC solid solutions agreed with results reported by Miraglia et al. [17].

D. Bellon et al. reported effect of addition of Zr over hydrogen sorption of BCC  $TiCrV_{0.9}$  [33] alloys  $TiCrV_{0.9}$ ,  $TiCrV_{0.9}Zr_{0.2}$  and  $TiCrV_{0.7}Zr_{0.4}$ . Replacing V by Zr lead to decrease in hydrogen capacity from 3.8wt% to 2.0wt%, but absorption kinetics significantly improved with increase in concentration of Zr.

Hang et al. studied the  $Ti_{10}V_{84-x}Fe_6Zr_x$  ( $x=1-8$ ) for hydrogenation behaviour with increase in content of Zr [34]. The XRD pattern and microstructure analysis revealed growth of secondary Laves phases with rise of Zr concentration. Though the introduction of secondary phase reported faster kinetics, the hydrogen capacity reduced with Zr. The improvement in kinetics reported due to coexistence of Laves phases and BCC phase. The hydrogen capacity reduced due reduction in BCC phase abundance.

Basak et al. tried substitution of Zr at 5at% on V-site of  $Ti_{0.85}VFe_{0.15}$  [35]. The hydrogenation properties of  $Ti_{0.85}VFe_{0.15}$  was compared with  $Ti_{0.85}V_{0.95}Fe_{0.15}Zr_{0.05}$ . The substitution of Zr improved the hydrogenation although hydrogen capacity reduced to 3.5wt% from 3.7wt%. Same reasoning was given that the presence of secondary phase resulted in enhanced kinetics and reduced hydrogen capacity.

The effect of additives Nb and 4% $Zr_7Ni_{10}$  over hydrogenation behaviour of  $TiCr_{1.1}V_{0.9}$  had been reported by Martínez and Santos [36].  $TiCr_{1.1}V_{0.9}$ ,  $TiCr_{1.1}V_{0.45}Nb_{0.45}$  and  $TiCr_{1.1}V_{0.9} + 4wt\% Zr_7Ni_{10}$  were casted. It was found that additives enhanced the kinetics of hydrogen absorption. The change in absorption rate took place due to change in microstructure. The additives introduced a secondary phase which was rich in content of additive compared with matrix phase.

The occurrence of secondary phase has been consistently reported upon addition of Zr-Ni based additives which shows synergy along with main phase for hydrogen absorption.

The overall literature review for Ti-V-Cr system with effects of additives can be tabulated as shown in **Table 2.2**.

**Table 2.2 Effects of additives/substitutes over hydrogen sorption.**

Sr. No.	Chemical Composition	Additive/ Substitute	Highlights	Ref. No.
1	33Ti-30V-37Cr	4wt% $Zr_7Ni_{10}$	<ul style="list-style-type: none"> <li>• Dramatic improvement of activation kinetics.</li> <li>• BCC+ Network of Zr-Ni rich intergranular phase.</li> <li>• The ease of activation observed due to presence of secondary phase.</li> </ul>	17
2	52Ti-12V-36Cr 42Ti-21V-37Cr	4wt% $Zr_7Ni_{10}$	<ul style="list-style-type: none"> <li>• BCC turns into BCC+ Network of Zr-Ni rich intergranular phase.</li> <li>• Coexistence of secondary phase reported responsible for short incubation and fast intrinsic hydrogen absorption.</li> </ul>	18-19
3	$TiCrV_{0.9}$ , $TiCrV_{0.9}Zr_{0.2}$ $TiCrV_{0.7}Zr_{0.4}$	Zr	<ul style="list-style-type: none"> <li>• Hydrogen absorption rate significantly improved with increase in concentration of Zr.</li> </ul>	33
4	$Ti_{10}V_{84-x}Fe_6Zr_x$	Zr ( $x = 1 - 8$ )	<ul style="list-style-type: none"> <li>• The activation behaviour had greatly enhanced due to addition of Zr.</li> <li>• Hydrogen capacity decreased with concentration of Zr.</li> </ul>	34
5	$Ti_{0.85}VFe_{0.15}$ $Ti_{0.85}V_{0.95}Fe_{0.15}Zr_{0.05}$	Zr at 5at%	<ul style="list-style-type: none"> <li>• The substitution of Zr improved the hydrogenation although hydrogen capacity reduced.</li> </ul>	35
6	$TiCr_{1.1}V_{0.9}$	Nb, 4% $Zr_7Ni_{10}$	<ul style="list-style-type: none"> <li>• Additives acted as catalysts to enhance the kinetics of hydrogen absorption.</li> <li>• The change in absorption rate took place due to change in microstructure.</li> </ul>	36

### 2.3.2 Effect of mechanical deformations on hydrogen sorption properties

Mechanical deformation of alloys may create internal or surface lattice defects [37]. These irregularities are favourable for nuclei formation and growth of the hydride phase. This may change the kinetics of hydrogen absorption/desorption. The dislocations act as a nucleation points for chemical reactions which may improve activation behaviour. Ball milling, cold rolling, forging, high pressure torsion (HPT) deformation, Equal Angular Channel Pressing (ECAP), grinding, filing etc. are some of the mechanical deformation techniques used nowadays [38].

The general default effects of mechanical deformations are strain fields and high-density defects. The hard-secondary phase, high density of defects (dislocations/twins) and cracks could create nonuniform strain fields. It will be beneficial for nucleation and growth of metal hydride phase. Therefore, increasing the number of heterogeneous sites could improve activation kinetics [39].

Mechanical grinding and mechanical alloying was utilized by Hu et al. for getting  $\text{TiCr}_2$  [40]. Mechanical grinding showed absorption and desorption of  $\sim 0.7$  and  $\sim 0.5$  wt% respectively. Mechanically alloyed samples revealed absorption and desorption of  $\sim 1.0$  and  $\sim 0.4$  wt% respectively. The mechanical alloying reported as an effective way to synthesize alloys for improved hydrogen sorption characteristics compared to mechanical grinding.

Cho et al. processed the cast of  $\text{Ti}_{0.32}\text{Cr}_{0.43}\text{V}_{0.25}$  (at. %) using combination of ball milling and further followed by heat treatment to study the effect on hydrogen sorption characteristics [41]. The tungsten carbide(WC) and stainless steel(SS) balls and vials were tested for pulverisation of alloys. The WC milled alloy powders revealed WC contamination and caused some compositional changes in matrix during heat treatment at 1473 K for 2 hrs. However, the contaminant peaks were not found in XRD of milled samples with SS balls and vial. The ball milling reduced the crystallite size to 23-30 nm. Both XRD analysis and TEM results agreed with each other. The pressure-concentration-isotherms exhibited reduction in total, effective hydrogen capacity, steep plateau for milled samples. The reduction in hydrogen absorption was reported to be due to contamination and steep plateau was found to be due to increased strain after ball milling.

The improvement in activation was observed by X. B. Yu et. al. when 10wt%  $\text{LaNi}_{3.75}\text{Co}_{0.75}\text{Mn}_{0.4}\text{Al}_{0.3}$ / carbon nanotubes ball milled with cast of Ti-28V-15Mn-10Cr

[42-43].  $\text{LaNi}_{3.75}\text{Co}_{0.75}\text{Mn}_{0.4}\text{Al}_{0.3}$  and Ti-28V-15Mn-10Cr were prepared by magnetic levitation melting and water cooled. The crush of (Ti-28V-15Mn-10Cr + 10wt%  $\text{LaNi}_{3.75}\text{Co}_{0.75}\text{Mn}_{0.4}\text{Al}_{0.3}$ ) processed for ball milling in steel vial with the ball to powder weight ratio of 10. The particles of Ti-28V-15Mn-10Cr covered with layer of nano-particles of  $\text{LaNi}_{3.75}\text{Co}_{0.75}\text{Mn}_{0.4}\text{Al}_{0.3}$ . The nano-composite layer acted as gateways for hydrogen and thus resulted into improved hydrogenation. The same sort of process followed for lab made carbon nanotubes. Ball milling Ti-28V-15Mn-10Cr with carbon nano-tubes was reported to have improved hydrogenation.

The effect of ball milling and cold rolling on hydrogen sorption characteristics of  $\text{TiV}_{1.6}\text{Mn}_{0.4}$  alloy was studied by Couillaud et al. [44]. As cast alloys showed nanocrystalline structure with crystallite size about 17 nm. The crystallite size and lattice parameter greatly reduced by both methods: ball milling and cold rolling. The as cast alloy absorbed hydrogen about 3.48wt% at 423 K and had reversibility of 1.8wt%. However, ball milled and cold rolled samples didn't absorbed hydrogen even after 10 cycles of hydrogenation/dehydrogenation. The reason behind non-absorption of hydrogen was remained unexplainable.

Singh et al studied the effect of ball milling on hydrogen sorption characteristics of  $\text{Ti}_{0.32}\text{Cr}_{0.43}\text{V}_{0.25}$  alloy [45]. Tungsten carbide (WC) balls and vial used for pulverizing the as-cast  $\text{Ti}_{0.32}\text{Cr}_{0.43}\text{V}_{0.25}$  alloy. The peaks of tungsten were rising with duration of ball milling, arising due to contamination of sample. Ball milling did not affect bulk compositional structure. The increasing lattice strain was measured through milling duration while the crystallite size was reduced to smallest size within first 1 hr. Pressure-concentration isotherms revealed decrease in total and effective hydrogen capacity with ball milling.

Ball milling is well-known technique used for getting nanocrystallinity, modifying surfaces, mechanical alloying which can produce wide variety of materials [38, 41-43].

### ***Effect of particle size***

The respective effect of particle size and nanocrystallinity on hydrogen sorption kinetics of metal hydrides has been investigated by many researchers. For example, Dornheim et al. showed improved kinetics with reduced particle size by reactive ball milling for  $\text{MgH}_2$  [37].

Reduced crystallinity and particle size could facilitate activation. Bobet et al. had shown that reduction in particle size resulted in increased specific surface area which gave rise to surface reactions and accelerated hydrogen absorption [46].

Effect of particle size of ball milled  $\text{MgH}_2$  has also been investigated by Varin et al. [47]. They distinguished the respective contribution of reduced particle size and the presence of a metastable phase ( $\gamma\text{-MgH}_2$ ) on the dehydrogenation kinetics.

The critical review is done on effect of mechanical deformations over hydrogen absorption. The tabulated summary of review is as shown in **Table 2.3**.

**Table 2.3 Effects of mechanical deformations over hydrogen sorption.**

Sr. No.	Chemical Composition	Synthesizing process	Highlights	Reference No.
1	$\text{TiCr}_2$	1.Mechanical Grinding, 2.Ball milling	<ul style="list-style-type: none"> <li>• Mechanical alloying is effective way to synthesize alloys.</li> </ul>	40
2	$\text{Ti}_{0.32}\text{Cr}_{0.43}\text{V}_{0.25}$	ball milling + heat treatment	<ul style="list-style-type: none"> <li>• WC and SS balls and vials both testified.</li> <li>• WC peak increasing with milling duration indicates increasing contamination.</li> <li>• No peaks of SS in XRD but still adverse effect on hydrogenation.</li> <li>• Reduced total, effective hydrogen capacity, steep plateau for milled samples.</li> </ul>	41
3	Ti-28V-15Mn-10Cr + 10% $\text{LaNi}_{3.75}\text{Co}_{0.75}\text{Mn}_{0.4}\text{Al}_{0.3}$	Cast Ti-28V-15Mn-10Cr milled with cast of 10% $\text{LaNi}_{3.75}\text{Co}_{0.75}\text{Mn}_{0.4}\text{Al}_{0.3}$	<ul style="list-style-type: none"> <li>• Ball to powder ratio 10</li> <li>• Layer of nano particles enhanced hydrogenation.</li> </ul>	42
4	Ti-28V-15Mn-10Cr + Carbon Nano tube	Cast Ti-28V-15Mn-10Cr milled with cast of Carbon Nano tube.	<ul style="list-style-type: none"> <li>• Ball to powder ratio 10</li> <li>• Layer of nano tubes particles enhanced hydrogenation.</li> </ul>	43
5	Mg-Ti(Bulky) Mg-Stainless steel(Bulky)	Accumulative roll bonding	<ul style="list-style-type: none"> <li>• Desorption at 623 K at which pure Mg hardly desorb.</li> <li>• First hydrogenation was improved with number of fold and roll(FA) operations.</li> <li>• Hydride nucleation sites at the heterogeneous locations like cracks and interference of phase layers.</li> </ul>	38
6	$\text{TiV}_{1.6}\text{Mn}_{0.4}$	1.Ball milling 2.Cold rolling	<ul style="list-style-type: none"> <li>• As cast-nanocrystalline structure with crystallite size about 17 nm.</li> <li>• Crystallite size and lattice parameter greatly reduced by both milling and rolling. Textured alloy along Bragg peak (200) in cold rolled</li> </ul>	44

			sample. • As cast absorbed hydrogen but milled and rolled samples does not absorbed even after 10 cycles.	
<b>Effect of particle size</b>				
7	MgH <sub>2</sub>	Reactive ball milling	• improved kinetics with reduced particle size	37
8	Mg + 10 wt% WO <sub>3</sub> Mg + 5 wt% Cr <sub>2</sub> O <sub>3</sub>	Mechanical milling Mechanical grinding	• Both oxides have an important catalytic effect on absorption and desorption. • Particle size influenced with milling speed and B/P weight ratio. • Reduced particle size improves rate of absorption and desorption.	46
9	Commercial nanocrystalline MgH <sub>2</sub>	Controlled mechanical milling, B/P=10	• Desorption temperature decreases with reduced particle size. • After threshold particle size, desorption temperature decreases rapidly. • Long milling more than 10 hrs introduce $\gamma$ -MgH <sub>2</sub> which coexists with $\beta$ -MgH <sub>2</sub> • Additive effect of rapid change in desorption temperature may be combined effect of reduced particle size and $\gamma$ -MgH <sub>2</sub>	47

### 2.3.3 Effect of heat treatment on hydrogen sorption properties

The heat treatment is an efficient way to change the phase compositions, its distribution and crystallographic parameters [22-23]. The as cast samples with additives could contain metastable phases and the hydrogen sorption properties may be associated with metastability of secondary phases. Thus, there is need of studying the BCC alloys after heat treatment. The heat treatment lead to homogenized microstructure.

Young et al. investigated the effect of annealing at various temperatures between 1073 K -1373 K on hydrogen storage properties of Ti<sub>15.6</sub>Zr<sub>2.1</sub>V<sub>40.0</sub>Cr<sub>11.2</sub>Mn<sub>6.9</sub>Co<sub>1.4</sub>Ni<sub>22.5</sub>Al<sub>0.3</sub> [48]. BCC phase, TiNi and C14 Laves phase was observed in microstructures of as cast samples. Annealing at 1073 K and 1173 K had introduced Zr and TiO<sub>2</sub> phases with decrease of C14 and increase of TiNi catalytic phase. The Ti<sub>2</sub>Ni and  $\sigma$ -VNi phases had originated after 1073 K -1373 K respectively. The effective hydrogen storage properties was observed for the sample annealed at 1173 K for 12 hr due to supportive balance between hydrogen absorbing BCC phase and catalytic TiNi+C14 phases.



Cho et al. reported the effect of heat treatment on  $\text{Ti}_{0.32}\text{Cr}_{0.43}\text{V}_{0.25}$  [49]. The heat treatment improved absorption-desorption capacities and flatness of plateau. Cyclic performance was excellent. The effective hydrogen capacity remained 2wt% even after 1000<sup>th</sup> cycle. The kinetics improved with cycling for first few cycles and remained same afterwards. At 504<sup>th</sup> cycle, the sample absorbed 98% of its full capacity within 2 min. XRD patterns revealed increase in amorphous contents with number of cycles.

Cho et al. reported improvement in the flatness of plateau without loss of total and reversible hydrogen capacity after heat treatment [50]. The heat-treated  $\text{Ti}_{0.16}\text{Zr}_{0.05}\text{Cr}_{0.22}\text{V}_{0.57}$  alloy showed the maximum total and effective hydrogen capacity of 3.55 and 2.14 wt% respectively.

The effect of heat treatment at 1273 K for 1 hr on crystal structure, microstructure, hydrogen sorption and corrosion rate of  $\text{Ti}_{34}\text{V}_{40}\text{Cr}_{24}\text{Fe}_2$  alloy was investigated by J. Mohammed Abdul et al. [51]. One of the heat treated sample was quenched and the other cooled in the furnace itself. All samples exhibited BCC as a main phase combined with some secondary Laves phases. The abundance of Laves phases reduced for annealed samples while disappeared for quenched sample. The Ti-rich phase precipitated after annealing. The hydrogenation behaviour was enhanced after annealing but corrosion rate was higher.

Maohua Rong et al. presented the effect of heat treatment on crystal structure, microstructure, hydrogen storage and thermal stability of  $\text{V}_{68}\text{Ti}_{20}\text{Cr}_{12}$  alloy [52]. The BCC phase did not change after heat treatment for 12 hours at 973 K. The kinetics of absorption/desorption has improved greatly due to the homogeneous composition and perfect structure. The slope of heat treated sample reported flatter than as cast alloy. The heat treatment is reported as beneficial mainly for improvement in kinetics of hydrogenation and de-hydrogenation.

X. Liu et al. investigated the influence of additive Ce and heat treatment on hydrogenation of  $\text{Ti}_{32}\text{Cr}_{46}\text{V}_{22}$  [53]. The alloys were casted with and without additive using magnetic levitation melting. The as cast samples were heat treated at 1673 K for 5 min. and quenched further using iced water. The plateau slope was flattened because of homogenization of phase composition, refined microstructure and low oxygen concentration. The heat treated  $\text{Ti}_{32}\text{Cr}_{46}\text{V}_{22}\text{Ce}_{0.4}(\text{at}\%)$  absorbed 3.65wt% and desorbed 2.00 wt% at 298 K, 2.52 wt% at 333 K under hydrogen pressure of 0.1 MPa.

The degraded performance of  $\text{Ti}_{0.32}\text{Cr}_{0.43}\text{V}_{0.25}$  due to ball milling could be explained on the basis of surface contamination [41]. The milled samples were heat treated further at 1473 K for 2 hrs, 1473 K for 8 hrs, 1073 K for 2 hrs and 1273 K for 2 hrs. The WC milled samples exhibited tungsten contamination. This contamination created compositional changes during heat treatment at 1473 K for 2 hrs. PCT results revealed increase in total and effective hydrogen capacities of heat treated samples. The improvement in hysteresis and phase transformation had observed and was found to be optimal at 1473 K.

Z. Hang et al reported the effect of heat treatment at 1373 K for 8 hrs. and 1523 K for 5 min. followed with water cooling to room temperature over hydrogen sorption characteristics of  $\text{Ti}_{10}\text{V}_{77}\text{Cr}_6\text{Fe}_6\text{Zr}$  [34]. It was found that the optimum temperature was 1523 K on the basis of desorption hydrogen capacity of 1.82wt% and decomposition plateau pressure of 0.75 MPa. As cast samples revealed BCC phase with C14 secondary phase. The plateau was flattened, and abundance of BCC was increased after heat treatment. However, the hydrogen capacity was reduced. The as cast and heat treated samples showed desorption capacity of 1.82 and 1.44wt% respectively at 333 K.

The effect of heat treatment followed by compression/cold rolling of single-phase Ti–22Al–27Nb alloy was studied [54]. The samples, compressed/cold rolled at different percentage of deformation were quenched from 1473 K. The specimens were compared using PCT at 373 K. The mild deformed samples without heat treatment were performed forward and reverse transformation between metal, mono hydride( $\beta$ -phase) and di-hydride( $\gamma$ -phase). However heavy deformations were found to be not useful. The quenched sample showed slow transformation from  $\beta$  to  $\gamma$  phase and were found to be hard towards reverse transformation. The best hydrogen absorption in mild deformed sample was explained on the basis of well uniformly aligned lattice arrangement and screw dislocation.

After a brief review over influence of heat treatments over the hydrogen absorption, the overall literature review is tabulated in **Table 2.4**. The main effects of heat treatment have been observed as enlargement in unit cell, change in microstructure, phase composition and phase distribution, reduction/increase in BCC phase and an appearance of Laves phases. These changes are leading to change in hydrogenation behaviour. The main observations are hydrogen capacity related with phase abundance of BCC phase. The

kinetics of hydrogenation has explained on the basis of coexistence of Laves phases with BCC phase.

**Table 2.4 Effects of heat treatment over hydrogen sorption.**

Sr. No.	Chemical Composition	Heat treatment parameters	Highlights	Reference No.
1	TiFe <sub>1-x</sub> M <sub>x</sub> (M = Cr, Mn)	1173 K	<ul style="list-style-type: none"> <li>• No activation required if secondary phase present.</li> <li>• Increase in abundance of second phase accelerates hydrogenation, lowers plateau pressure.</li> <li>• Homogenization treatment reduced activation rate.</li> </ul>	55
2	(41Ti-59Cr) <sub>100-x</sub> -V <sub>x</sub> (x = 5, 15, 30, 60)		<ul style="list-style-type: none"> <li>• Ti-V heat treated alloy- hysteresis decreased significantly with repetitive cycles.</li> <li>• Effective capacity decreased rapidly till 20<sup>th</sup> cycle and gradually afterwards till 50<sup>th</sup> cycle.</li> <li>• After 50<sup>th</sup> cycle, particle size decreases with V-content.</li> </ul>	56
3	Ti <sub>2</sub> CrV with additive ZrFe <sub>1.8</sub> V <sub>0.2</sub>	1173 K 2 days	<ul style="list-style-type: none"> <li>• The coexistence of Laves phase with BCC led to rapid hydrogenation.</li> <li>• The reduction of hydrogen capacity with increase in concentration of additive.</li> <li>• 5at% ZrFe<sub>1.8</sub>V<sub>0.2</sub> as optimized amount of additive.</li> </ul>	57
4	Ti <sub>15.6</sub> Zr <sub>2.1</sub> V <sub>40.0</sub> Cr <sub>11.2</sub> Mn <sub>6.9</sub> Co <sub>1.4</sub> Ni <sub>22.5</sub> Al <sub>0.3</sub>	1073 to 1373 K	<ul style="list-style-type: none"> <li>• BCC phase, TiNi and C14 Laves phase present before annealing.</li> <li>• 1073 K and 1173 K had introduced Zr and TiO<sub>2</sub> phases, decrease C14, increase TiNi.</li> <li>• The effective hydrogen storage properties presented by sample annealed at 1173 K for 12 hr due to supportive balance between hydrogen absorbing BCC phase and catalytic TiNi+C14 phases.</li> </ul>	48
5	Ti <sub>0.32</sub> Cr <sub>0.43</sub> V <sub>0.25</sub>	1653 K 20 K/min, 1 min, Water quenched	<ul style="list-style-type: none"> <li>• Heat treatment improved absorption-desorption capacities and flatness of plateau.</li> <li>• Cyclic performance was excellent.</li> <li>• Increase in amorphous nature with number of cycles.</li> </ul>	49
6	Ti <sub>0.16</sub> Zr <sub>0.05</sub> Cr <sub>0.22</sub> V <sub>0.57</sub>	1473 K, 8 Hrs.	<ul style="list-style-type: none"> <li>• Improved the flatness of plateau without loss of total and effective capacity.</li> </ul>	50
7	Ti <sub>34</sub> V <sub>40</sub> Cr <sub>24</sub> Fe <sub>2</sub>	1273 K, 1 hr	<ul style="list-style-type: none"> <li>• BCC as a main phase combined with some secondary Laves phases.</li> <li>• Reduced Laves phases after annealing and disappeared after quench.</li> <li>• Ti-rich phase precipitates after annealing.</li> <li>• Improved hydrogenation but high corrosion rate.</li> </ul>	51

8	$\text{Ti}_{30}\text{Cr}_{50}\text{V}_{20}$ (Arc-melt) $\text{Ti}_{27.8}\text{Cr}_{42.2}\text{V}_{25}\text{Fe}_5$ (VIM)	1473-1673 K, 1 min to 6 hrs.	<ul style="list-style-type: none"> <li>• No beneficial thermodynamics and absorption capacities.</li> <li>• Increase in lattice constant and refinement of grains achieved due to fast cooling rate.</li> </ul>	52
9	$\text{V}_3\text{TiNi}_{0.56}$	973-1473 K, 24 hrs Furnace cooling	<ul style="list-style-type: none"> <li>• Almost fattened plateau in between 1073-1273 K. At 1173K, the BCC phase had expanded grain size</li> <li>• Reduction in catalytic phase TiNi caused decrease in cyclic performance and hydrogen absorption rate.</li> <li>• Optimized temperature 1073-1173 K.</li> </ul>	21
10	$\text{Ti}_{32}\text{Cr}_{46}\text{V}_{22} + \text{Ce}$	1673 K 5 min. Ice-Quenched	<ul style="list-style-type: none"> <li>• The plateau slope was flattened because of homogenization of phase composition, refined microstructure and low oxygen concentration.</li> </ul>	53
11	$\text{Ti}_{0.32}\text{Cr}_{0.43}\text{V}_{0.25}$	Ball milling + 1473 K, 2 hrs, 1473 K, 8 hrs, 1073 K, 2 hrs. 1273 K, 2 hrs.	<ul style="list-style-type: none"> <li>• Adverse effect from ball milling, surface contamination low down absorption rate.</li> <li>• WC contamination caused compositional and structural changes at 1473 K.</li> <li>• Increase in total and effective hydrogen capacities of heat treated samples.</li> <li>• Improvement in hysteresis and phase transformation.</li> </ul>	41
12	$\text{Ti}_{10}\text{V}_{77}\text{Cr}_6\text{Fe}_6\text{Zr}$	1373 K, 8 hrs. 1523 K, 5 min. water cooling	<ul style="list-style-type: none"> <li>• Optimum temperature 1523 K</li> <li>• Flattened plateau, BCC phase abundance increase, reduced hydrogen capacity.</li> </ul>	34
13	Ti-22Al-27Nb	compression/cold rolling + quenched from 1473 K	<ul style="list-style-type: none"> <li>• Mild deformation leads to improvement in hydrogenation and showed easy reversible transformations.</li> <li>• Heavy deformations not beneficial.</li> <li>• Heat treatment made hard transformations from metal to mono-hydride and then di-hydride and reversibility.</li> </ul>	54

## 2.4 Phase Diagrams

From literature review, the choice was made to study effect of Zr-Ni additives, heat treatment and mechanical deformations on the hydrogen sorption characteristics of 52Ti-12V-36Cr BCC alloy. Thus, the Ti-V-Cr ternary diagram is explored. The key points of ternary diagram are listed in following sections.

### *Isothermal sections through Ti-V-Cr system at 1273 K*

Figure 2.2 shows the isothermal section of Ti-V-Cr system at 1273 K [58]. Various Laves phases like  $\alpha\text{-TiCr}_2$ ,  $\beta\text{-TiCr}_2$  and  $\gamma\text{-TiCr}_2$  are reported with stoichiometry  $\text{AB}_2$ . An annealing at elevated temperature may turn  $\beta\text{-TiCr}_2$  into stable  $\alpha\text{-TiCr}_2$  or intermediate metastable phase  $\gamma\text{-TiCr}_2$  while cooling. The  $\alpha\text{-TiCr}_2$  i.e. Laves phase C15 has cubic structure.  $\beta\text{-TiCr}_2$  i.e. Laves phase C14 has ternary hexagonal structure. The

crystallographic parameters for C14 and C15 have been registered by various researchers [59-60]. However, crystallographic parameters for  $\gamma$ -TiCr<sub>2</sub> were not reported. According to Murray, the ternary hexagonal form of TiCr<sub>2</sub> ( $\beta$ -TiCr<sub>2</sub>) is observed at higher temperature than cubical form of TiCr<sub>2</sub> ( $\alpha$ -TiCr<sub>2</sub>) and have higher concentration of chromium [59]. The allotropic form  $\gamma$ -TiCr<sub>2</sub> occurs only above  $\sim 1543$  K. The various solids phases occurred in Ti-V-Cr systems and their crystallographic data is reported by Enomoto et al. [58] as listed in *Table 2.5*.

The BCC 52Ti-12V-36Cr i.e. the composition being selected for study lies in the region ( $\beta$  +  $\alpha$ -TiCr<sub>2</sub>) on the ternary diagram as shown in **Figure 2.2**. That indicates that the multiphase system could be originated with Laves phase  $\alpha$ -TiCr<sub>2</sub> in BCC phase. The position of Laves phase based BCC alloy may lead to 60wt% BCC while 40% of  $\alpha$ -TiCr<sub>2</sub>. The details about the phases referred from *Table 2.5*.

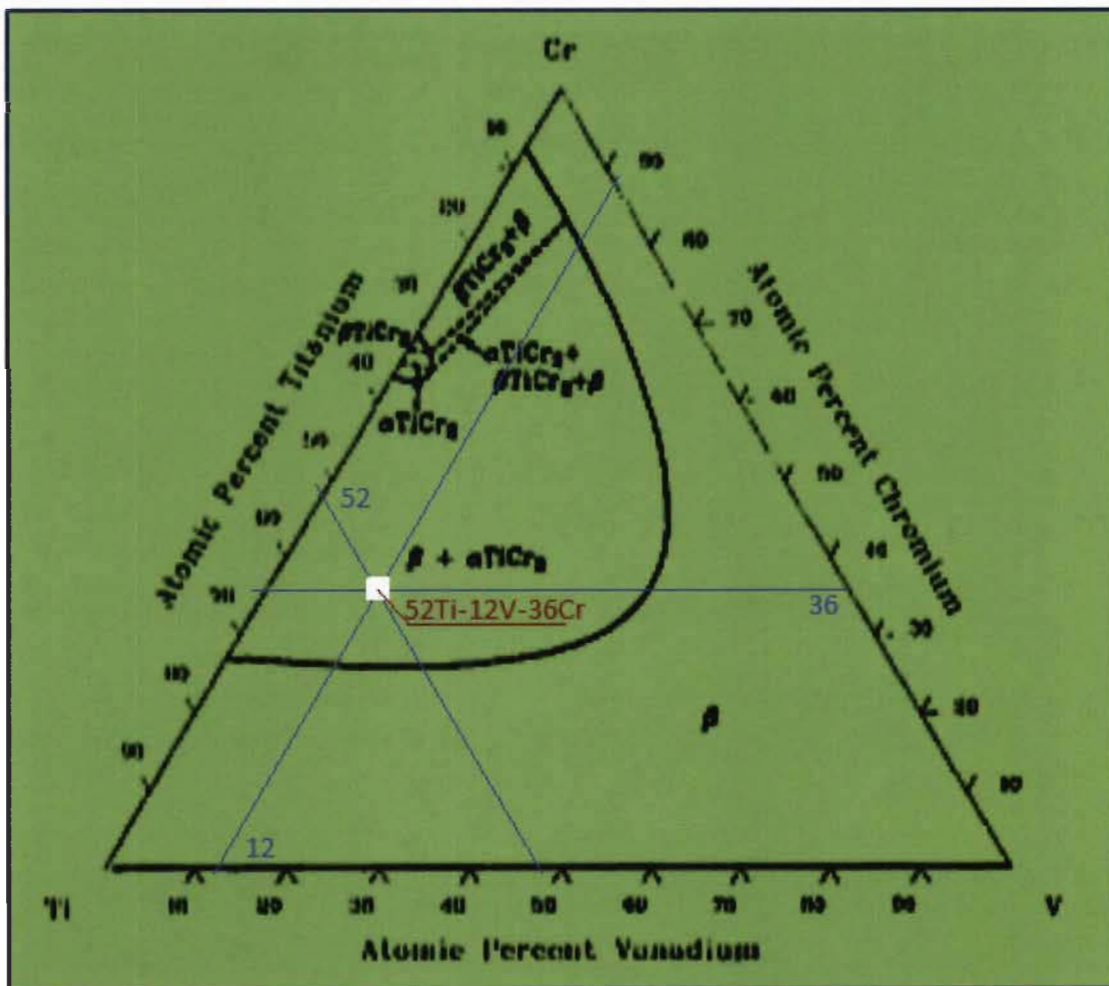


**Figure 2.2** Isothermal sections through Ti-V-Cr system at 1273 K [58]

**Table 2.5** Crystallographic data of Ti-V-Cr system [58]

Phase	Composition range (at%)	Space Group	Pearson Symbol	Strukturbericht designation	Lattice Parameters (nm)		Cell Volume (Å <sup>3</sup> )
					<b>a</b>	<b>c</b>	
$\alpha$ -Ti	0-0.2 Cr 0-3 V	$P6_3/mmc$	$hP_2$	A3	0.2951	0.4684	35.66
$\beta$ -Ti	0 – 100Cr 0 – 100V	$Im-3m$	$cI_2$	A2	0.3307		36.17
$\alpha$ -TiCr <sub>2</sub>	63 – 65Cr 0 – 7.5V	$Fd-3m$	$cF24$	C15	0.6957		333.10
$\beta$ -TiCr <sub>2</sub>	64 – 66Cr 0 – 4V	$P6_3/mmc$	$hP_{12}$	C14	0.4921	0.7945	168.17
$\gamma$ -TiCr <sub>2</sub>	64 – 66Cr	$P6_3/mmc$	$hP_{24}$	C36	-	-	327.5

The cell volumes of each phase reported by Enomoto [58] are evaluated by Mohammed [61] using AtomWorks. Various researchers also have reported the cell volumes of each phase. The experimentally obtained cell volumes are summarized. He has been found the agreement among themselves.

**Chapter III**

**MATERIAL SYNTHESIS &  
CHARACTERIZATION**

### 3.1 Overview

This chapter describes the choice of raw materials and procedures for alloy synthesis and characterization. It describes some background based on which the alloy compositions were evaluated. Secondly, it provides information about raw materials used. Sequentially, after that, it gives information about some standard equipment used for synthesizing and characterization of alloys. The research is concluded on the basis of results obtained after implementation of these material characterization techniques.

### 3.2 Weight% and atomic%

Normally, alloy compositions are specified by atomic percent or weight percent of each element. The conversions from atomic percent to weight percent and vice versa are evaluated using Eq. 3.1 and Eq. 3.2 respectively [62].

$$wt\%_j = \frac{at\%_j \times W_j}{\sum at\%_i \times W_i} \times 100 \dots \dots Eq. 3.1$$

$$at\%_j = \frac{wt\%_j / W_j}{\sum wt\%_i / W_i} \times 100 \dots \dots Eq. 3.2$$

Where,

$at\%_i$  – Atomic percent of element i.

$at\%_j$  – Atomic percent of element j.

$wt\%_i$  – Weight percent of element i.

$wt\%_j$  – Weight percent of element j.

$W_i$  – Atomic weight of element i.

$W_j$  – Atomic weight of element j.

$i, j$  – Elements in Alloy



The respective atomic % and weight % for each alloy is presented in *Table 3.1*. Also, the weight of each element required to prepare a sample of 3 grams are reported in *Table 3.1*.






**Table 3.1 Atomic percent, weight percent and weights of each element**

<b>52Ti-12V-36Cr</b>					
	Ti	V	Cr	Zr	Ni
<b>wt%</b>	<b>50.1</b>	<b>12.3</b>	<b>37.6</b>	-	-
<b>at%</b>	<b>52.00</b>	<b>11.99</b>	<b>36.00</b>	-	-
<b>Sample 3 gm</b>	<b>1.502 g</b>	<b>0.369 g</b>	<b>1.129 g</b>	-	-
<b>52Ti-12V-36Cr + 4wt%Zr<sub>7</sub>Ni<sub>10</sub></b>					
<b>wt%</b>	<b>48.057</b>	<b>11.802</b>	<b>36.14</b>	<b>2.084</b>	<b>1.916</b>
<b>at%</b>	<b>50.547</b>	<b>11.665</b>	<b>34.994</b>	<b>1.1503</b>	<b>1.643</b>
<b>Sample 3 g</b>	<b>1.442 g</b>	<b>0.354 g</b>	<b>1.0842 g</b>	<b>0.0625 g</b>	<b>0.058 g</b>
<b>52Ti-12V-36Cr + 4wt%Zr</b>					
<b>wt%</b>	<b>48.057</b>	<b>11.803</b>	<b>36.140</b>	<b>4</b>	-
<b>at%</b>	<b>50.845</b>	<b>11.733</b>	<b>35.20</b>	<b>2.221</b>	-
<b>Sample 3 g</b>	<b>1.442 g</b>	<b>0.354 g</b>	<b>1.084 g</b>	<b>0.12 g</b>	-
<b>52Ti-12V-36Cr + 2.22wt%Zr</b>					
<b>wt%</b>	<b>48.95</b>	<b>12.02</b>	<b>36.81</b>	<b>2.22</b>	-
<b>at%</b>	<b>51.364</b>	<b>11.85</b>	<b>35.56</b>	<b>1.22</b>	-
<b>Sample 3 g</b>	<b>1.47 g</b>	<b>0.36 g</b>	<b>1.104 g</b>	<b>0.067 g</b>	-
<b>52Ti-12V-36Cr + 4wt%Ni</b>					
<b>wt%</b>	<b>48.1</b>	<b>11.8</b>	<b>36.2</b>	-	<b>3.87</b>
<b>at%</b>	<b>50.28</b>	<b>11.60</b>	<b>34.813</b>	-	<b>3.29</b>
<b>Sample 3 g</b>	<b>1.444 g</b>	<b>0.355 g</b>	<b>1.086 g</b>	-	<b>0.116 g</b>

### 3.3 Raw materials

The highly pure raw materials were purchased from Alpha Aesar. The specifications of purchased raw materials are reported in **Table 3.2** along with their physical appearance in **Figure 3.1-3.5**.

**Table 3.2- Raw elements.**

Titanium(Ti): Sponge, 3-19 mm (0.12-0.75 in.), 99.95%(Metal basis)  <i>Figure 3.1- Titanium</i>	Vanadium(V): Granules, 1-3 mm (0.04-0.12 in.), 99.7%(Metal basis)  <i>Figure 3.2 Vanadium</i>	Chromium: Pieces, irregular, 99%(Metal basis)  <i>Figure 3.3 Chromium</i>
Zirconium(Zr): Sponge, 0.8-25.4 mm (0.03-1.0 in.), 99.5%(Metal basis)  <i>Figure 3.4 Zirconium</i>	Nickel(Ni): Wire, Ø 2.0 mm (0.08 in.), 99.95%(Metal basis)  <i>Figure 3.5 Nickel</i>	

### 3.4 Arc melting

As per required composition, the raw materials were measured for their weights listed in **Table 3.1** using electronic weight balance. This mixture of raw materials was arc melted using a Centorr Associates Inc, USA arc melter.

Arc-melting is a fast and clean way of producing alloys of electrically conductive materials. An electric arc is produced between a pointed electrode and conductive raw materials which heats the raw materials above their melting point, fusing them into pellet. In order to reach a homogeneous alloy, each pellet was turned over 3-4 times and re-melted. Arc melting was performed under an argon atmosphere to avoid oxidation. The pellets were cooled inside the furnace itself with waiting time of 5 minutes. The arc melting apparatus used in this investigation is shown in **Figure 3.6**. It can process about 10-15 grams of material in one melting charge.



**Figure 3.6- Arc melter (Centorr Associates Inc, USA).**

The selected compositions have 5 elements, titanium, vanadium, chromium, zirconium and nickel. The melting and boiling points of each are reported in **Table 3.3**. It could be seen that the lowest boiling point is still 773 K higher than the highest melting point. Thus, proper stoichiometry could be expected from casting as there is a slight possibility of vaporization of elements

**Table 3.3 Melting points of Ti, V, Cr, Zr and Ni [63-67]**

Element	Ti	V	Cr	Zr	Ni
Melting Point (K)	1943	2183	2180	2127	1728
Boiling point (K)	3560	3580	2844	4582	2686

### 3.5 Ball milling

High impact energy ball miller Spex Certiprep 8000M shown in *Figure 3.7* was used for mechanical alloying and to pulverize alloy powders.



*Figure 3.7- Ball miller Spex 8000M.*

The Spex Certiprep 8000M can shake the vial to and fro approximately 1080 cycles per minute. A Stainless-Steel vial model 8007M from Spex Certiprep was used [68]. This vial has a body and cap with liner made of hardened steel 440C stainless steel. It has dimensions as 6.35 cm diameter x 7.62 cm height with hardness of Rockwell C55-60, internal volume -55 cc.

The combination of balls of  $\frac{1}{2}$  in. (12.7 mm) and  $\frac{1}{4}$  in. (6.35 mm) was used which ensures the breakage of coarser as well finer particles due to two different sizes of balls [69]. The stainless-steel balls were chosen as tungsten carbide balls are the source of more wear and contamination of the sample powder [41]. The ball to powder weight ratio was maintained between 10 and 15 [41,42-43,45-47].

The total weight of balls measured  $B = 41.78$  gm.

The sample pellets  $P = 4$  gm or 3 gm.

$$B/P = 10 \text{ or } 14$$

### 3.6 Heat treatment

Heat treatment was carried out using a tube furnace made by Barnstead Thermolyne. Pellets were annealed at temperature 1273 K for 1 week under constant argon flow. The pellet was cooled inside furnace itself until it reaches the room temperature to avoid oxidation of pellet surface.

A wide range of heat treatment temperature and holding time for Ti-V-Cr has been reported by various researchers. The temperatures and holding time reported by researchers lies between 1073 -1673 K and 5 min.- 2 weeks respectively [48] Young et al. also reported the optimized heat treatment temperature 1273 K for Ti-V-Cr system on the basis of maximum abundance of BCC phase [48].

The experimental set up for heat treatment is shown in **Figure 3.8**. 21100 type tube furnace is a mini and inexpensive furnace, ideally suits for industrial or laboratories. It is intended for applications requiring temperatures up to 1373 K for manual control based system and up to 1473 K for electronic single set point control based system. The furnace chamber is heated using electric heating elements embedded in refractory material.



**Figure 3.8- Heat treatment set-up with Tube furnace (Barnstead thermolyne).**

With proper precautions, the casted pellets to be compared for hydrogenation were placed in Alumina crucible. All samples were processed simultaneously in order to ensure identical conditions. A black layer was formed due to residual oxygen in argon gas. This layer was removed by polishing papers and washed away using acetone.



### 3.7 X-ray diffraction(XRD)

X-ray diffraction (XRD) is a well-known technique used to determine crystal structure, lattice parameter, crystallite size and phase identification of the material. It is based on the Bragg's Law which states that constructive interference occurs when *Equation 3.4* is satisfied.

$$n\lambda = 2d_{hkl}\sin\theta_{hkl} \dots\dots Eq. 3.4$$

Where,

$\lambda$  – wavelength,  $\theta_{hkl}$  – Bragg angle and  $d_{hkl}$  – interatomic spacing between hkl planes.

The interatomic spacing between various planes is related with Miller indices and lattice parameters. For cubic system, it is given by *Equation 3.5* as,

$$d_{hkl} = \frac{a}{\sqrt{h^2 + l^2 + k^2}} \dots\dots Eq. 3.5$$

Where,

$a$  – Lattice constant/parameter of crystal,  $h, l, k$  – Miller indices of of Bragg's plane.

The XRD patterns were acquired using the D8 Focus BRUKER X-ray powder diffractometer shown in *Figure 3.9*. The data was collected for angles between 30°-110° with a step size of 0.1°.

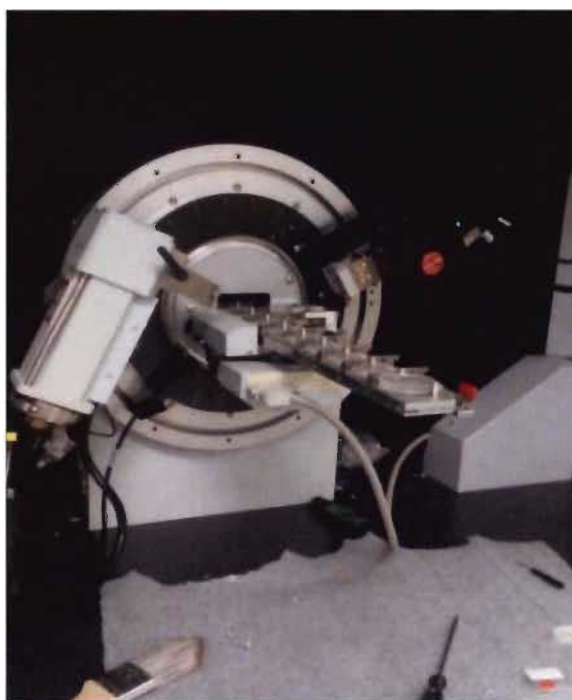


*Figure 3.9 – D8 Focus BRUKER X-ray Powder Diffractometer.*

The XRD patterns were analyzed using Rietveld refinement. Rietveld refinement is a method used to refine selected parameters to minimize the error function between experimental data pattern and calculated pattern assessed based upon hypothesized crystal structure and instrumental parameters [70-71]. The hypothesized crystal structures are defined using space group, lattice parameter, atomic positions, atomic site occupancies and atomic thermal parameters. The additional requirement for refinement is appropriate background function and peak profile. After providing approximate details, the selected parameters could be refined one by one. The method of least square method is used to fit the profile which minimise error function. Rietveld refinement can be used to confirm or reject hypothetical crystal structure and refine unit cell parameters, atomic positions, atomic site occupancies and thermal parameters. It can also provide the information of crystallite size, microstrain and weight percentage of each phase in case of multi-phase crystalline materials.

The crystal structure related information can be obtained using websites (Crystallography Open Database <http://www.crystallography.net/>) [72], databases (PDF4 from the ICDD, Linus Pauling File from ASM International, Cambridge Structure Database) and Literature. Rietveld refinement was performed using Bruker TOPAS [70-71].

### 3.8 Scanning Electron Microscopy (SEM)

SEM is a technique used to produce highly resolved micro images of samples by scanning the surface with focused beam of electrons. The schematic for scanning electron microscope is shown in **Figure 3.10**. The high beam of electrons produced using electron gun are focused and moved on sample surface using electro-magnetic lenses. When electron beam interacts with the sample surface, the various signals with information of surface's topology and chemical composition are obtained. The SEM can achieve the resolution better than 1 nm. It can be used in different modes to collect various kinds of images.

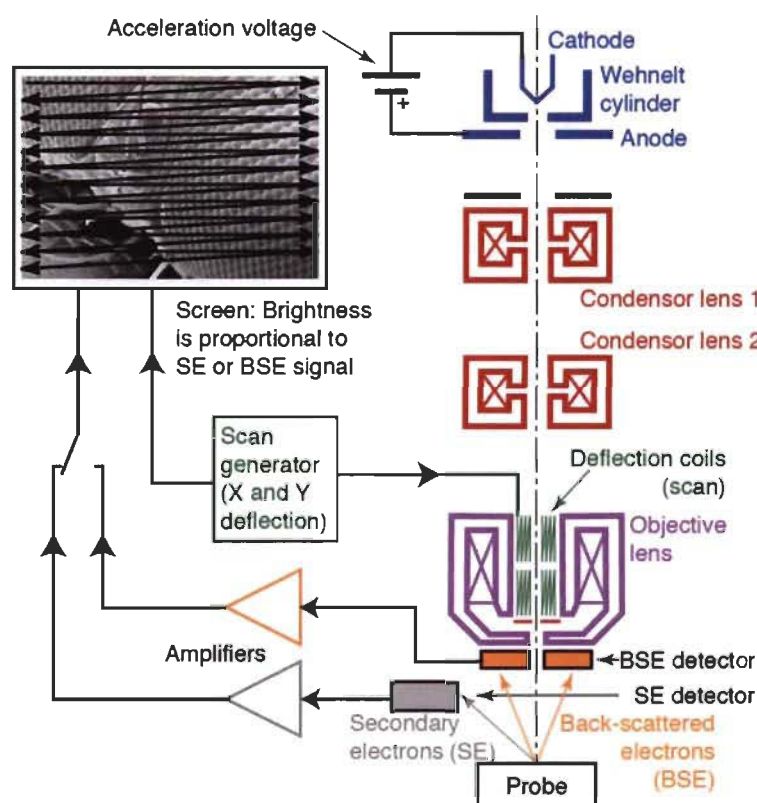


**Figure 3.10** Schematic of Scanning Electron microscope [73].

Normal modes of SEM are secondary electron (SE) and back scattered mode. In secondary electron mode, low energy secondary electrons detected using special detector for it. These secondary electrons detection depends upon topography of surface. Thus, this mode is used to collect topographical information at different magnifications. Back scattering (BSE) mode capture images from electrons of the primary beam that are scattered at high angle. The intensity of back scattered electrons is proportional to the atomic number of the element. Thus, a region with heavy elements creates more intense back scattered electron signal and is seen as a brighter region. It creates images showing chemical contrast and



their abundance. This mode could provide information about phase distribution but do not identify chemical elements present.

All the SEM images were captured using JEOL JSM-5500 model shown in **Figure 3.11** with specification of resolution of 1.0 nm (15 kV), 1.5 nm (1 kV), accelerating voltage 0.1 to 30 kV and magnification 25 to 1,000,000. The back scattered images are further analysed for phase abundance using Image J software [74-75].

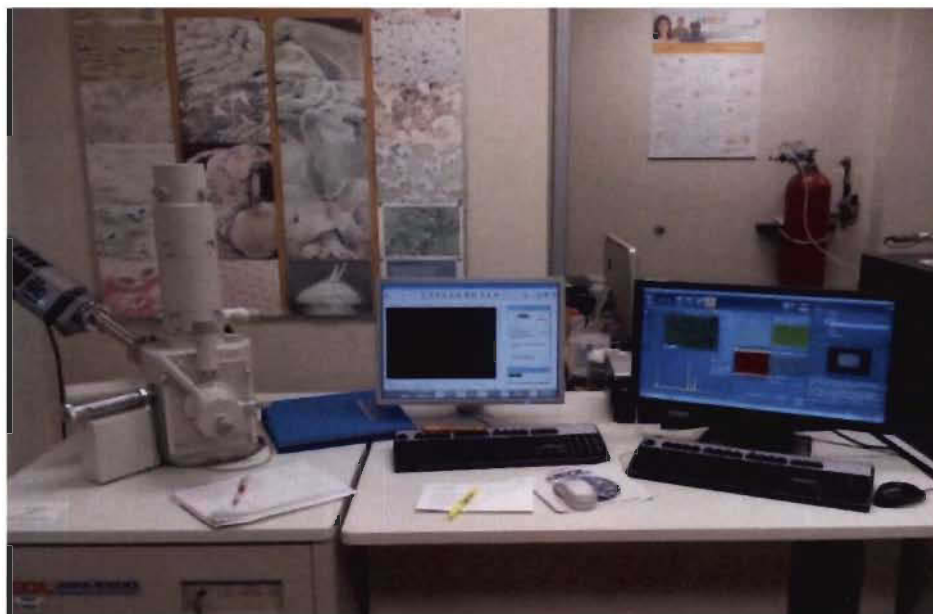


**Figure 3.11-** JSM-5500 with master and slave installed with Oxford Instruments software.

### **3.9 Energy Dispersive X-ray Spectroscopy(EDS)**

Energy dispersive X-ray spectroscopy is well known technique used for micro chemical analysis. It is popularly known as EDX or EDS. It is based on the principle of characteristic X-rays. Each element has unique atomic structure producing unique X-ray emission spectrum. EDS is installed on the microscope and measure the chemical compositions according to X-ray spectrum produced. It can determine bulk nominal compositions, area, line and point mapping.

The microscope JEOL JSM 5500 was equipped with EDS attachment from Oxford Instruments<sup>®</sup> default software for micro composition analysis and elemental mapping.

### 3.10 Hydrogenation Characterization

The first hydrogenation kinetics of the samples was performed at room temperature under hydrogen pressure of 2 MPa. The hydrogenation kinetics of alloy powders were studied using computer connected homemade Sievert's type apparatus shown in **Figure 3.12**. The sample holder is shown in **Figure 3.13**. To avoid oxidation, the casted pellets were crushed inside the glove-box using mortar-pestle and filled in sample holder.

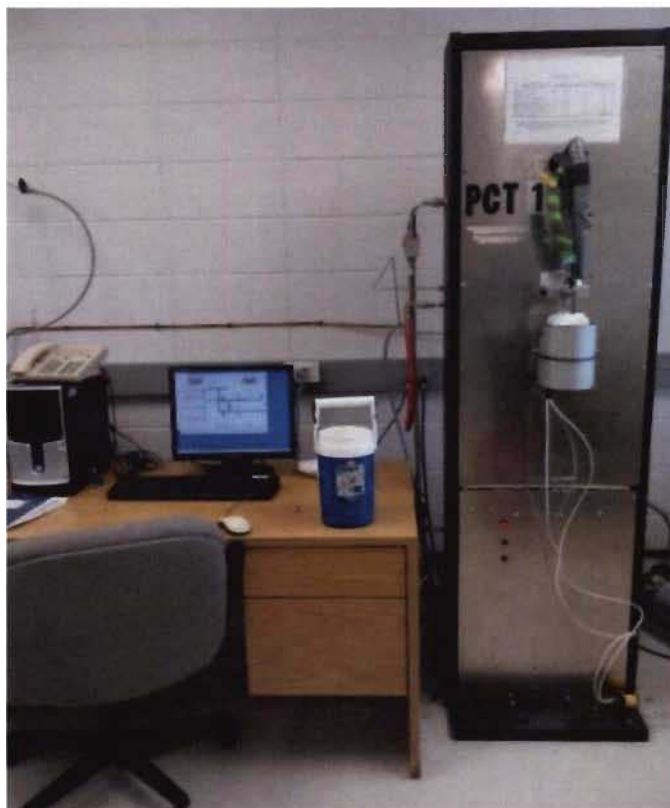


*Figure 3.12- Hydrogen Titration System.*

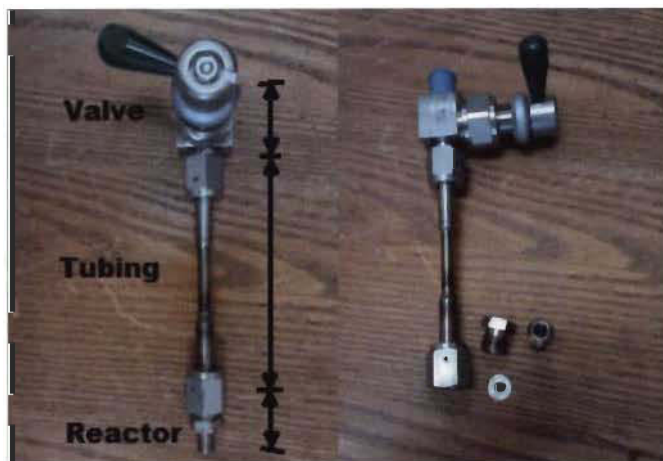


*Figure 3.13- PCT Sample Holder.*

For isothermal hydrogen absorption/desorption, the temperature of sample was kept constant by mounting reactor inside water bath temperature controller for temperature less than 353 K and heating coil furnace for temperature 353 K and above.

The apparatus is controlled through a Labview software. The homepage, as shown in **Figure 3.14**, provides many options to perform various hydrogen absorption/desorption characterizations such as hydrogen kinetics, desorption kinetics, cycling, PCT. The apparatus is schematically represented in **Figure 3.15**. It shows main parts of the system like hydrogen reservoirs, various valves, pressure and temperature detectors. There are two tubing lines for sample and reference sample connecting to hydrogen supply using valves-V3, V4, vacuum pump using valve-V5 and evacuation using valve-V2. The differential gauge is used to measure difference between sample and reference lines which is related to amount of hydrogen absorbed in sample.

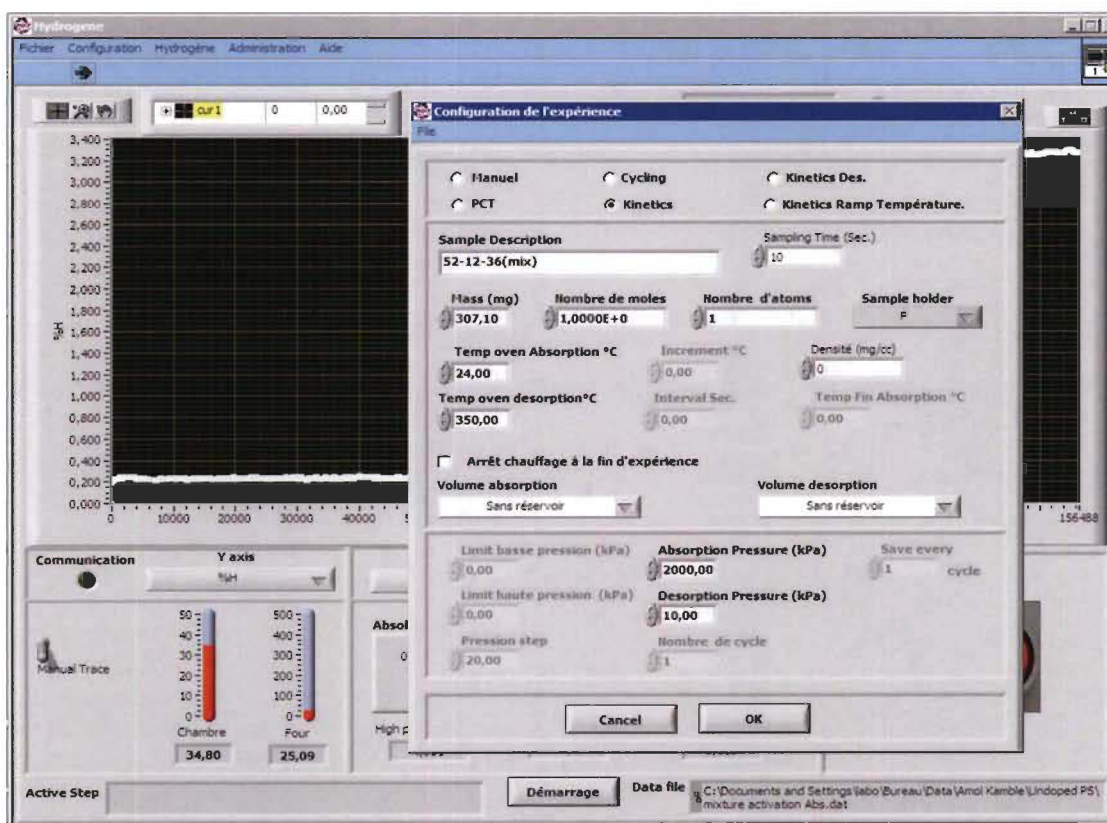


Figure 3.14- GUI Hydrogene Home page.

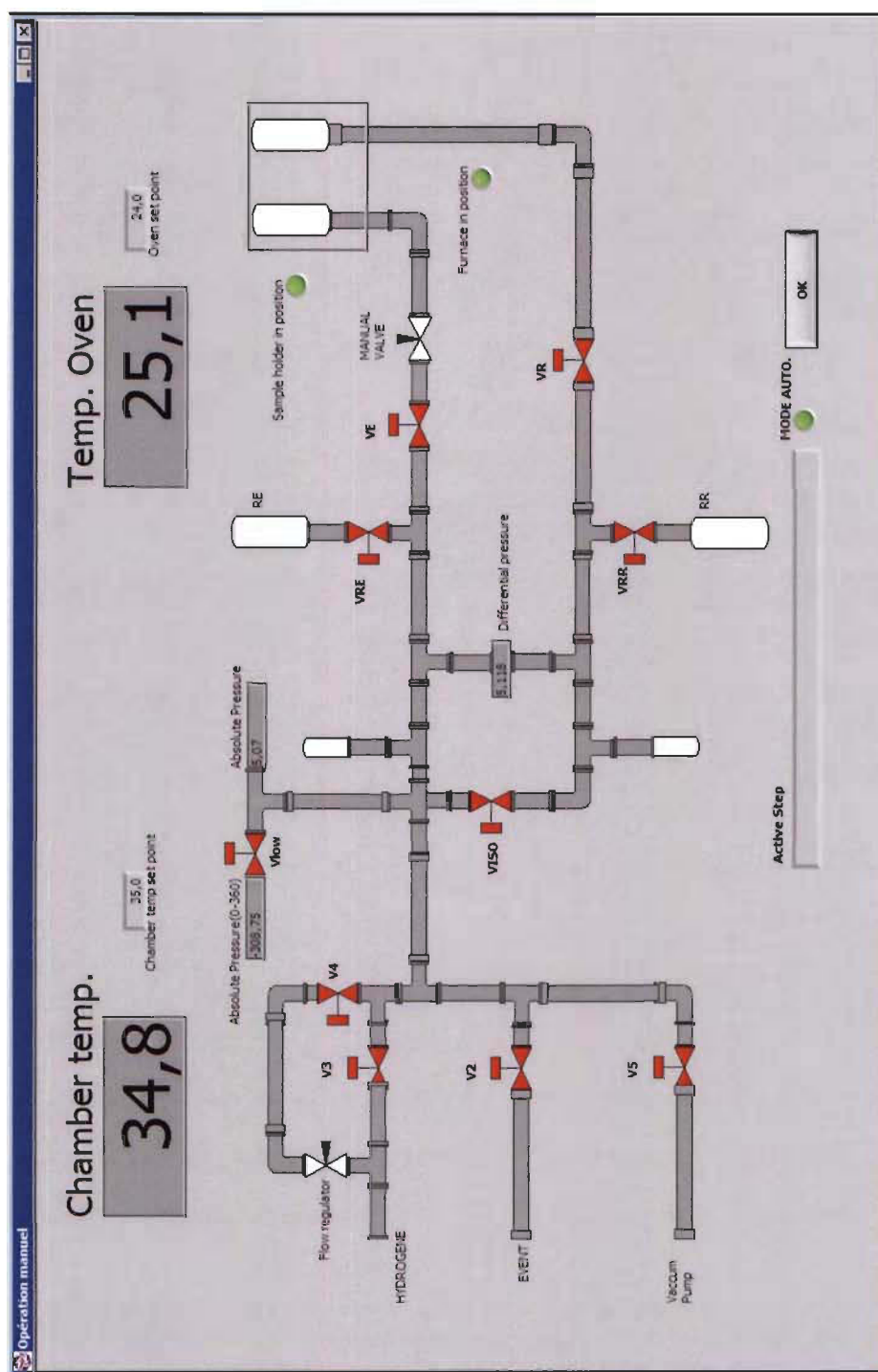


Figure 3.15- Operation manual Interface.

### *Dynamic vacuum*

Before initiating any hydrogen sorption measurements, the sample is always placed under dynamic vacuum pressure at less than 10 kPa for 1 hr. This will remove adsorbed gaseous associated with the samples' surface and carry out cleaning process.

Procedure-

1. Open the software Hydrogene on computer attached with system and select Manual mode.
2. Open operational manual. Confirm all valves are closed(red).
3. Click V2, VISO, VR and VE to open(green) them to evacuate system pressure below 120 kPa reading in absolute pressure gauge.
4. Once the system absolute pressure gauge below 120 kPa, click V2 to turn it close(red).
5. Click V5 to turn it open(green) to develop vacuum in tubing and wait till the vacuum pressure shown by absolute high-pressure gauge below 10-5 kPa so that any foreign gases/air suck outside. It will clean our tubing.
6. Click V5 to close(red) it as the vacuum pressure below 5 kPa and click V4 to open(green) it to pressurize the system with hydrogen which push out the foreign gases/air outside and clean it. Wait till the absolute high-pressure gauge reading near about 100 kPa.
7. Repeat the steps '5' and '6' two more times.
8. Click V5 to open(green) it to develop vacuum inside system.
9. Once the absolute high-pressure gauge reading goes below 5 kPa open valve manual valve (MV) manually so that sample powder will be under dynamic vacuum.
10. Note down the time as the valve MV opened and wait for 1 hr of dynamic vacuum.
11. Close the valve MV after one hour and click V5 to close(red) it. Now sample is ready for experiment.

***Kinetic absorption***

For measuring first hydrogenation we need to conduct kinetic measurement. To select kinetic program from home page GUI, click in sequence as Configuration→Experience →Kinetic (Fill experiment parameters as shown in **Figure 3.16**)→OK.


**Figure 3.16-** Kinetic program parameters.

Procedure (Auto kinetic mode):

1. Select 'Kinetic mode' using GUI of hydrogen software.
2. Set experiment parameters and click OK.
3. To start auto measurements, click **Démarrage** start command on Hydrogene home page. It will ask file name and location to save the measurements. Provide the details and click OK.
4. Message Box to confirm closing of valve MV. Confirm and close valve MV. Click **Oui** Yes.
5. Evacuation to 30 kPa. (for absolute pressure, greater than 110kPa, Closed Valves- MV, V3, V4, VRR, VRE, V5 and open valves-V2, VISO, VR, VE, V2) (for absolute pressure between 30kPa-110kPa, Closed Valves- MV, V3, V4, VRR, VRE, V2 and open valves-V2, VISO, VR, VE, V5)



6. Pump to 150 kPa. (Closed Valves- MV, V3, V2, VRR, VRE, V5 and open valves-V2, VISO, VR, VE, V4).
7. Absorption preparation time-60 sec.
8. Message box to open valve MV. Open valve MV and click OK.
9. Absorption- pressurize hydrogen till P2. (P2 is the auto calculated pressure to pressurize principle system volume V2 using ideal gas equation at constant temperature so that set absorption pressure P1 would achieve when valve VE is opened to start absorption by releasing hydrogen into sample holder volume.) (Closed Valves- V3, V2, VR, VE, V5 and open valves-MV, VISO, V4, VRR, VRE).
10. Absorption temperature attainment duration-60 sec. (If sample holder temperature is within limit of tolerance of absorption set temperature, step '11' will be taken immediately. Otherwise another 60 sec time will be added each time till the sample holder temperature reach to set value within limit of tolerance.) (Closed Valves- V3, V2, VR, VE, V5, V4 and open valves-MV, VISO, VRR, VRE).
11. Absorption- As set conditions attained the sample interacted with sample. (Closed Valves- V3, V2, V5, V4 and open valves-MV, VR, VE, VISO, VRR, VRE).
12. Wait till the achievement of activation followed by saturation of hydrogen capacity.

Once hydrogen capacity is saturated, click  stop command to stop the measurements.

## **Chapter IV**

### **EFFECT OF ADDITION OF Zr, Ni AND Zr-Ni IN 52Ti-12V-36Cr ALLOY**



## 4.1 Overview

This chapter describes the choice of elements and alloys added to 52Ti-12V-36Cr alloy. The microstructure, crystal structure and hydrogen storage properties of all these compounds are reported and discussed.

## 4.2 Choice of additives

Recently, Miraglia et al. showed that a dramatic improvement of activation kinetics could be achieved by first casting a BCC alloy of composition 33Ti-30V-37Cr, adding 4wt% of  $Zr_7Ni_{10}$  and recasting the mixture [17]. Later, Bibienne et al studied the BCC alloy 52Ti-12V-36Cr melted together with 4 wt%  $Zr_7Ni_{10}$  [18] and reported short incubation time prior to activation. These results point out that minor secondary phases are favourable for hydrogen absorption properties of metal hydrides [17-20].

The BCC 52Ti-12V-36Cr alloy was tested by Bibienne et al. was added with 4 wt%  $Zr_7Ni_{10}$  only. In order to find the exact role of Zr and Ni, 4wt%Zr and 4wt%Ni were selected as additives and compared with 4wt%  $Zr_7Ni_{10}$ . Additionally, 2.2wt%Zr was selected as an additive because this is the fractional amount of Zr in  $Zr_7Ni_{10}$ . Thus, BCC 52Ti-12V-36Cr alloy was studied without additive and with four different additives: 4wt%  $Zr_7Ni_{10}$ , 4wt% Zr, 2.2wt% Zr, 4wt% Ni.

## 4.3 Experimental procedures

### *Material Synthesis*

The raw materials Ti (Sponge, 3-19 mm, 99.95%), V (Granules, 1-3 mm, 99.7%), Cr (Pieces, irregular, 99%), Ni (Wire, diameter 2mm, 99.95%) and Zr (Sponge, 0.8-25.4 mm, 99.5%) were purchased from Alfa Aesar. Chunks of all raw elements were mixed according to the nominal composition and arc-melted. In order to get homogeneous samples, the cast pellets were turned-over and remelted two more times. The as-cast pellets were processed as shown in **Figure 4.1**. To avoid oxidation, the sample pellets were crushed into powder using a mortar and pestle in an argon-filled glove-box.

### *Material characterization*

X-ray diffraction (XRD) patterns of each sample powder before and after first hydrogenation was recorded on D8 Focus Bruker X-ray powder diffractometer with Cu  $K_\alpha$  radiation and analyzed with Topas software [70-71].

Scanning Electron Microscopy, Energy Dispersive Spectroscopy (EDS) was performed on all alloys in order to determine the microstructure and chemical phase composition. The uncertainty on element abundance determined by EDS has been evaluated to be  $\pm 1$  at%. For each micrograph, the fractions of the surface occupy by each phase were determined by using ImageJ software [74-75].

First hydrogenation of 300-400 mg sample was measured at 298K under 2 MPa hydrogen pressure using a homemade hydrogen titration system.

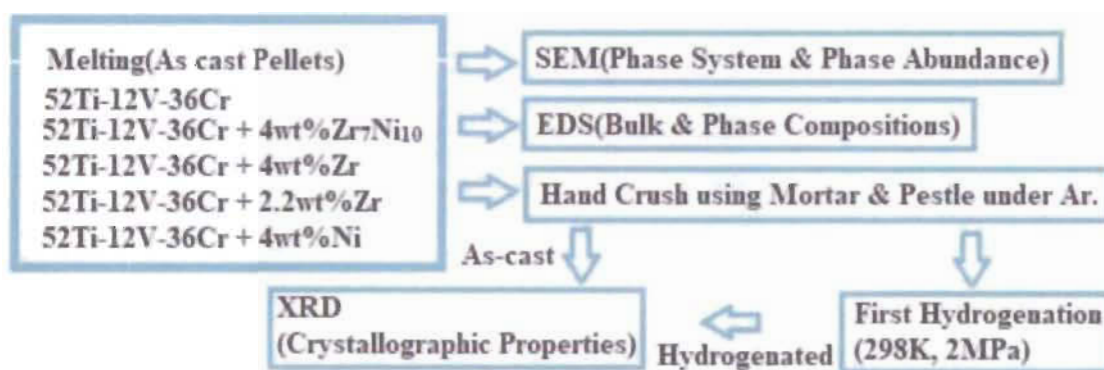


**Figure 4.1-** Flow chart of synthesis & characterization of BCC 52Ti-12V-36Cr alloy with and without additive.

## 4.4 Results and discussion

### 4.4.1 Microstructure of as-cast BCC 52Ti-12V-36Cr with/without additive

**Figure 4.2** shows the microstructure of as cast alloy 52Ti-12V-36Cr without and with additives. The alloy without additive is essentially single phase with only a small amount of black intergranular precipitation. With additives, a multi-phase system is produced as shown in **Figure 4.2(b-e)**. All compositions have a similar microstructure which is made of a dark matrix phase, a bright secondary phase and less abundant black precipitates. Analogous microstructure has been reported in the literature [17-19]. The precipitation of black phase is more important in case where Ni is present as additive. In fact, the biggest proportion of black phase is seen for the alloy with 4wt.% Ni addition.

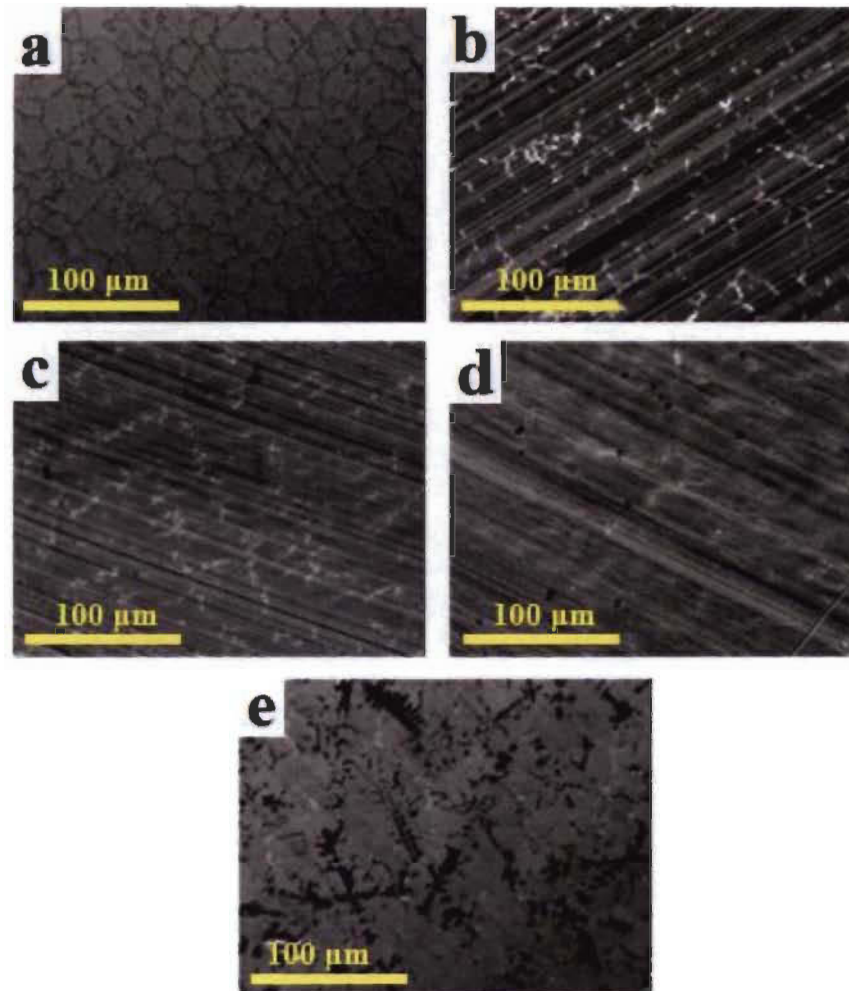


**Figure 4.2-** Backscattering electrons (BSE) SEM micrographs of the as-cast BCC 52Ti-12V-36Cr (a) without additives and with additives (b) 4wt%  $Zr_7Ni_{10}$ , (c) 4wt%Zr, (d) 2.2wt%Zr and (e) 4wt%Ni.

The fractions of areas occupied by each phase were determined using ImageJ [74-75]. The analyzed micrographs of each composition for dark, bright and black phases are shown in **Figure 4.3**. The black region indicates the fractional occupied by respective phase. The summary of analysis is presented in **Table 4.1**. It shows that alloys with additives had a lower dark phase abundance. As expected, the alloy with only 2.2 wt.% of Zr has a smaller amount of bright phase. Addition of pure nickel increases the amount of black phase while addition of pure zirconium had the opposite effect.

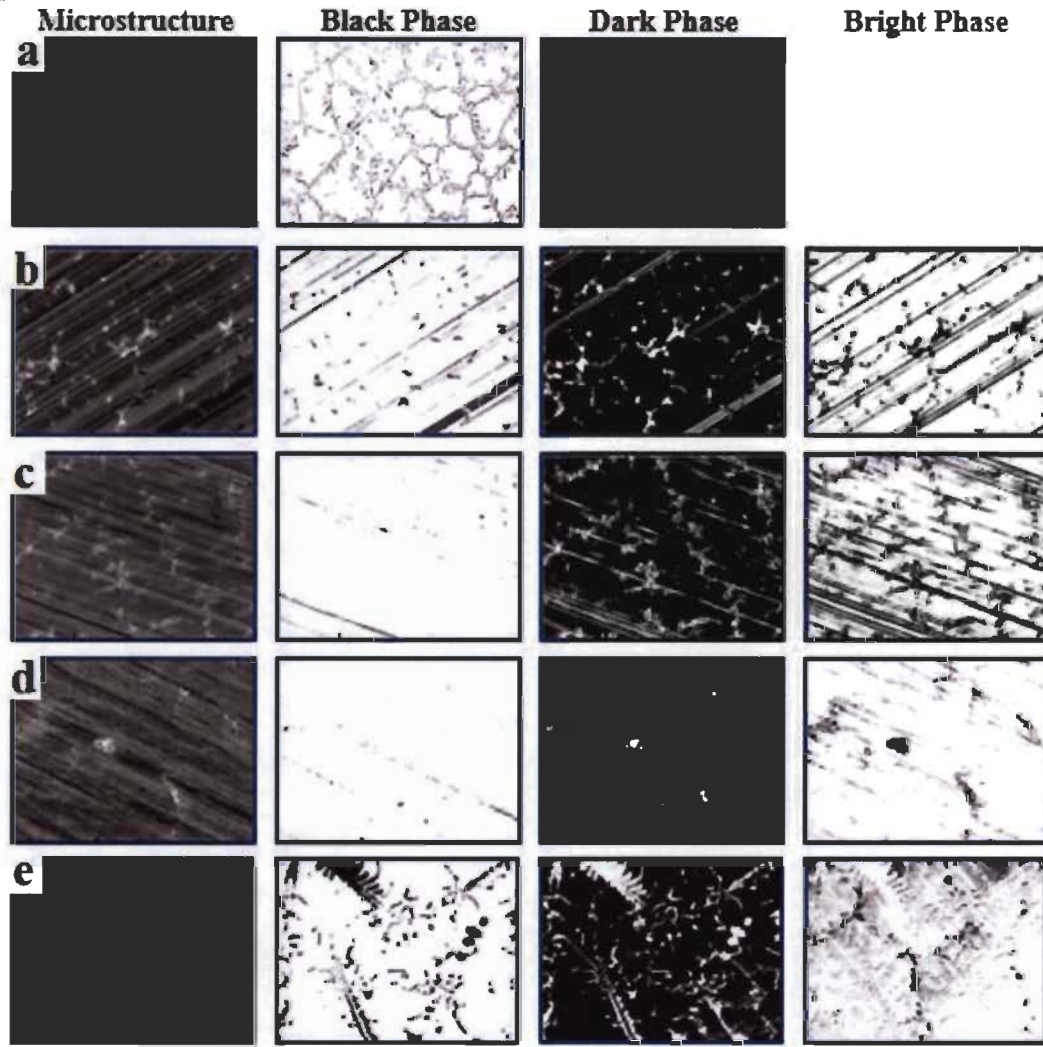


**Figure 4.3-** ImageJ analysis of as-cast BCC 52Ti-12V-36Cr (a) without additives and with (b) 4wt%  $Zr_7Ni_{10}$ , (c) 4wt%Zr, (d) 2.2wt%Zr and (e) 4wt%Ni additives.

**Table 4.1-** Fraction of area (in %) occupied by each phase in as cast 52Ti-12V-36Cr alloys with and without additives. Uncertainty on each measurement is  $\pm 1\%$

Additive	Dark	Bright	Black
Without	97	-	3
4wt% $Zr_7Ni_{10}$	84	14	2
4wt%Zr	90	10	< 1
2.2wt%Zr	94	5	1
4wt%Ni	85	9	6

#### 4.4.2 Results of Energy Dispersive X-ray Spectroscopy (EDS)

Different additives resulted into different abundance of secondary phase in the alloy. Most likely, this will lead to different chemical compositions of the different phases. Before measuring the individual phase's chemical composition, the bulk composition was investigated in order to verify that the alloy had globally the nominal composition. Bulk chemical composition was measured using Energy Dispersive X-ray Spectroscopy (EDS) and the results are presented in **Table 4.2**. For all alloys, the measured bulk compositions agree with the nominal compositions

**Table 4.2-** Element abundances as measured from EDS for bulk compositions of as cast 52Ti-12V-36Cr alloys with and without additives. Uncertainties on measured composition are  $\pm 1$  at%.

Additive		Ti	V	Cr	Zr	Ni
Without	Nominal composition	52	12	36	-	-
	Bulk measured composition	53	12	36	-	-
4wt%Zr <sub>7</sub> Ni <sub>10</sub>	Nominal composition	50.6	11.7	35.0	1.2	1.6
	Bulk measured composition	51	11	34	1	2
4wt%Zr	Nominal composition	50.9	11.7	35.2	2.2	-
	Bulk measured composition	52	11	34	2	-
2.2wt%Zr	Nominal composition	51.4	11.9	35.6	1.2	-
	Bulk measured composition	52	11	35	1	-
4wt%Ni	Nominal composition	50.3	11.6	34.8	-	3.3
	Bulk measured composition	50	14	33	-	3

The composition of each phase was then measured. **Figure 4.4** shows the localisation of each measurement for all alloys. The grooves seen on a few micrographs are due to the roughness of the polishing. Except for the bare alloy, multiple measurements were taken on each individual phase. For all phases, individual measurement agrees amongst themselves. Here, we report the chemical composition of the three spots corresponding to the dark phase, black phase, and bright phase.



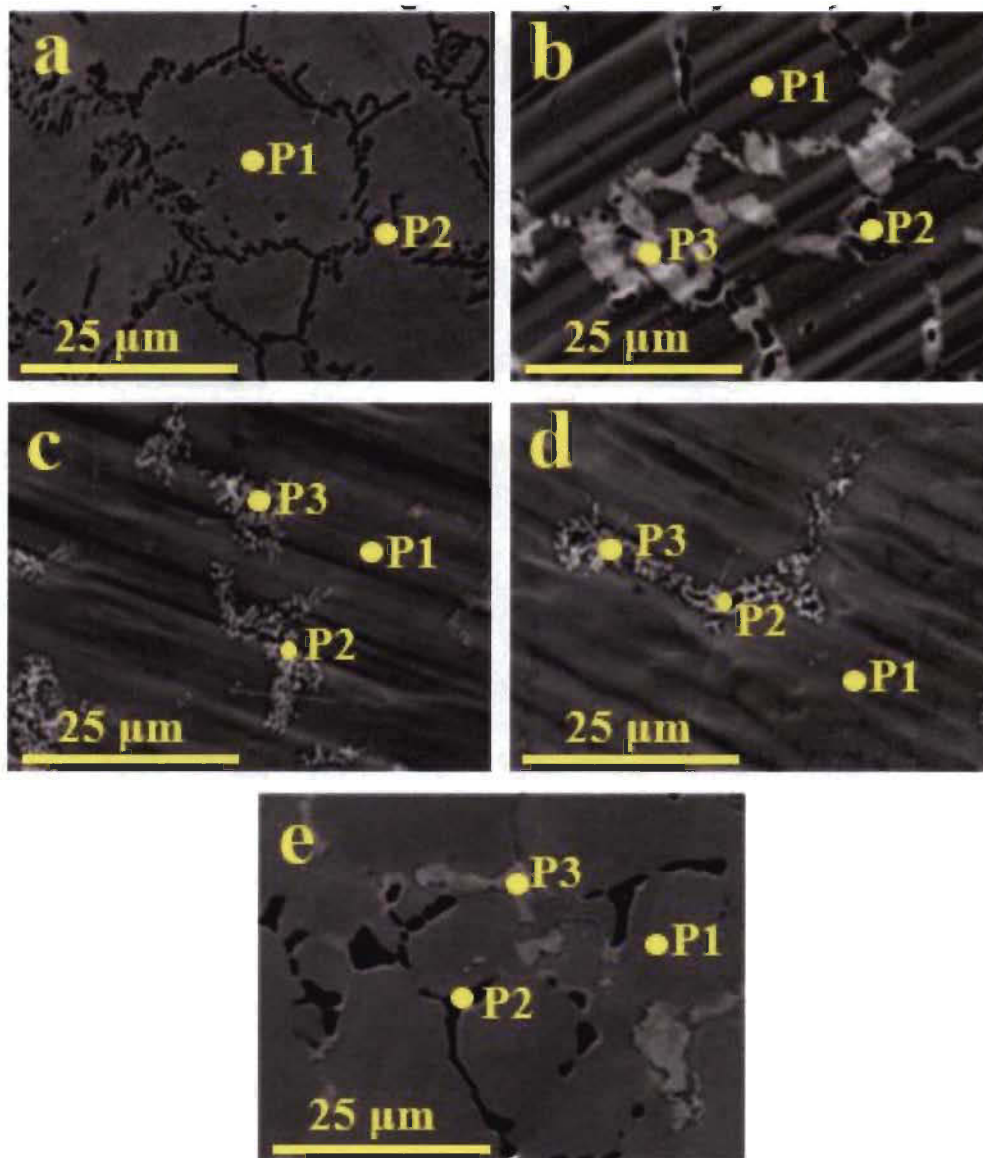


**Figure 4.4-** Point mapping on micrographs of the as-cast BCC 52Ti-12V-36Cr (a) without additives and with (b) 4wt%  $Zr_7Ni_{10}$ , (c) 4wt%Zr, (d) 2.2wt%Zr, and (e) 4wt%Ni additives.

The dark phase compositions of each sample are reported in *Table 4.3*. We see that, for most of the alloys, the dark phase has a composition very close to 52Ti-12V-36Cr. Only the alloys having Ni-containing additive shows a noticeable deviation from this stoichiometry i.e. the Ti content is lower than the nominal one. Dark phase has a low concentration of the elements Zr and/or Ni. Only in the case with 4wt% Ni additive the concentration of nickel in the dark phase is non-negligible. From table 4.3, it is observed that the dark BCC phase could not accommodate Zr and/or Ni atoms from the additive and thus forcing the formation of a secondary phase.

**Table 4.3- Composition of dark phases in as-cast BCC 52Ti-12V-36Cr alloys with and without additives.**

Additive	Ti	V	Cr	Zr	Ni
Without	53	12	35	-	-
4wt%Zr <sub>7</sub> Ni <sub>10</sub>	50	12	36	1	1
4wt%Zr	52	12	34	1	-
2.2wt%Zr	53	10	36	1	-
4wt%Ni	49	12	34	-	4

The atomic compositions of black phase in each sample are reported in **Table 4.4**. It is clear that the black phase has a high concentration of titanium, being essentially pure titanium for Ni-containing additive. For pure zirconium additive, the titanium content in the dark phase much less compared to the alloys with other additives. In these cases, chromium and vanadium content of black phase are also quite important. It is interesting to note that, even if nickel favoured the formation of black phase, nickel isn't present in that phase. It should be pointed out that, contrary to the dark and bright phases, we do not claim that the dark phase has the same crystal structure in all alloys. This is quite evident by comparing the composition of the dark phase for 4 wt.%Ni and for 2.2wt.%Zr. For 4wt.% Ni the black phase is essentially titanium precipitates while for the 2.2wt.% Zr the amount of Ti is much smaller and thus the dark phase has more likely another crystal structure than the HCP structure of titanium.

**Table 4.4- Composition of black phases in as-cast BCC 52Ti-12V-36Cr alloys with and without additives.**

Additive	Ti	V	Cr	Zr	Ni
Without	75	8	18	-	-
4wt%Zr <sub>7</sub> Ni <sub>10</sub>	91	1	2	5	0
4wt%Zr	60	12	26	2	-
2.2wt%Zr	55	9	29	6	-
4wt%Ni	97	2	1	-	0

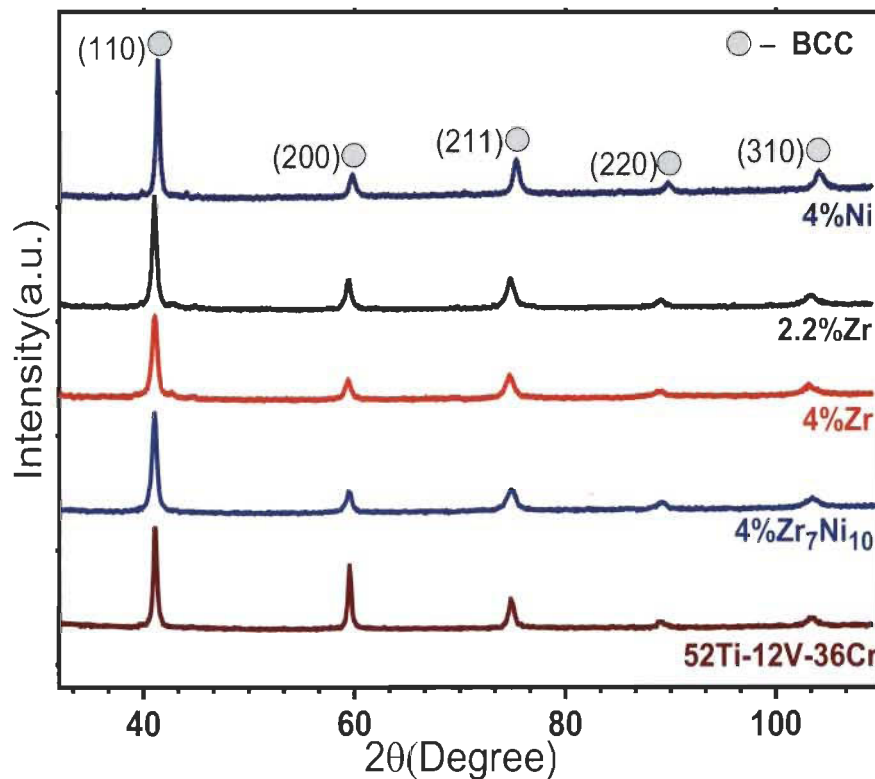
The phase composition for bright phases are reported in **Table 4.5**. There is no bright phase in sample without additive. For the alloys with additives, the bright phase is mainly constituted by titanium and chromium. Concentration of chromium is reduced when the additive contains nickel. In fact, it seems that nickel substitute with chromium in that phase. Even if zirconium and nickel are present in small concentration in this phase, it is still the phase that contains the maximum amount of these two elements as compared to the other phases in all alloys. Considering the relative proportion of each phase, we could conclude that most of the zirconium/nickel is inside the bright phase. Similar situation has been reported in literature [48-49, 54]

**Table 4.5- Composition of bright phases in as-cast BCC 52Ti-12V-36Cr alloys with and without additives.**

Additive	Ti	V	Cr	Zr	Ni
Without	-	-	-	-	-
4wt%Zr <sub>7</sub> Ni <sub>10</sub>	40	7	38	8	7
4wt%Zr	42	9	40	9	-
2.2wt%Zr	43	8	42	7	-
4wt%Ni	44	8	36	-	12

#### 4.4.3 X-ray diffraction (XRD) of as-cast alloys

The X-ray diffraction (XRD) patterns for as-cast BCC 52Ti-12V-36Cr with and without additive are shown in **Figure 4.5**. In the as-cast state, all alloys have the BCC crystal structure (S.G. Im-3m) [18]. Because of the relatively small abundance of secondary phases, the Bragg peaks of these phases are not noticeable in the patterns.

**Figure 4.5- XRD patterns of as-cast BCC 52Ti-12V-36Cr alloys with and without additives.**

Rietveld refinement was performed on all these patterns [70-71]. The refinement results are summarized in **Table 4.6**.



**Table 4.6-** Crystal structure parameters as determined by Rietveld refinement of 52Ti-12V-36Cr with and without additive. The number in parentheses is the error on the last significant digit.

Additive	As-cast-BCC( <i>Im-3m</i> )	
	a(Å)	Crystallite Size(nm)
Without	3.1066(5)	19.8(8)
4wt%Zr <sub>7</sub> Ni <sub>10</sub>	3.1110(7)	11.3(2)
4wt%Zr	3.1116(7)	10.3(2)
2.2wt%Zr	3.1091(6)	13.1(3)
4wt%Ni	3.0933(4)	17.1(3)

From **Table 4.6**, it seems that addition of zirconium had for effect of reducing the crystallite size of the BCC phase even if this element is almost absent in BCC. On the other hand, adding nickel does not drastically change the crystallite size even if the amount of nickel in the BCC phase is relatively high.

#### 4.4.4 First hydrogenation of as-cast BCC 52Ti-12V-36Cr with and without additive

The first hydrogenation curves of BCC 52Ti-12V-36Cr alloys with and without additive are shown in **Figure 4.6**. All curves show similar shape. There is some incubation time followed by a quick absorption. Clearly, the incubation time is strongly dependent on the nature of the additive, but all additives reduced the incubation time by at least one order of magnitude. Therefore, we could conclude that multiphase have a positive effect on incubation time. **Table 4.7** list the incubation time, full capacity, and slope at mid-capacity for all samples.

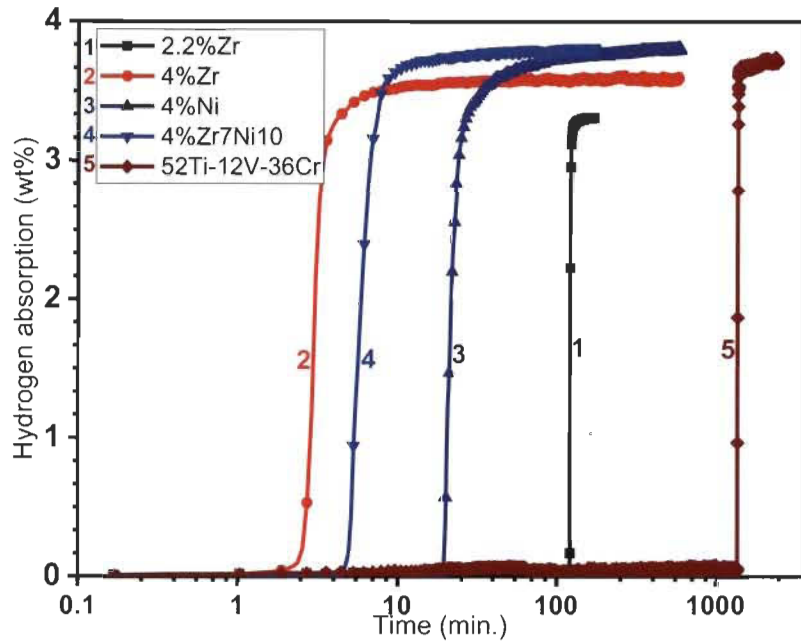


**Figure 4.6-** First hydrogenation of as-cast BCC 52Ti-12V-36Cr alloys with and without additives.

**Table 4.7-** Hydrogenation characteristics of BCC 52Ti-12V-36Cr with and without additive.

Additive	Incubation time (min)	Hydrogen Capacity (H%)	Intrinsic kinetics (H%/min)
Without	1340	$3.7 \pm 0.1$	$0.98 \pm 0.03$
4wt%Zr <sub>7</sub> Ni <sub>10</sub>	4	$3.8 \pm 0.1$	$1.70 \pm 0.05$
4wt%Zr	2	$3.6 \pm 0.1$	$6.7 \pm 0.2$
2.2wt%Zr	120	$3.3 \pm 0.1$	$2.55 \pm 0.08$
4wt%Ni	19	$3.8 \pm 0.1$	$0.91 \pm 0.03$

From **Figure 4.6** and **Table 4.7**, it is clear that the main effect of additives is to reduce incubation time. The alloys with additive showed a reduction of incubation time of at least one order of magnitude and for some additives, up to more than two order of magnitudes. The effect on capacity and intrinsic kinetics was much weaker. The intrinsic kinetics was faster by a factor of 7 for the best case. We see that zirconium is most effective to reduce incubation time but just 2.2 wt% of zirconium is not sufficient for getting a better capacity. Also, incubation time and intrinsic kinetics seems to be correlated. Shorter incubation time means it gives faster intrinsic kinetics. In the case of nickel, its effect on incubation time is not as efficient as zirconium but it makes the capacity much higher. Therefore, the best compromise in terms of high capacity and short incubation time is given by the additive Zr<sub>7</sub>Ni<sub>10</sub>. For this additive, the capacity reached is quite close to the theoretical full capacity of 4.08 wt.%.

#### 4.4.5 X-ray diffraction(XRD) after hydrogenation

All as-cast alloys with and without additive absorbed hydrogen and, as expected their patterns show a FCC (Face Centered Cubic) crystal structure (S.G. Fm-3m) [48] as presented in *Figure 4.7*.

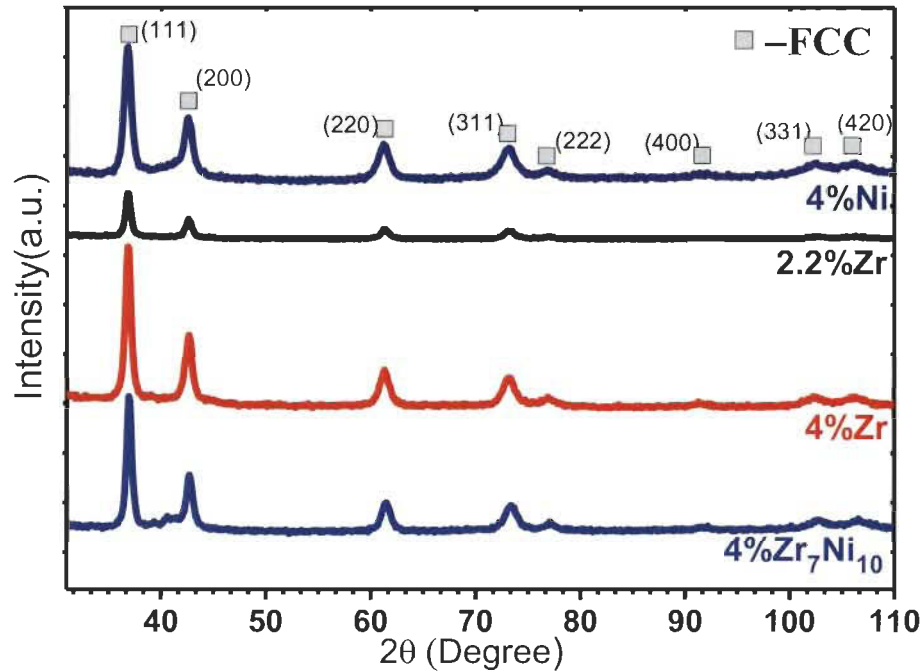


*Figure 4.7-* XRD patterns of hydrogenated BCC 52Ti-12V-36Cr alloy with and without additives.

All patterns were analysed by Rietveld refinement [70-71] and the results are reported in *Table 4.8*.

*Table 4.8-* Rietveld refinement of BCC 52Ti-12V-36Cr with and without additive.

Additive	As-cast-BCC(Im-3m)		Hydrogenated-FCC(Fm-3m)		
	a(Å)	Crystallite Size(nm)	a(Å)	Crystallite Size(nm)	Microstrain (%)
Without	3.1066(5)	19.8(8)			
4wt%Zr <sub>7</sub> Ni <sub>10</sub>	3.1110(7)	11.3(2)	4.334(1)	12.0(6)	1.00(6)
4wt%Zr	3.1116(7)	10.3(2)	4.3444(9)	11.6(4)	1.10(4)
2.2wt%Zr	3.1091(6)	13.1(3)	4.341(2)	9.6(4)	0.5(1)
4wt%Ni	3.0933(4)	17.1(3)	4.330(1)	10.8(4)	1.06(5)

The lattice parameters of all hydrogenated alloys are practically the same, as well as their crystallite size. The hydrogenated alloys also presented a small amount of microstrain due to expansion of the unit cell upon hydrogenation.

## 4.5 Conclusion

The effect of Zr and/or Ni additives to 52Ti-12V-36Cr alloy was investigated. It was found that all as-cast alloys have a main BCC phase but the ones with additives present a microstructure made up of at least one secondary phase.

Without additive, the first hydrogenation of 52Ti-12V-36Cr is prolonged. Adding Zr and/or Ni drastically reduced the incubation time of hydrogenation. Additives have also an impact on the intrinsic kinetics of activation.

The sample with 4wt%Zr additive exhibited the smallest incubation time and fastest intrinsic kinetic. It seems that the presence of zirconium influences the incubation time and kinetics. In the case of nickel addition, it favored an increase of capacity. Thus, due to synergetic effect, the additive 4wt%Zr<sub>7</sub>Ni<sub>10</sub> stands as most effective additive with low incubation time and better hydrogen capacity.

## **Chapter V**

### **EFFECT OF HEAT TREATMENT ON 52Ti-12V- 36Cr WITH ADDITIVES**

## 5.1 Overview

In the previous chapter the effect of adding Zr, Ni, and Zr-Ni alloy to BCC 52Ti-12V-36Cr alloy has been reported. As the microstructure plays an essential role in the hydrogen storage behaviour of these alloys and considering the fact that the as-cast alloys are in a metastable state, it is important to study the effect of heat treatment on these compounds. Therefore, all compositions reported in chapter 4 were heat treated and their morphology, crystal structure, and hydrogen sorption properties investigated and compared to as-cast alloys.

## 5.2 Experimental procedures

### *Material Synthesis and Characterization*

The process flow chart for synthesising heat treated samples is as shown in *Figure 5.1*.

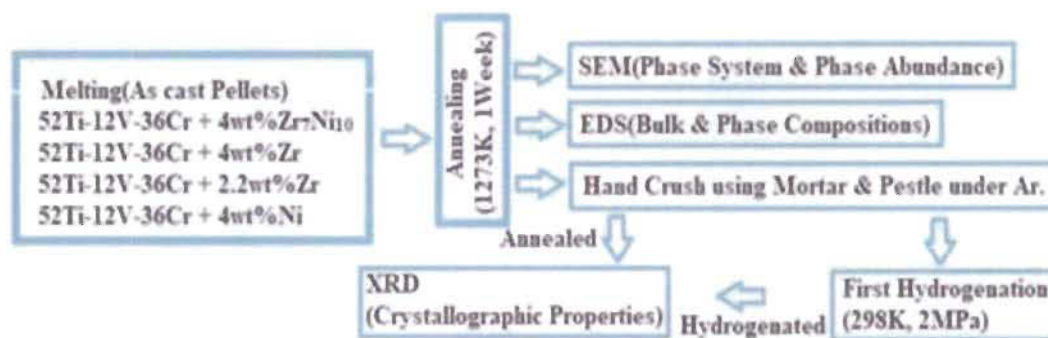


**Figure 5.1-** Flow chart of the synthesis process, heat treatment and characterization.

The pellets of as cast BCC 52Ti-12V-36Cr with 4wt% Zr<sub>7</sub>Ni<sub>10</sub>, 4wt% Zr, 2.2wt% Zr and 4wt%Ni were synthesized in same manner as described in Chapter 4. As cast samples were further heat treated under argon atmosphere at 1273K for one week in a Branstead Thermolyne type tubular furnace. To avoid oxidation of hot pellets, pellets were cooled to room temperature under argon inside furnace itself. As the surface of heat treated pellets was oxidized due to residual oxygen in the argon flow, the surface was removed using sand paper and acetone. To avoid oxidation, the sample pellets were crushed into powder using a mortar and pestle inside an argon-filled glove-box.

The samples are characterized using XRD, SEM, EDS and first hydrogenation in similar way as described in chapter 4.

### 5.3 Results and discussion

#### 5.3.1 Microstructural study of heat treated BCC 52Ti-12V-36Cr with additive

The alloy's microstructure before and after heat treatment of BCC 52Ti-12V-36Cr with/without additive are presented in *Figure 5.2*. The parallel lines seen in some micrographs are due to grinding media.

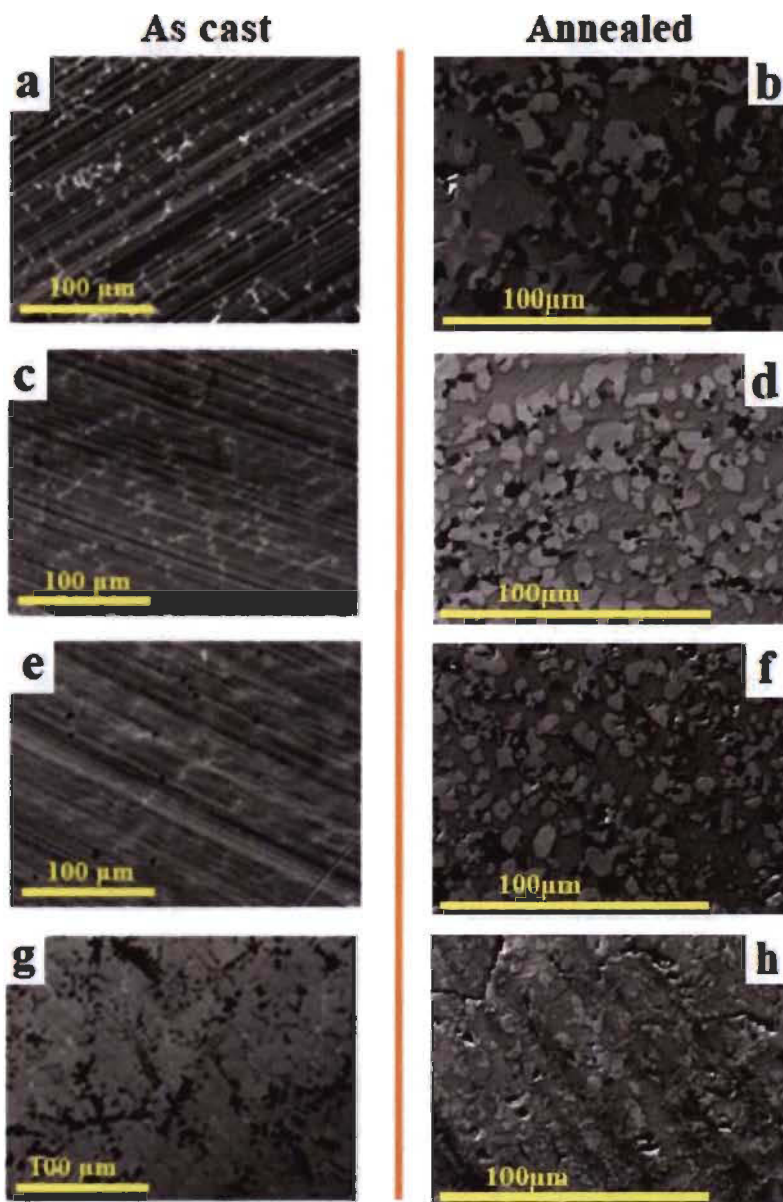


*Figure 5.2-* Backscattering electrons (BSE) SEM micrographs of the as cast(Left) and heat treated(Right) BCC 52Ti-12V-36Cr with (a,b) 4wt% Zr<sub>7</sub>Ni<sub>10</sub>, (c,d) 4wt%Zr, (e,f) 2.2wt%Zr and (g,h)4wt%Ni additives.

The as cast samples with additive showed similarity, all have a main dark phase with a network of minor bright phase and some black precipitates.

The micrographs of heat treated samples show an important difference compared to their as-cast counterparts. The network of minor bright phase seen in the alloy before heat treatment is completely broken after heat treatment. Also, the relative proportion of each phase drastically changed upon heat treatment. The fractional area occupied by each phase was measured using ImageJ [74-75] and the results are presented in **Table 5.1**.

**Table 5.1- Fraction area (in %) occupied by each phase in as-cast and heat-treated BCC 52Ti-12V-36Cr with additive. Uncertainty on each measurement is  $\pm 1\%$**

Additive	As-cast			Heat treated		
	Dark	Bright	Black	Dark	Bright	Black
4wt%Zr <sub>7</sub> Ni <sub>10</sub>	84	14	2	34	52	14
4wt%Zr	90	10	<1	30	56	14
2.2wt%Zr	94	5	1	29	52	19
4wt%Ni	85	9	6	36	56	8

From this table, we could see that the black precipitates abundance significantly increased upon heat treatment except with the 4wt%Ni additive. For all alloys, the abundance of dark phase significantly decreases while the bright phase abundance increases. It could be noticed that the black phase usually precipitates alongside or within the bright phase. The overall phase distribution has completely changed with heat treatment. Before heat treatment, the fraction area of dark phase was about 85-95%, bright phase about 4-14% and black phase about 2-5%. After annealing, the abundance of dark phase was greatly reduced while the abundance of bright phase significantly growth. The black precipitates are much larger than in the as-cast alloys, It should be noticed that the black phase always precipitated beside bright phase. In the case of 4wt%Ni additive, the behaviour of the black phase was different. The abundance of black phase decreases after heat treatment for this alloy.



### 5.3.2 Energy Dispersive X-ray Spectroscopy (EDS) of heat treated alloys

In order to understand more about phases and their compositions, Energy Dispersive Spectroscopy (EDS) was performed. The EDS measurements for bulk composition are presented in **Table 5.2**. For all samples, the bulk measured composition agreed with the nominal one.

**Table 5.2-** Element abundances as measured for bulk compositions of heat treated 52Ti-12V-36Cr alloys with additives. Uncertainties on measured composition are  $\pm 1$  at%.

Additive		Ti	V	Cr	Zr	Ni
4wt%Zr <sub>7</sub> Ni <sub>10</sub>	Nominal	50.55	11.67	34.99	1.15	1.64
	Bulk Measured	54	11	32	1	2
4wt%Zr	Nominal	50.85	11.73	35.2	2.22	-
	Bulk Measured	52	12	34	2	-
2.2wt%Zr	Nominal	51.36	11.85	35.56	1.22	-
	Bulk Measured	53	11	35	1	-
4wt%Ni	Nominal	50.28	11.61	34.81	-	3.3
	Bulk Measured	51	12	33	-	4

A EDS point mapping was carried out for measuring the chemical composition of each individual phase. The measurements were taken at multiple locations on micrographs. *Figure 5.3* shows the localization of representative points. For each phase in each alloy, measurements on different localization agree among themselves within experimental error. The phase compositions for dark phases and bright phases before and after heat treatment are reported in **Table 5.3** and **Table 5.4** respectively.

For as-cast samples, dark phase has chemical composition near the bulk nominal composition for all additives. It should be pointed out that nickel seems to be much easier to enter the dark phase than zirconium. It also seems that nickel replace titanium in the dark phase.

For heat treated samples, the dark phase chemical composition change depending on the type of additive. The titanium abundance in the dark phase increases with amount of zirconium in additive and the chromium abundance decreases in the same proportions except for 2.2 wt.% Zr additives. When both zirconium and nickel are added, the main effect is an important reduction of vanadium content compared to the heat treated samples with other additives.

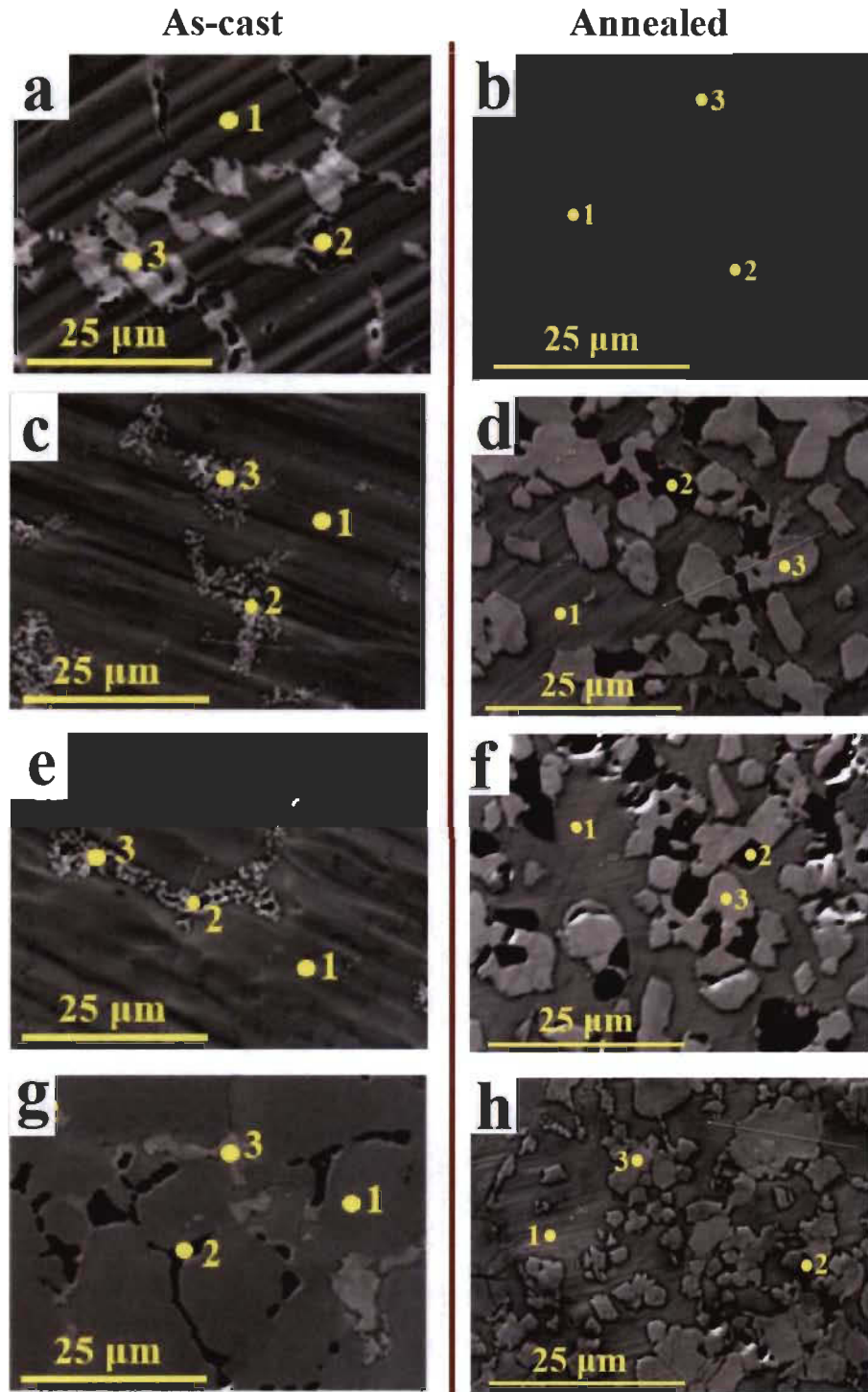


*Figure 5.3- Point mapping of dark phase (1), black phase (2) and bright phase (3) on micrographs of as cast (left) and annealed (right) BCC 52Ti-12V-36Cr with (a,b)4wt%  $Zr_7Ni_{10}$ , (c,d)4wt%Zr, (e,f)2.2wt%Zr and (g,h)4wt%Ni additives.*

**Table 5.3- Chemical composition of dark phases in 52Ti-12V-36Cr alloys with additives. Uncertainties on measured composition are  $\pm 1$  at%.**

Additive	As-cast (at%)					Heat treated (at%)				
	Ti	V	Cr	Zr	Ni	Ti	V	Cr	Zr	Ni
4wt%Zr <sub>7</sub> Ni <sub>10</sub>	50	12	36	1	1	59	7	29	2	3
4wt%Zr	52	12	34	1	-	61	15	23	<1	-
2.2wt%Zr	53	10	36	1	-	56	15	28	1	-
4wt%Ni	49	12	34	-	4	53	16	29	-	2

From **Figure 5.2** and **Figure 5.3**, it could be seen that a minor secondary bright phase coexists with primary dark phase. The composition of this bright phase before and after heat treatment is shown in **Table 5.4**. In the as-cast alloys, the composition of the bright phase does not change much with the proportion or nature of additive. However, it seems that nickel has a tendency to substitute for chromium.

**Table 5.4- Chemical composition of bright phases in 52Ti-12V-36Cr alloys with additives. Uncertainties on measured composition are  $\pm 1$  at%.**

Additive	As-cast (at%)					Heat treated (at%)				
	Ti	V	Cr	Zr	Ni	Ti	V	Cr	Zr	Ni
4wt%Zr <sub>7</sub> Ni <sub>10</sub>	40	7	38	8	7	33	10	54	3	<1
4wt%Zr	42	9	40	9	-	32	9	55	4	-
2.2wt%Zr	43	8	42	7	-	31	9	56	4	-
4wt%Ni	44	8	36	-	12	62	4	14	-	20

After heat treatment, the chemical composition of the bright phase drastically changed. The most important change was seen for the 4 wt.% Ni additive. The proportion of titanium increased, and nickel is the second most abundant element in that phase. The other alloys have very similar chemical composition. In fact, the stoichiometry is near TiCr<sub>2</sub>.

The phase composition for black precipitates was measured to be basically titanium precipitates and is shown in **Table 5.5**.

**Table 5.5- Chemical composition of black phases in 52Ti-12V-36Cr alloys with additives. Uncertainties on measured composition are  $\pm 1$  at%.**

Additive	As-cast (at%)					Heat treated (at%)				
	Ti	V	Cr	Zr	Ni	Ti	V	Cr	Zr	Ni
4wt%Zr <sub>7</sub> Ni <sub>10</sub>	91	1	2	5	0	87	3	8	1	1
4wt%Zr	60	12	26	2	-	95	1	1	3	-
2.2wt%Zr	55	9	29	6	-	95	1	1	3	-
4wt%Ni	97	2	1	-	0	64	6	27	-	3

For Zr based alloys, a significant increase in concentration of Ti with decrease of Cr and V was precipitated in black phase after heat treatment while an important reduction in concentration of Ti in black phase was observed for Ni based alloys. The precipitation behavior of Ti is exactly reversed after heat treatment.

### 5.3.3 Crystal structures before hydrogenation

In section 4, we have reported the x-ray diffraction patterns of these as-cast alloy. It was found that all alloys have single phase BCC crystal structure with a lattice parameter changing very slightly around 3.1 Å with the amount and nature of additive. The amount of secondary (bright and black phases) being too small to be detected by X-ray diffraction [18].

The XRD patterns for heat treated BCC 52Ti-12V-36Cr with additive are shown in *Figure 5.4*. These patterns are quite similar to each other and clearly indicate multi-phase alloys.

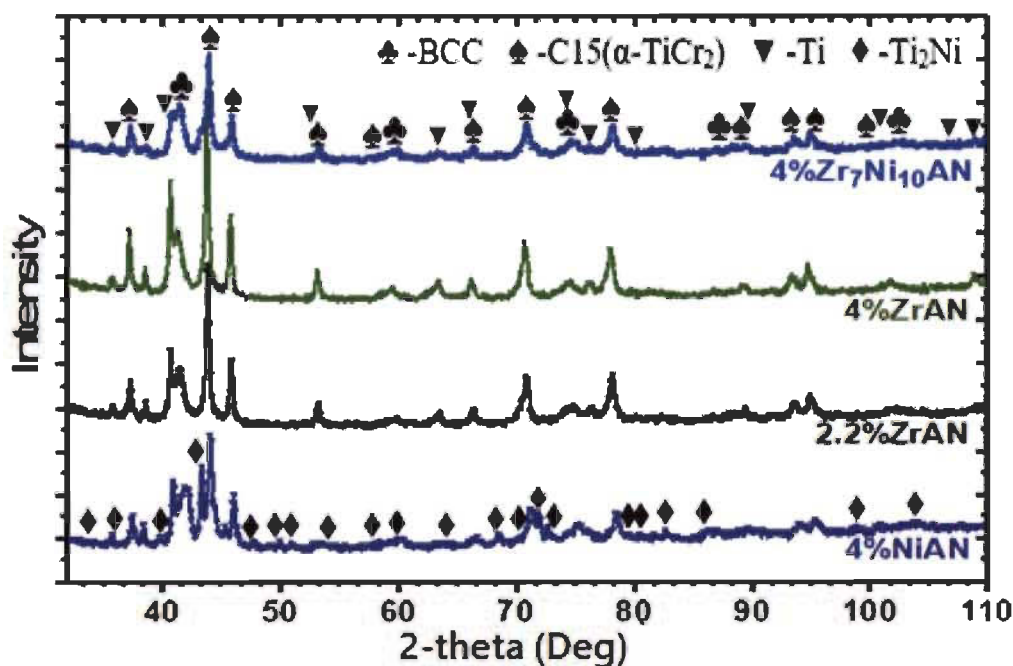


*Figure 5.4-* XRD patterns of heat treated BCC 52Ti-12V-36Cr alloys with additive.

Rietveld refinement was performed on all these patterns. The refinement [70-71] results are summarized in *Table 5.6*.

**Table 5.6-** Crystal structure parameters as determined by Rietveld refinement of heat treated 52Ti-12V-36Cr with additive. The number in parentheses is the error on the last significant digit.

Additive	Crystal structure	Phase Abundance (wt.%)	Lattice Parameter(Å)	Crystallite Size(nm)	Cell Volume(Å <sup>3</sup> )
4wt%Zr <sub>7</sub> Ni <sub>10</sub>	BCC	31	a = 3.148(1)	6.6(3)	31.19(3)
	α-TiCr <sub>2</sub>	55	a = 6.989(2)	12.6(3)	341.4(3)
	Ti	13	a = 2.968(1), c = 4.779(4)	16(2)	36.45(4)
4wt%Zr	BCC	30	a = 3.1579(9)	5.8(2)	31.49(3)
	α-TiCr <sub>2</sub>	55	a = 7.0002(7)	24.1(6)	343.0(1)
	Ti	15	a = 2.9736(4), c = 4.7774(8)	63.662	36.58(1)
2.2wt%Zr	BCC	28	a = 3.1463(8)	6.3(3)	31.15(2)
	α-TiCr <sub>2</sub>	53	a = 6.9922(9)	21.9(5)	341.9(1)
	Ti	19	a = 2.9717(6), c = 4.778(2)	22(2)	36.54(2)
4wt%Ni	BCC	38	a = 3.123(2)	4.7(3)	30.47(5)
	α-TiCr <sub>2</sub>	45	a = 6.961(2)	12.5(5)	337.3(3)
	Ti	12	a = 2.947(1), c = 4.802(4)	47(15)	36.11(4)
	Ti <sub>2</sub> Ni	6	a = 11.087(3)	140(60)	1363(1)

The XRD patterns of heat treated alloys revealed three main phases: BCC [S.G. Im-3m] [18], Laves phase C15 (α-TiCr<sub>2</sub> type) [S.G. Fd-3m] and Ti [S.G. P63/mmc]. In the case of 4wt%Ni additive, there were additional peaks of minor phase of Ti<sub>2</sub>Ni type [S.G. Fd-3m]. Compared to the as-cast samples that were essentially 100% BCC, the abundance of the BCC phase of heat treated alloys was greatly reduced to about 30% with an increase of lattice parameters up to 3.15 Å. The change in lattice parameter may be accommodation to change in phase composition [17]. The crystallite size also reduced from the range 10-20 nm before heat treatment to the range 4.5-6.5 nm after heat treatment. Usually, heat treatment results in increasing crystallite size contrary to what is observed here. However, in the present case, heat treatment transformed an alloy that was essentially single-phase BCC to a multiphase alloy. Also, the chemical composition of the BCC changed with heat treatment. These may be the reasons why crystallite size decreased upon heat treatment.

The C15 (α-TiCr<sub>2</sub>) phase in heat treated samples has an abundance near 45-55% as shown in **Table 5.5**. The bright phase of all samples has reported abundance of 52-56% in **Table 5.1** and ratio of concentrations of Ti/Cr near to 2 as shown in **Table 5.4**. It indicates that C15 could be considered as the bright phase. In a similar way, Ti phase seen in the

diffraction patterns could be associated with the black phase. For all phases in all alloys, no microstrain was found from Rietveld refinement. This is consistent with the process of heat treatment which is well known to relieve stresses.

### 5.3.4 First hydrogenation of heat treated BCC 52Ti-12V-36Cr with additive

The first hydrogenation behaviour of the as-cast alloys has been reported in chapter 4 and the key parameters of hydrogenation behaviour were discussed. It was found that the as cast without additive is very hard to activate with incubation time of 22 hours. When casted with additives, the incubation time had greatly reduced to 2-20 min. The presence of zirconium in additive has impact on kinetics of hydrogen absorption while the nickel improved hydrogen capacity. The additive 4wt%  $Zr_7Ni_{10}$  has been reported as most effective additive with an incubation time of 4 min, hydrogen capacity of 3.76% and fast intrinsic kinetics.

The first hydrogenation curves for heat treated samples compare to as cast samples are as shown in **Figure 5.5**. The key hydrogen storage properties are tabulated in **Table 5.7** after analysing the first hydrogenation curves.

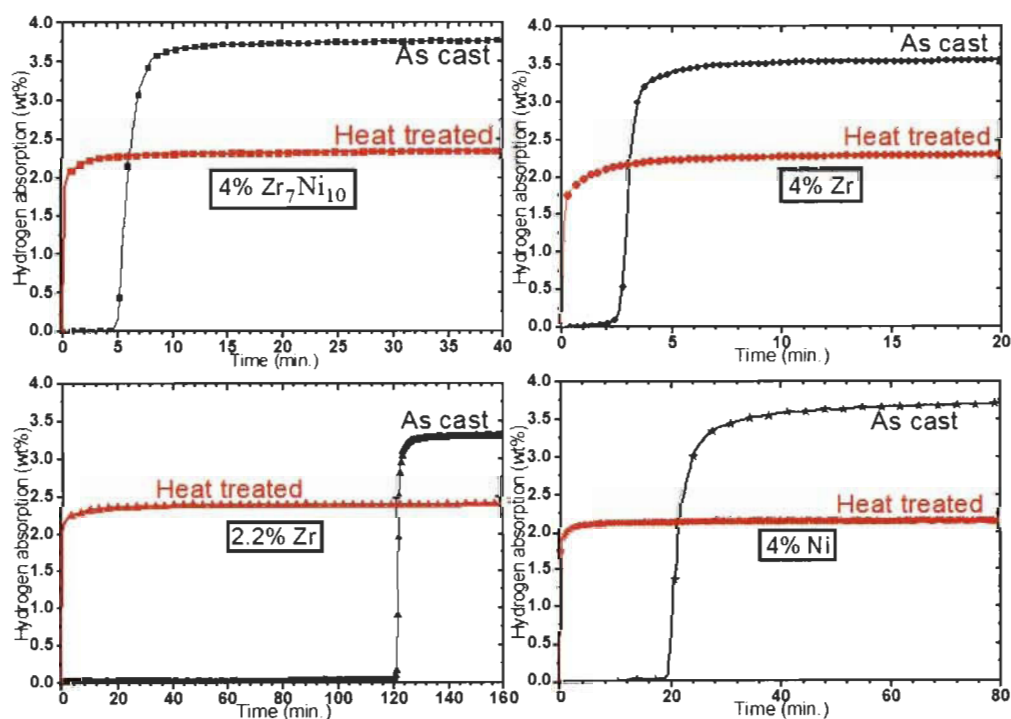


**Figure 5.5-** First hydrogenation curves of heat treated BCC 52Ti-12V-36Cr with additive.

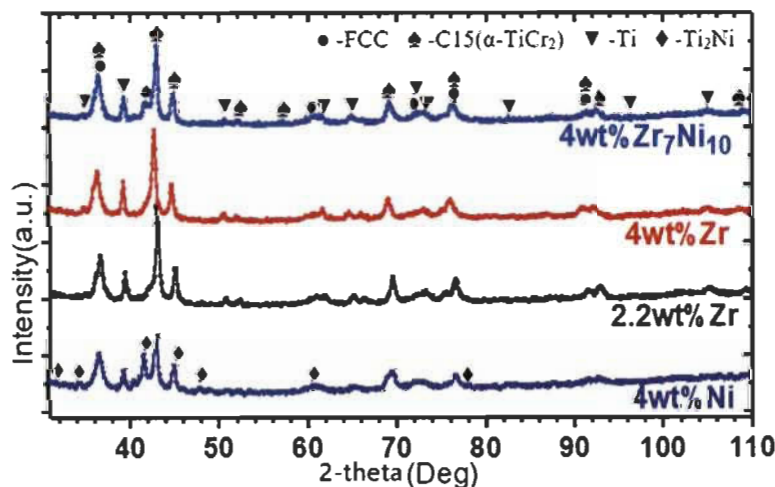
**Table 5.7-** Hydrogen storage properties of heat treated BCC 52Ti-12V-36Cr with additive.

Additive	Hydrogen Capacity (H%)	Intrinsic kinetics (H%/min)
4wt%Zr <sub>7</sub> Ni <sub>10</sub>	2.25±0.07	5.6±0.2
4wt%Zr	2.30±0.07	5.0±0.2
2.2wt%Zr	2.35±0.07	5.7±0.2
4wt%Ni	2.20±0.07	4.9±0.2

It is clear from **Figure 5.6** that heat treatment essentially eliminates incubation time. This is probably due to change in phase composition and refined microstructure with reduced crystallite size. After the incubation time, all as-cast samples showed very fast hydrogen absorption kinetics and the same hydrogen capacity. Unfortunately, the hydrogen capacity of all samples was reduced by 40 % after heat treatment. This diminution of capacity is most probably due to the reduction of the BCC phase upon heat treatment as shown in the diffraction patterns.

### 5.3.5 X-ray diffraction(XRD) of heat treated BCC 52Ti-12V-36Cr with additive after hydrogenation

The XRD patterns for hydrogenated as cast samples has been reported in chapter 4. All as cast samples exhibited single phase FCC crystal structure due to rearrangement of lattice points during hydrogenation. The XRD patterns for heat treated samples after hydrogenation are shown in **Figure 5.6**. The complex patterns indicating multi-phase system.

**Figure 5.6-** XRD patterns of hydrogenated crush of heat treated BCC 52Ti-12V-36Cr with additive.

Rietveld refinement was performed on all patterns to determine change in lattice parameter, crystallite size and phase abundance after hydrogenation. The results are presented refinement are abridged in **Table 5.8** [70-71].

For all alloys, three phases were identified: an FCC phase, a C15 Laves phase and Ti. In the case of 4wt%Ni, additional  $Ti_2Ni$  type phase was also present. The abundance of the FCC phase could be seen to be close to the BCC phase abundance after heat treatment. This confirms that the BCC phase was fully hydrogenated and transformed into an FCC phase ( $\gamma$ -dihydride phase). However, the fully hydride phase has a theoretical capacity of 4 wt.%. Considering that the proportion of the FCC phase is between 25 and 36% then, the hydrogen capacity should be between 1 wt.% and 1.4 wt.%. This clearly does not match the measured capacity. That means there should be some more phases which are absorbing hydrogen. Thus, we measured the expansion of cells after hydrogenation of the other phases present in the diffraction patterns.

**Table 5.8- Rietveld refinement of hydrogenated heat treated BCC 52Ti-12V-36Cr with additive.**

Additive	Crystal structure	Phase Abundance (%)	Hydrogenated			
			Lattice Parameter a, c (Å)	Cell Volume (Å <sup>3</sup> )	Crystallite Size (nm)	Microstrain (%)
4wt%Zr <sub>7</sub> Ni <sub>10</sub>	FCC	36(2)	a = 4.37(2)	83.5(1)	50(70)	0.85(3)
	$\alpha$ -TiCr <sub>2</sub>	58(2)	a = 7.13(2)	362.1(3)	12.7(4)	
	Ti	6(5)	a = 3.05(2), c = 5.07(2)	40.8(1)	11(10)	
4wt%Zr	FCC	25(1)	a = 4.37(2)	83.4(1)	7.3(2)	0.52(2)
	$\alpha$ -TiCr <sub>2</sub>	46(2)	a = 7.15(2)	364.8(2)	13.0(3)	
	Ti	30(2)	a = 3.04(3), c = 5.11(3)	40.9(2)	15.8(9)	
2.2wt%Zr	FCC	33(1)	a = 4.37(2)	83.2(1)	6.0(5)	0.41(2)
	$\alpha$ -TiCr <sub>2</sub>	52(1)	a = 7.12(2)	360.1(2)	15.4(3)	
	Ti	16(7)	a = 3.04(3), c = 5.10(1)	40.8(2)	14.8(9)	
4wt%Ni	FCC	30(2)	a = 4.36(3)	83.1(1)	15(8)	0.63(3)
	$\alpha$ -TiCr <sub>2</sub>	47(3)	a = 7.12(2)	360.7(4)	12.4(6)	
	Ti	9.3(1)	a = 3.03(3), c = 5.14(3)	40.9(1)	12(3)	
	Ti <sub>2</sub> Ni	14(2)	a = 11.53(3)	1534(2)		

The change in unit cell volume of each phase for all samples is reported in *Table 5.9*. By dividing the change of unit cell volume by the number of formula units per unit cell, the volume expansion per formula unit could be estimated. Number of formula units per unit



cell for Laves phase C15, hexagonal  $\alpha$ -Ti, and  $\text{Ti}_2\text{Ni}$  are respectively 4, 2 and 32. Using the criterion that a hydrogen atom produces a volume expansion between 2 and 3  $\text{\AA}^3$  it was possible to estimate the number of hydrogen atoms per formula unit. These results are reported in **Table 5.9**. It shows that Laves phase C15 and  $\alpha$ -Ti seem to be mono-hydrided and additional the  $\text{Ti}_2\text{Ni}$ -like phase in the 4wt%Ni additive may be dihydride.

The heat treated samples with additive have multi-phase system, containing BCC, Lave's phase C15 and  $\alpha$ -Ti. However, even if these alloys are multiphase and more than one phase absorbs hydrogen, the kinetics of hydrogenation showed curves without obvious change of slope and/or kinks. Thus, the curve looks like absorption of a single-phase alloy. This is consistent with the gateway mechanism proposed in previous papers where the secondary phase is acting as a gateway for hydrogen to enter the main phase and thus making the activation easier [17-18].

**Table 5.9- Change in unit cell volume of phases other than BCC due to hydrogenation of BCC 52Ti-12V-36Cr with additive.**

Additive	Phase	Expansion of unit Cell Volume, ( $\text{\AA}^3$ )	Expansion per formula unit ( $\text{\AA}^3$ )	Number of H atoms per formula unit
4wt%Zr <sub>7</sub> Ni <sub>10</sub>	Laves C15	20.7	2.58	1
	Ti	4.33	2.16	1
4wt%Zr	Laves C15	21.77	2.72	1
	Ti	4.34	2.17	1
2.2wt%Zr	Laves C15	18.24	2.28	1
	Ti	4.26	2.13	1
4wt%Ni	Laves C15	23.4	2.93	1
	Ti	4.34	2.17	1
	$\text{Ti}_2\text{Ni}$	171.2	5.3	2

## 5.4 Conclusion

Heat treatment had for effect of turning the BCC phase found in as-cast alloys into a complex multi-phase structure. For all compositions, similar multi-phase microstructures with BCC, C15 and Ti precipitates were observed after heat treatment. However, there was a drastic change in phase composition and distribution compared to the as-cast alloys.

Investigation of the first hydrogenation of heat treated alloys showed that they readily absorb hydrogen without any incubation time but with an important reduction of total capacity. The elimination of incubation time is probably caused by synergy between multi-

phase hydrogen absorption, change in phase compositions and homogenization of microstructure.

The heat treatment had greatly reduced the hydrogen capacity. The reduction in hydrogen capacity is probably due to the reduction of BCC phase abundance. The Laves phase C15 and Ti-precipitates were formed during heat treatment but, upon hydrogenation they seem to have turned into monohydrides. The hydrogenation showed single slope hydrogen absorption like single phase alloys even if they contain more than one phase. It indicates synergy among the phases for hydrogen absorption and a gateway mechanism.

## **Chapter VI**

### **EFFECT OF MECHANICAL DEFORMATION ON BCC ALLOY 52Ti-12V-36Cr**

## 6.1 Overview

Looking at adverse effect of reduced hydrogen capacity after heat treatment even though incubation is eliminated, it was decided to check the effect of mechanically deformed and nanocrystalline BCC alloy powders for improvement in hydrogenation behaviour. This chapter compares the addition of additive in cast of BCC 52Ti-12V-36Cr alloy either at melting together or mechanically alloyed at milling. The more simpler and fast composition BCC 52Ti-12V-36Cr with additive Zr was chosen for study on effect of mechanical deformation. The chapter includes the description of alloy synthesis mechanically and its characterization.

## 6.2 Experimental procedures

### *Material Synthesis and characterization*

The process flow diagram for synthesising BCC alloy with Zr additive in two different ways in which Zr was added is shown in **Figure 6.1**.

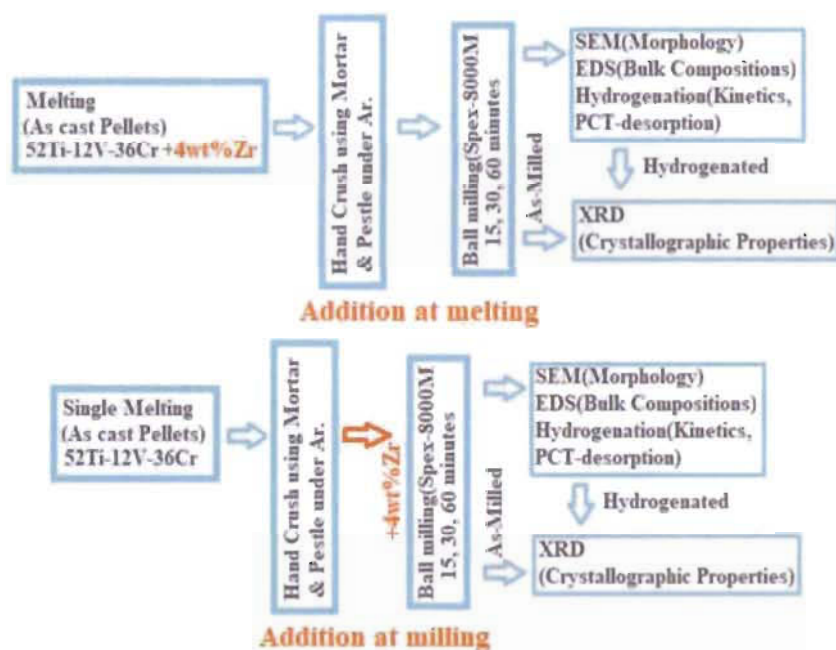


**Figure 6.1-** Synthesis and characterization of melted and ball milled BCC 52Ti-12V-36Cr with Zr.

The pellets of 52Ti-12V-36Cr and 52Ti-12V-36Cr + 4wt%Zr were prepared using an arc melting apparatus. The pellets of bare alloy were ball milled with Zr for 15, 30 and 60 minutes. The cast of 52Ti-12V-36Cr + 4wt%Zr pellets were ball milled for 15, 30 and 60

minutes. The materials are characterized using XRD, SEM and homemade hydrogen titration techniques in similar way as described in Chapter 4.

### 6.3 Results and discussion:

#### 6.3.1 X-ray diffraction(XRD) of ball milled of as cast of BCC 52Ti-12V-36Cr + 4wt%Zr

The XRD pattern of as cast BCC 52Ti-12V-36Cr with additive 4wt% Zr reproduced from section 4.3.3, shown in **Figure 6.2-a**. It has BCC crystal structure (S. G.- Im-3m) [18]. The Rietveld refinement [70-71] of BCC 52Ti-12V-36Cr with and without additive reported in section 4.3.3. The lattice parameter has negligible rise due to addition of 4wt%Zr while the BCC crystal structure remained same. The significant reduction in crystallite size has reported after addition of Zr. The cast of BCC 52Ti-12V-36Cr with additive 4wt% Zr ball milled for 15 min, 30 min and 60 min. The XRD patterns are presented in **Figure 6.2-b, c, d** respectively. All samples have BCC crystal structure (S.G Im-3m). The ball milling does not change the crystal structure. The peak broadening has been observed with increase in ball milling duration which confirms the reduced crystallite size with ball milling.

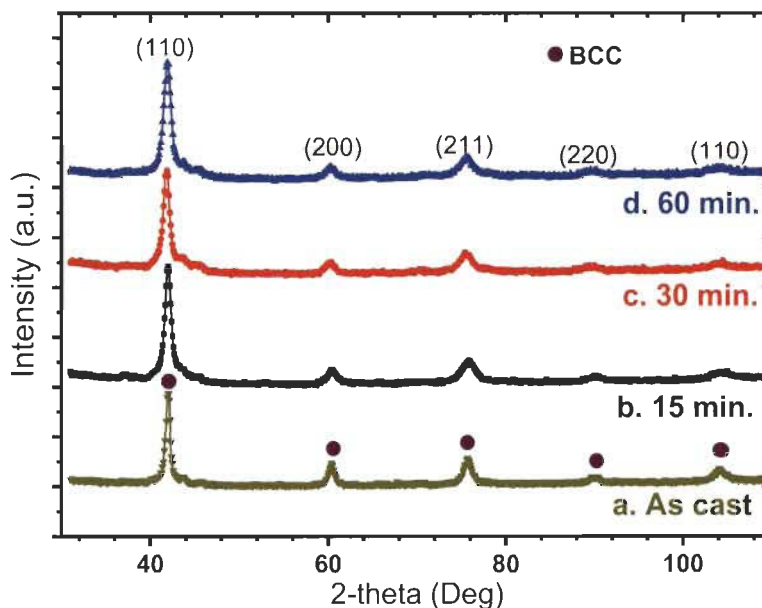


**Figure 6.2-** XRD patterns of (a) cast BCC 52Ti-12V-36Cr+4wt%Zr milled for (b) 15 min, (c) 30 min, (d) 60 min

The refinement results are tabulated in **Table 6.1**. The lattice parameters have negligible change after milling. The crystallite size has reduced further from 10 nm to 5 nm.

In order to change the surface morphology of samples, the additive 4wt%Zr is added at the time of milling instead of melting with BCC alloy. The XRD patterns of BCC alloy milled with Zr for 15, 30 and 60 minutes are presented in **Figure 6.3**. In case of Zr-addition at milling, all samples exhibit mainly BCC crystal structure (S.G Im-3m) with small minor peaks. These minor peaks may be of Zr, which was not well merged with BCC during milling. The minor peaks were found to diminish with increased milling duration. It concludes that the merging of Zr in BCC alloy increases with milling time. The ball milling of 60 minutes may not be sufficient to change the crystal structure. The peak broadening has been observed with ball milling which confirms the reduced crystallite size with ball milling.

**Table 6.1-** Refinement of cast BCC 52Ti-12V-36Cr+4wt%Zr milled for 15 min, 30 min, 60 min.

Sample	As-cast-BCC(Im-3m)	
	a(Å)	Crystallite Size(nm)
BCC 52Ti-12V-36Cr	3.1066(5)	19.8(8)
BCC 52Ti-12V-36Cr + 4wt%Zr	3.1116(7)	10.3(2)
BM15	3.1056(6)	7.2(3)
BM30	3.1092(5)	5.4(2)
BM60	3.1161(4)	5.2(3)

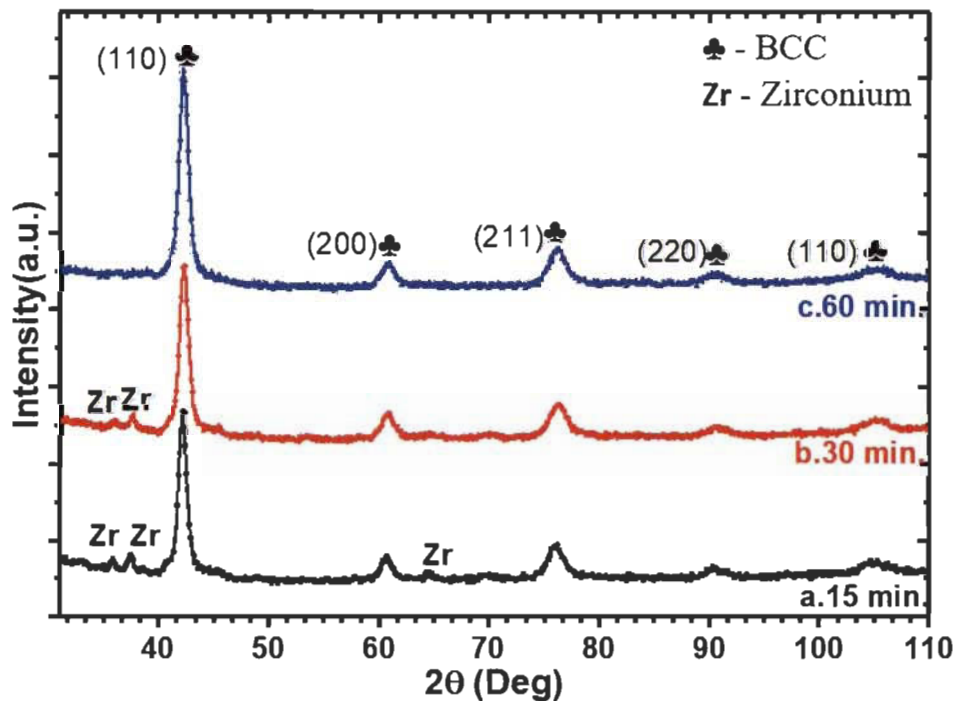


**Figure 6.3-** XRD patterns of cast BCC 52Ti-12V-36Cr milled with 4wt%Zr for (a) 15 min, (b) 30 min, (c) 60 min.

### 6.3.2 First Hydrogenation of BCC 52Ti-12V-36Cr with addition of Zr either at melting or at milling.

The first hydrogenation of milled BCC 52Ti-12V-36Cr+4wt%Zr for 15, 30 and 60 minutes are shown in **Figure 6.4** using curves b, d, f respectively while for the unmilled sample it is presented by curve a. In case of Zr addition at milling, hydrogenation presented by curves c, e and g for milling duration of 15, 30 and 60 minutes respectively. Samples milled for 30 and 60 minutes were not absorbing hydrogen. However, sample milled for 15 minutes absorbed hydrogen, there is drastic reduction in intrinsic kinetics which is reduced more if Zr added at milling instead of melting. The kinetics of samples milled for 15 minutes were too slow to absorb all hydrogen capacity during test duration and reached to  $3.2 \pm 0.1$  wt% and  $2.6 \pm 0.08$  wt% in case of Zr addition at melting and milling respectively.

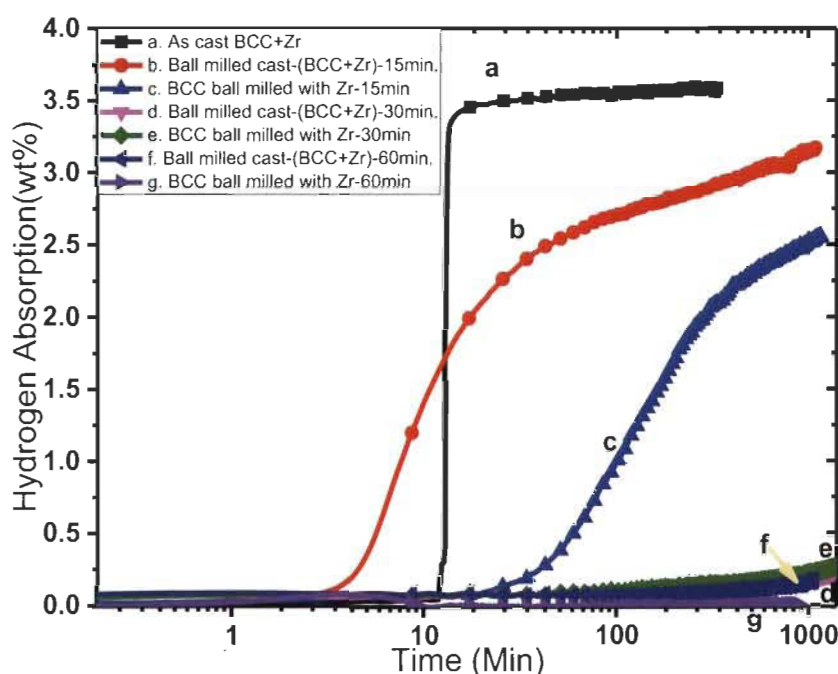


**Figure 6.4-** First hydrogenation curves of (a)as cast BCC 52Ti-12V-36Cr+4wt%Zr milled for (b)15 min, (d)30 min, (f)60 min and cast BCC 52Ti-12V-36Cr milled with 4wt%Zr for (c)15 min, (e)30 min, (g)60 min.

The key hydrogen storage properties for various samples, which absorbed hydrogen are reported in **Table 6.2**. The behaviour of hydrogenation completely changed after ball milling and adverse effect is observed. It's quite difficult to understand the change in mechanism of hydrogenation after ball milling.

**Table 6.2- Hydrogen sorption properties**

Sample	Cast(BCC+4wt%Zr)	Ball milled (BCC+4wt%Zr) for 15 min	BCC ball milled with 4wt%Zr for 15 min
Incubation(min)	12	5	20
Hydrogen capacity (H%)	$3.6 \pm 0.1$	$3.25 \pm 0.1$	$2.65 \pm 0.08$
Kinetics(H%/min)	$6.66 \pm 0.2$	$0.084 \pm 0.003$	$0.0070 \pm 0.0002$

The intrinsic kinetics of casted (BCC+4wt%Zr) is reduced by order of two after milling for 15 minutes. Probably, this is the reason that the full hydrogen capacity recorded before ball milling is not observed after ball milling during the test of 20 hrs. The saturation process was very slow. Thus, it was impractical and time consuming to wait till the full hydrogen capacity for such a degraded sample when we have sample cast(BCC+4wt%Zr) absorbing fast to full capacity of  $3.6 \pm 0.1$  wt% within 10 minutes.

The change in mode of Zr addition from melting to milling also showed reduced intrinsic kinetics, in fact its detrimental. The intrinsic kinetics is reduced by the order of three compared to unmilled cast of alloy with Zr.

### **6.3.3 Scanning Electron Microscopy of BCC 52Ti-12V-36Cr with addition of Zr either at melting or at milling.**

As the samples milled for 15 minutes, showed absorption in both cases of Zr addition, they are studied further for microscopy and spectroscopy in order to understand the change in hydrogenation behaviour after change in event of Zr addition. The back scattered SEM image for the sample is presented in **Figure 6.5-a**. The particles showed rounded edges which confirms the wear taken place on the edges of particles. This indicates rounding of edges due to rolling action during ball milling.

The BSE micrograph for previously casted BCC 52Ti-12V-36Cr milled with 4wt%Zr for 15 min. is shown in **Figure 6.5-b**. The particles observed with rounding of edges due to frictional interaction during ball milling. The bright phase observed localized at the edges or within cracks. It shows inhomogeneous covering of BCC particles by bright secondary phase.



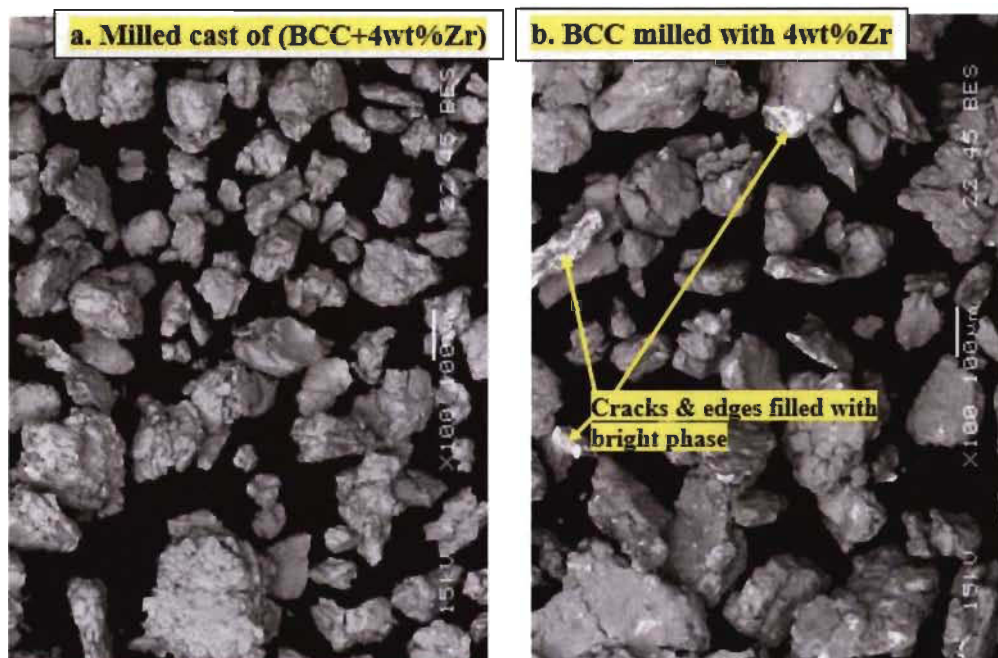


**Figure 6.5-** BSE of (a) milled as cast of BCC 52Ti-12V-36Cr+4wt%Zr and (b) cast BCC 52Ti-12V-36Cr milled with 4wt%Zr for 15 min.

#### 6.3.4 Energy Dispersive Spectroscopy of BCC 52Ti-12V-36Cr with addition of Zr either at melting or at milling.

The elemental mapping was performed on powders obtained after milling of 15 minutes in both cases of Zr addition. The mapping is presented in **Figure 6.6-a** for Zr addition at melting and in **Figure 6.6-b** for Zr addition at milling.

In case of Zr addition at melting, the measured compositions have good agreement with nominal compositions as reported in **Table 6.3**. The elemental mapping showed homogeneous distribution of all elements present with every particle.

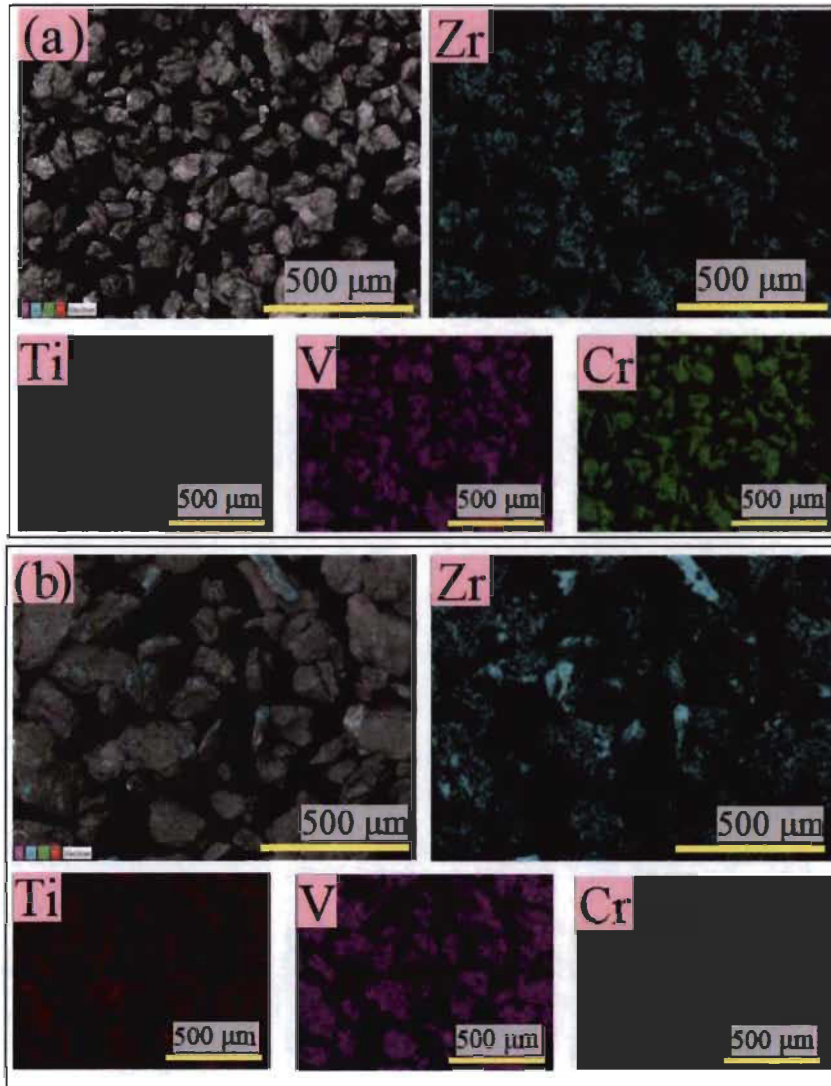


**Figure 6.6-** Elemental mapping of (a) milled of as casted (BCC 52Ti-12V-36Cr+4wt%Zr) and (b) cast of BCC 52Ti-12V-36Cr milled with 4wt%Zr for 15 minutes.

**Table 6.3-** EDS of ball milled BCC 52Ti-12V-36Cr+4wt%Zr for 15, 30 and 60 min.

The uncertainty measured on each measurement is  $\pm 1$  at%.

Description	Ti	V	Cr	Zr
Nominal Composition	50.85	11.73	35.2	2.22
Bulk measured (15 min.)	51.8	12.4	32.9	2.9
Bulk measured (30 min.)	53.3	12.2	32.1	2.4
Bulk measured (60 min.)	52.1	12.7	33.1	2.1

In case of Zr addition at milling, the elemental mapping showed presence of titanium, vanadium and chromium distributed homogeneously along each particle. The presence of zirconium was not homogeneous and gathered at bright sites. It was mostly localized at edges and cracks of particles with higher concentration. The heterogeneously located

bright sites were measured for chemical composition and are reported in **Table 6.4**. These seem to be pure chunks of zirconium. Thus, the bright phase observed in BSE micrographs at the edges and cracks of particles is nothing but the zirconium rich region. The heterogeneity in zirconium distribution over the surface could be the resulted from change in frictional and compressive interaction of zirconium with BCC particles at the surface and edges/cracks during rolling motion.

**Table 6.4- EDS of cast of BCC 52Ti-12V-36Cr milled with 4wt%Zr for 15, 30 and 60 min. The uncertainty measured on each measurement is  $\pm 1$  at%.**

Description	Ti	V	Cr	Zr
Nominal Composition	50.85	11.73	35.2	2.22
Bulk measured (15 min.)	51.8	12.9	30.4	4.9
Bulk measured (30 min.)	51.8	13.1	28.9	6.2
Bulk measured (60 min.)	52.1	12.8	28.5	6.6
Bright Site	19.3	3.4	4.7	72.6

The bulk measured compositions were not agreed with the nominal composition. The concentration of zirconium was double the zirconium in nominal composition. This could be explained on the basis of amount of BCC particles and zirconium sticking with the wall of vial during ball milling. The amount of BCC alloy powder poured in vial was very high compared to the amount of Zr added. The BCC powder was striking with wall of the vial. The possibility of sticking BCC particle is more which may lead to increase in concentration of Zr in bulk compositions.

The wear on edges is due to frictional interaction between particles and vial which could be suspected for resulting into surface contamination. The surface contamination may be too small that remains undetected during XRD. This could be the reason behind adverse effect of reduced kinetics. The effect of too small surface contamination leading to reduced kinetics by two order of magnitude, even the increase in specific surface area for absorption with ball milling, remains unexplainable. Probably, there could be something else other than small contamination, that or collectively with surface contamination reduced the kinetics of hydrogen absorption to great extent almost by two order of magnitude.

The partial reason behind the adverse effect on hydrogenation due to ball milling is already discussed for ball milled-(BCC+4wt%Zr). But the additional adverse effect could be originated from heterogeneity in concentration of zirconium at localized sites and surface of the particles.

### 6.3.5 Pressure-Temperature-Concentration Desorption of BCC 52Ti-12V-36Cr with Zr

The PCT desorption isotherm at 483K was recorded for unmilled cast of BCC 52Ti-12V-36Cr with 4wt%Zr, ball milled cast of BCC 52Ti-12V-36Cr with 4wt%Zr for 15 minutes and cast of BCC 52Ti-12V-36Cr milled for 15 minutes with 4wt% Zr and plotted as curves a-c in *Figure 6.7*.

An unmilled sample revealed the 1.5wt% of reversible hydrogen. In case of milled sample with Zr addition at melting, it has very less reversibility compared with unmilled sample. The reduced reversible capacity could be explained with surface contamination during ball milling. However, mean desorption plateau pressure remains nearly same after ball milling. This indicates no influence of ball milling on thermodynamics which could be expected from materials with same composition.

In case of Zr addition at milling, it has same amount of reversible hydrogen compared with unmilled sample. However, there is improvement in desorption pressure. An improvement in desorption pressure might be originated either due to change in surface morphology with heterogeneous Zr-rich covering layer over core of BCC alloy particles or from change in bulk composition due to different sticky nature of alloy and Zr powder added for milling.

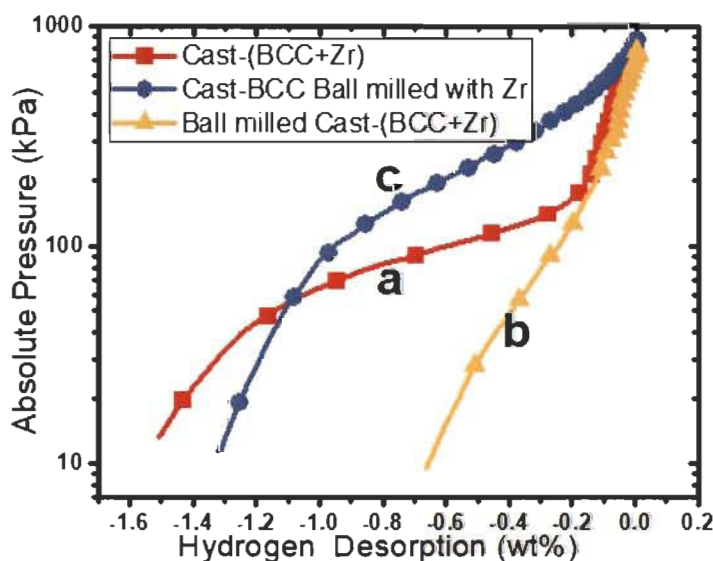


*Figure 6.7-* PCT desorption curves at 483K of (a) BCC 52Ti-12V-36Cr+4wt%Zr, (b) ball milled (BCC52Ti-12V-36Cr+4wt%Zr) for 15 min and (c) cast BCC52Ti-12V-36Cr ball milled with 4wt%Zr for 15 min.

## 6.4 Conclusion

The addition of Zr at milling and at melting was investigated for changes in hydrogenation. In case of addition of Zr at melting, the Zr was well merged with BCC alloy showing BCC crystal structure while in case of Zr addition at milling leads to heterogenous Zr amongst BCC alloy. This created extra minor peaks of Zr in BCC crystal structure. It changed surface morphology having Zr particles over BCC particles.

Milling created the adverse effect of slow absorption with intrinsic kinetics reduced by two order of magnitude in case of Zr addition at melting and by three order of magnitude in case of Zr addition at milling. The detrimental effect of slow kinetics and less reversibility is still not totally understood. An additional adverse effect of reduced intrinsic kinetics in case of Zr addition at milling could be resulted from change in bulk composition or change in surface morphology. There is improvement in desorption pressure probably due to heterogeneous Zr on BCC alloy powder.

**Chapter VII**

**EFFECT OF PARTICLE SIZE IN 52Ti-12V-  
36Cr ALLOY WITH AND WITHOUT  
ADDITIVES**

## 7.1 Outline

This chapter describes the effect of particle size on hydrogenation behaviour of BCC alloy with and without addition of Zr. The main emphasis was on the kinetics of the first hydrogenation, the so-called activation. This is a serious problem for the industry and this work was to investigate if a simple particle size reduction could have some effect on activation kinetics and the hydrogen capacity of the material. By studying the alloy with and without Zr addition, the relative effect of chemical composition and particle size was evaluated.

## 7.2 Experimental procedures

### *Material Synthesizing*

The pellets of BCC 52Ti-12V-36Cr with and without 4wt% Zr were casted in similar manner as explained in previous studies. The schematic of experimental procedure is as shown in **Figure 7.1**. To avoid oxidation, the sample pellets were crushed using a mortar and pestle in an argon filled glove-box.

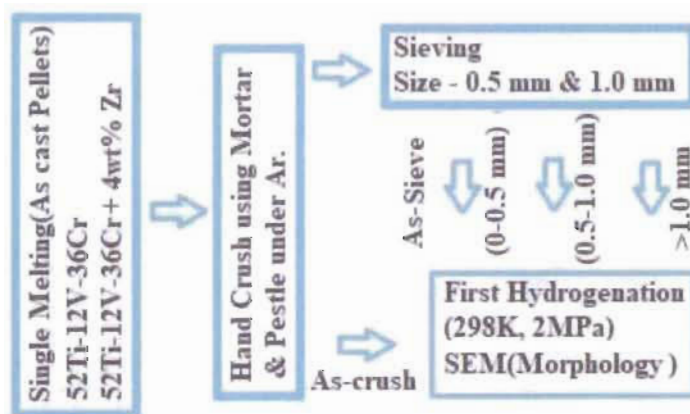


**Figure 7.1-** Flow chart for synthesis and characterization of sieved BCC 52Ti-12V-36Cr with and without Zr.

For this type of investigation, the selection of range of particle size to be studied as well as the mean to reduce the particle size is crucial. Ball milling is a well-known and easy way to reduce particle size. However, this technique is too energetic for the present purpose. It induces a reduction of crystallite size down to nanoscale and thus could change the intrinsic hydrogen storage kinetics of the material. Moreover, previous tests indicated that ball milling could actually made an alloy totally inert toward hydrogen. Therefore, we used a simple crushing of the as-cast pellet using a mortar and pestle. Sample powder was



sieved inside the glove box. Two sieves of size 0.5 mm and 1.0 mm were used to collect the powder in three different particle size ranges: diameters of less than 0.5 mm, diameters between 0.5 and 1.0 mm and diameters bigger than 1 mm. Crushing and sieving were done in a glove box to prevent oxidation.

### ***Material characterization***

Scanning Electron Microscopy was performed using JEOL scanning electron microscope JSM-5500 and micrographs analysed with ImageJ 1.50i software [74-75]. Particle size was measured as the mean Equivalent Circle Diameter (ECD) as determined with ImageJ. First hydrogenation on sample of 300-400 mg was performed at 298K under 2 MPa hydrogen pressure using a homemade hydrogen titration system.

## **7.3 Results and discussion**

### **7.3.1 Particle size analysis**

**Figure 7.2** shows a typical particle size distribution of the as-cast alloy 52Ti-12V-36Cr + 4wt%Zr after being crushed in a mortar and pestle. The alloy 52Ti-12V-36Cr had similar size distribution. This distribution was the basis for the decision to split the powder in three populations: particles of less than 0.5 mm, particles between 0.5 mm and 1 mm, and particles of sizes bigger than 1 mm. **Figure 7.3** shows, for the alloy 52Ti-12V-36Cr + 4wt%Zr, the micrographs of these three distributions as well as the powder before sieving.

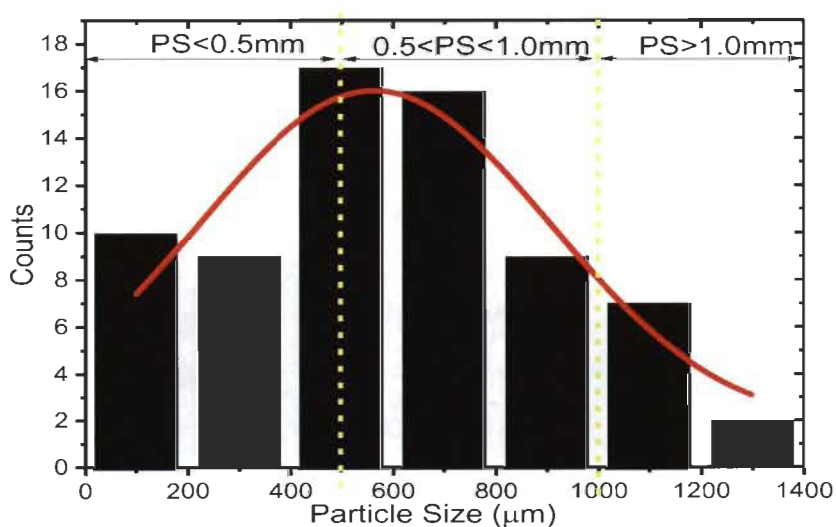


**Figure 7.2-** Particle size distribution of 52Ti-12V-36Cr + 4wt%Zr powder.



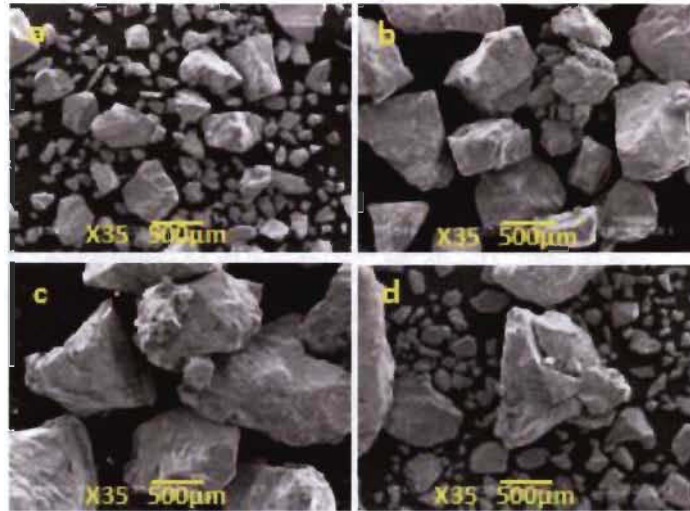


**Figure 7.3-** Secondary Electron Images of 52Ti-12V-36Cr + 4wt%Zr alloy (a) PS<0.5mm, (b) 0.5<PS<1.0mm, (c) PS>1.0mm and (d) as-crushed

The as-crushed image shows that the particles have irregular shape with sharp edges. This indicates that the hand crushing only broke the particles and had limited wear on the particle's surface. **Figures 7.3a-c** confirms the sieving process.

From SEM micrographs, the average particle size of each population was determined and is shown in **Table 7.1**.

**Table 7.1-** Average particle size of sample powder ( $\mu\text{m}$ ) for the alloy 52Ti-12V-36Cr + 4wt%Zr.

Sample	ECD ( $\mu\text{m}$ )
As crushed	560 $\pm$ 400
PS<0.5 mm	150 $\pm$ 60
0.5<PS<1.0 mm	770 $\pm$ 10
PS>1.0 mm	1120 $\pm$ 70

### 7.3.2 First hydrogenation

First hydrogenation (activation) kinetics of as-crushed powder and the three sieved samples for the 52Ti-12V-36Cr + 4wt%Zr alloy are shown on **Figure 7.4**. We see that all curves have the same general shape showing an incubation time followed by a very fast kinetics reaching the full hydrogen capacity of the alloy.

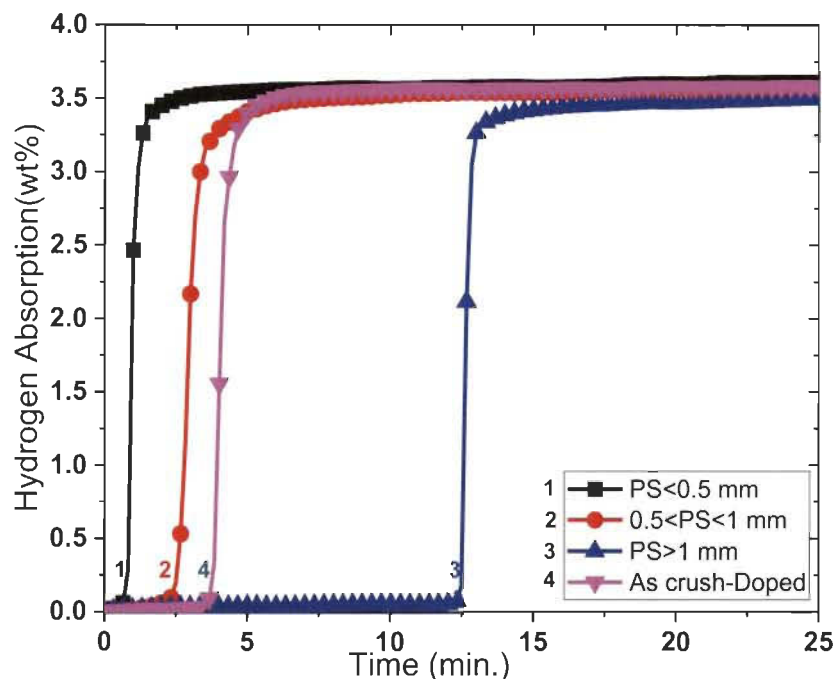


**Figure 7.4-** First hydrogenation curves of 52Ti-12V-36Cr doped with 4%Zr for different particle size and for the as-crushed sample.

It is clear that the main difference between the curves is the incubation time. These incubation times are listed in **Table 7.2**. As could be anticipated, incubation time is shorter for smaller particles. A smaller particle size means a higher specific surface area and thus greater area for metal-hydrogen interaction. Therefore, it may be expected that the reduction of particle size would have an effect on the hydrogenation kinetics as well. But, as seen in **Figure. 7.4**, the intrinsic kinetics (hydrogenation rate after incubation time) is very fast for all samples. Something, which is not expected in case if the kinetics is the function of the exposed surface. As the 52Ti-12V-36Cr + 4wt%Zr is a two-phase material, one possibility is that, upon crushing, some phase segregation may occur, resulting in the smaller particles having a higher proportion of the secondary phase and therefore exhibiting a shorter incubation time. But this means that the intrinsic kinetics would be noticeably faster for the smaller particles which is not what is seen. Moreover, as different particle size shows different incubation time, we expect that the as-crushed sample will show various activation steps coming from the different particle size of this particular sample. However, this is not what is seen. This behaviour is difficult to explain. Therefore, in order to distinguish between the effect of additive and particle size, we performed the same type of investigation with 52Ti-12V-36Cr alloy without additive.

**Table 7.2- Incubation of with ( $t_w$ ) and without ( $t_{w/o}$ ) additive samples.**

Sample Description	Incubation(min.)	
	( $t_w$ )	( $t_{w/o}$ )
As crushed	4	1340
PS<0.5mm ( $t_{-0.5}$ )	0.3	434
0.5<PS<1.0mm ( $t_{0.5-1.0}$ )	2	1280
PS>1.0mm ( $t_{+1.0}$ )	12	1520

**Figure 7.5** shows the activation kinetics of first hydrogenation of 52Ti-12V-36Cr alloy for the as-crushed sample and for sieved powders. From **Figure. 7.4** and **Figure 7.5**, we see that the effect of particle size is qualitatively the same for the with and without additive alloys.

As shown in **Table 7.2**, main difference is that the incubation time for the alloy with additive are much reduced compared to the without ones. **Table 7.3** shows the ratio of these incubation time for each size of particles.

It is clear that the effect of additive is more important for the small particles than for the big ones. Additive reduces the incubation time by at least two order of magnitude. It is known from previous investigation that these alloys have a microstructure made up of a main BCC phase and a zirconium rich secondary phase. Therefore, chemical composition and/or presence of a secondary phase play a more important role in the reduction of incubation time than the reduction of particle size.

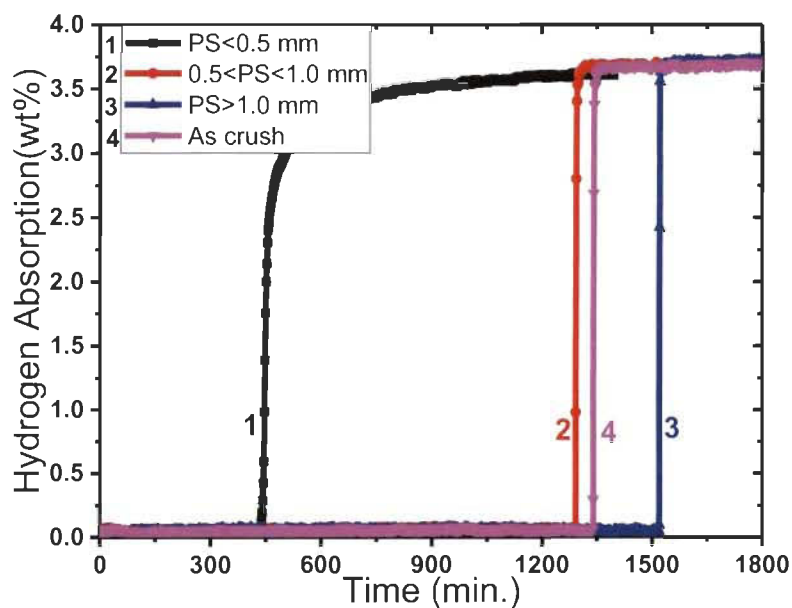


**Figure 7.5- First hydrogenation curves of 52Ti-12V-36Cr alloy for different particle size for the as-crushed sample.**

**Table 7.3- Ratio of incubation time of with and without additive samples with the same particle size.**

Sample Description	$\frac{t_{w/o}}{t_w}$
As-crushed	335
PS<0.5mm	1447
0.5<PS<1.0mm	640
PS>1.0mm	127

Even if the effect of particle size is much smaller than additive, it is still worthy to understand the effect of particle size. In this perspective, the ratio of incubation times over the small particles' incubation time was calculated. These ratios are shown in **Table 7.4**. For the bare sample, incubation time is only reduced by a factor 3.5 when small particles are used. On the other hand, small particles of the sample with additive are 40 times faster than the big particles. These results indicate that particle size reduction is beneficial for reduction of incubation time but there is a synergetic effect between additive and particle size deduction. Moreover, synergy between particle size and additive is more important for smaller particle size.

**Table 7.4- Effect of particle size on incubation**

Sample's ratio	Incubation(min.)	
	With additive	Without
$\frac{t_{0.5-1.0}}{t_{-0.5}}$	6.7	2.9
$\frac{t_{+1.0}}{t_{-0.5}}$	40	3.5

For both with and without additive samples the hydrogenation kinetic is very fast after incubation time. The intrinsic kinetics were compared by taking the slope of each curve at half capacity (i.e. 1.8 wt.%). Results are listed in **Table 7.5**. The intrinsic kinetics of the samples with additive is faster than their counterparts without additive. For the particles without additive, the intrinsic kinetic decreases with decreasing particle size with an almost ten-fold decreases between the bigger particle and smaller ones. Such a trend is not seen for the samples with additive. The intrinsic kinetics of the intermediate size particles is smaller than the kinetics shown by bigger and smaller particles. But the main fact is that there is only a small variation of intrinsic kinetics amongst the doped samples. This shows that intrinsic kinetics is mainly due to the presence of additive and particle size plays a negligible role.

**Table 7.5- Intrinsic kinetics of with and without additive samples.**

Sample Description	Intrinsic kinetics (%H/min.)	
	With	Without
As crush	$5.6 \pm 0.2$	$0.82 \pm 0.02$
PS<0.5mm	$9.0 \pm 0.3$	$0.110 \pm 0.003$
0.5<PS<1.0mm	$3.8 \pm 0.1$	$0.81 \pm 0.02$
PS>1.0mm	$6.8 \pm 0.2$	$0.98 \pm 0.03$

From these results, it is clear that the most important factor for reducing incubation time is the chemical nature of the alloys and to a much lesser extent the particle size. The reduction of incubation time with decreases of particle size could be explained, in part, by the increase of specific surface area when average particle size is smaller. However, the reduction of incubation time with particle size is too important to be explained just by this fact. One possible explanation could be that small particles have a higher proportion of surface defect per unit area than the big particles. A higher number of defects means that there are more sites available for nucleation of a new phase, in the present case the hydride phase, which will result in decrease of incubation time.

Another interesting fact shown by all samples is that the as-crushed sample act as a monolithic sample. From the results of the sieved samples, one could expect that the as crushed samples will show three different activation steps, corresponding to each population. On the contrary, the as-crushed sample showed a single activation time which is close to the weighted average of the individual activation times. Therefore, this is a proof that there is a strong synergy between particles during the activation process and that the powder always acts collectively no matter what the size distribution is.

## 7.4 Conclusion

The relative importance of particle size and chemical composition on the first hydrogenation (activation) of a Ti-V-Cr BCC solid solution alloy was investigated. It was found that the chemical composition and presence of a second phase has a much bigger impact on decrease of incubation time than reduction of particle size. Thus, the most efficient way to reduce activation time is to modify the chemical composition of the alloy. Moreover, doping has strong effect on the intrinsic kinetics of activation.

Reduction of particle size leads to a decrease of activation time, but it could not be explained by increase in specific area alone.

It was also found that activation is a monolithic process where a mixture of different particle size will have an incubation time proportional to the average particle size.

## Conclusion

---

The investigation of the effect of change in chemical composition, heat treatment, ball milling and particle size on hydrogen absorption of BCC alloys is carried out to eliminate the step of incubation time and select effective additive and synthesizing techniques.

Casting with Zr and/or Ni drastically reduced the incubation time of hydrogenation and improved rate of intrinsic kinetics. The influence may be probably due to the presence of secondary phase. The addition of Zr has influence on incubation and hydrogenation kinetics while Ni favoured an increase of capacity. With synergetic effect, 4wt%Zr<sub>7</sub>Ni<sub>10</sub> stood as effective additive with low incubation time and high capacity.

All heat treated samples showed a decrease of BCC phase abundance with increase of Ti-precipitates and Laves phase C15( $\alpha$ -TiCr<sub>2</sub>). The heat treatment has effect of change in phase composition and abundance. The heat treatment eliminates step of incubation probably due to change in phase composition and abundance but adversely reduce capacity due to reduction in BCC phase. The acceptance of annealing remains doubtful as reduced capacity can't be appreciated. Still the 2.2wt% hydrogen absorption is 1.5 - 2 times more than practically used materials like TiFe (1.5 wt%), LaNi<sub>5</sub> (1.2 wt%) etc. Thus, there may be future scope for heat treated materials in practical applications based upon cost of heat treatment process, thermodynamic properties and cyclability of heat treated samples.

As compared to heat treated samples with no incubation, cast alloy with additive Zr<sub>7</sub>Ni<sub>10</sub> with negligible incubation time has relatively high hydrogen capacity about 3.7 wt%. The charging time will be of ten seconds for heat treated samples compared to 3-4 min for as cast with additive. Thus, as-cast with additive stands suitable for practical applications as high hydrogen storage with negligible fuelling time if perform well during repetitive cycles of hydrogen absorption and desorption.

In case of addition of Zr during melting, the Zr was well merged with BCC alloy showing BCC crystal structure, However, in case of Zr addition during milling heterogenous Zr was found amongst BCC alloy, the presence of which. created extra minor peaks of Zr in BCC crystal structure. It changed surface morphology showing the presence of Zr particles over BCC particles. Milling created the adverse effect of slow absorption with intrinsic kinetics reduced by two order of magnitude in case of Zr addition at melting and by three order of magnitude in case of Zr addition at milling. The detrimental effect of slow



---

kinetics and less reversibility is still not totally understood. An additional adverse effect of reduced intrinsic kinetics in case of Zr addition at milling could be resulted from change in bulk composition or change in surface morphology. There is improvement in desorption pressure probably due to heterogeneous Zr on BCC alloy powder. The detrimental effect of ball milling made these samples not suitable for hydrogen storages and battery applications.

The relative importance of particle size and chemical composition on the first hydrogenation (activation) of a Ti-V-Cr BCC solid solution alloy was investigated. It was found that the chemical composition and presence of a second phase has a much bigger impact on decrease of incubation time than reduction of particle size. Thus, the most efficient way to reduce activation time is to modify the chemical composition of the alloy. Moreover, doping has strong effect on the intrinsic kinetics of activation. Reduction of particle size leads to a decrease of activation time, but it could not be explained by increase of specific area alone. It was also found that activation is a monolithic process where a mixture of different particle size will have an incubation time proportional to the average particle size.

At the end, casting BCC alloy together with 4wt%Zr<sub>7</sub>Ni<sub>10</sub> could be optimized chemical composition and synthesizing technique with negligible incubation time, fast hydrogenation kinetics and high capacity at room temperature under low pressure.

---

## References

- [1] <https://www.eia.gov/todayinenergy/detail.php?id=26212> Last accessed on August 12, 2018.
  - [2] <https://www.youtube.com/user/worldenergycouncil> Last accessed on August 12, 2018.
  - [3] Dincer, I. (2000). Renewable energy and sustainable development: a crucial review. *Renewable and Sustainable Energy Reviews*, 4(2), 157-175.
  - [4] Panwar, N. L., Kaushik, S. C., & Kothari, S. (2011). Role of renewable energy sources in environmental protection: A review. *Renewable and Sustainable Energy Reviews*, 15(3), 1513-1524.
  - [5] Akiba, E., & Iba, H. (1998). Hydrogen absorption by Laves phase related BCC solid solution. *Intermetallics*, 6(6), 461-470.
  - [6] Harris I. R. (1987). The potential of hydrogen in permanent magnet production. *Journal of the Less-Common Metals*, 131(1-2), 245-262.
  - [7] Schulz R, Huot J, Liang G, Boily S, Lalande G, Denis MC. et al. (1999). Recent development in the applications of nanocrystalline materials to hydrogen technologies. *Mater Science Engineering: A*, 267, 240-245.
  - [8] [https://www1.eere.energy.gov/hydrogenandfuelcells/tech\\_validation/pdfs/fcm01r0.pdf](https://www1.eere.energy.gov/hydrogenandfuelcells/tech_validation/pdfs/fcm01r0.pdf) Last accessed on August 12, 2018.
  - [9] Ashworth, M. A., Davenport, A. J., Ward, R. M., & Hamilton, H. G. C. (2010). Microstructure and corrosion of Pd-modified Ti alloys produced by powder metallurgy. *Corrosion Science*, 52(7), 2413-2421.
  - [10] Sakintuna, B., Lamari-Darkrim, F., & Hirscher, M. (2007). Metal hydride materials for solid hydrogen storage: A review. *International Journal of Hydrogen Energy*, 32(9), 1121-1140.
  - [11] <https://h2tools.org/lessons> Last accessed on December 18, 2018.
  - [12] Monterey Gardiner R. and Burke A. (2002). Comparison of hydrogen storage technologies: a focus on energy required for hydrogen input. *Fuel Chemistry Division Preprints*, 47(2), 794-795.  
[https://web.anl.gov/PCS/acsfuel/preprint%20archive/Files/47\\_2\\_Boston\\_10-02\\_0218.pdf](https://web.anl.gov/PCS/acsfuel/preprint%20archive/Files/47_2_Boston_10-02_0218.pdf)
  - [13] DOE: US Department of Energy. Website: (<http://www.doe.gov>) Last accessed on August 12, 2018.
  - [14] Darkrim FL, Malbrunot P, Tartaglia GP. (2002). Review of hydrogen storage by adsorption in carbon nanotubes. *International Journal of Hydrogen Energy*, 27, 193-202.
  - [15] Ellis, Arthur B.; et al. (1995). Teaching General Chemistry: A Materials Science
-

- 
- Companion (3rd ed.). Washington, DC: American Chemical Society. ISBN-10: 084122725X, ISBN-13: 9780841227255.
- [16] Qiu S-J, Chu H-L, Zhang Y, Sun L-X, Xua F, Cao Z. (2008). The electrochemical performances of Ti-V-based hydrogen storage composite electrodes prepared by ball milling method. *International Journal of Hydrogen Energy*, 33, 7471–7478.
- [17] Miraglia, S., de Rango, P., Rivoirard, S., Fruchart, D., Charbonnier, J., & Skryabina, N. (2012). Hydrogen sorption properties of compounds based on BCC Ti<sub>1-x</sub>V<sub>1-y</sub>Cr<sub>1+x+y</sub> alloys. *Journal of Alloys & Compounds*, 536, 1-6.
- [18] Bibienne, T., Bobet, J.-L., & Huot, J. (2014). Crystal structure and hydrogen storage properties of body centered cubic 52Ti–12V–36Cr alloy doped with Zr<sub>7</sub>Ni<sub>10</sub>. *Journal of Alloys & Compounds*, 607, 251-257.
- [19] Bibienne, T., Razafindramanana, V., Bobet, J.-L., & Huot, J. (2015). Synthesis, characterization and hydrogen sorption properties of a Body Centered Cubic 42Ti–21V–37Cr alloy doped with Zr<sub>7</sub>Ni<sub>10</sub>. *Journal of Alloys & Compounds*, 620, 101-108.
- [20] Banerjee S., Kumar A., Ruz P., Sengupta P. (2016). Influence of Laves phase on microstructure and hydrogen storage properties of Ti–Cr–V based alloy, *International Journal of Hydrogen Energy*, 41, 18130-18140.
- [21] Tsukahara, M., Takahashi, K., Mishima, T., Isomura, A., & Sakai, T. (1996). Heat-treatment effects of V-based solid solution alloy with TiNi-based network structure on hydrogen storage and electrode properties. *Journal of Alloys and Compounds*, 243(1), 133-138.
- [22] Okada, M., Kuriwa, T., Tamura, T., Takamura, H., & Kamegawa, A. (2002). Ti–V–Cr b.c.c. alloys with high protium content. *Journal of Alloys and Compounds*, 330–332, 511-516.
- [23] Young, K., Wong, D. F., & Wang, L. (2015). Effect of Ti/Cr content on the microstructures and hydrogen storage properties of Laves phase-related body-centered-cubic solid solution alloys. *Journal of Alloys and Compounds*, 622, 885-893.
- [24] Goodell P.D, Sandrock G.D., Huston E.L. (1980). Kinetic and dynamic aspects of rechargeable metal hydrides. *Journal of Less Common Metals* 73, 135–142.
- [25] Lang J., Eagles M., Conradi M. S., Huot J., (2014) Hydrogenation rate limiting step, diffusion and thermal conductivity in cold rolled magnesium hydride, *Journal of Alloys and Compounds*, 583, 116-120.
- [26] Nakamura Y., Oguro K., Uehara I. and Akiba E. (2000). X-ray diffraction peak
-

- 
- broadening and degradation in LaNi<sub>5</sub>-based alloys. *International Journal of Hydrogen Energy*, 25(6), 531-537.
- [27] Schlappbach L., (1992). Hydrogen in intermetallic compounds I and II., *Journal of Applied Physics*, 63-67. ISBN 978-3-540-46433-4
- [28] Murray J. L., (1987). The Ti-V system, Phase Diagrams of Binary Titanium Alloys. In J. L. Murray (Ed.), (pp. 319-327). Metals Park, OH USA: ASM International. ISBN 0871702487
- [29] Broom D. P. (2011). Hydrogen Storage Materials; The Characterisation of their storage properties. London: Springer-Verlag London Limited. ISBN 978-0-85729-220-9.
- [30] Qiu S-J, Chu H-L, Zhang Y, Sun L-X, Xua F, Cao Z. (2008) , The electrochemical performances of Ti-V-based hydrogen storage composite electrodes prepared by ball milling method. *International Journal of Hydrogen Energy*, 33, 7471–7478.
- [31] <https://energy.gov/eere/fuelcells/materials-based-hydrogen-storage>. Last accessed on August 12, 2018.
- [32] Charbonnier J, De RP, Fruchart D, Miraglia S, Rivoirard S, Skryabina N. Pulverulent intermetallic materials for the reversible storage of hydrogen. Google Patents; 2007. <https://patents.google.com/patent/US8257464>
- [33] Bellon, D., Martinez, A., Barreneche, D., & Santos, D. S. (2016). A structural study of the hydrogen absorption properties by replacing vanadium with zirconium in metal alloys. *Journal of Physics: Conference Series*, 687(1), 012057.
- [34] Hang, Z., Xiao, X., Tan, D., He, Z., Li, W., Li, S., . . . Chen, L. (2010). Microstructure and hydrogen storage properties of Ti<sub>10</sub>V<sub>84-x</sub>Fe<sub>6</sub>Zr<sub>x</sub> (x=1–8) alloys. *International Journal of Hydrogen Energy*, 35(7), 3080-3086.
- [35] Basak S., Shashikala K. and Kulshreshtha S. K. (2008). Hydrogen absorption characteristics of Zr substituted alloy. *International Journal of Hydrogen Energy*, 33(1), 350-355.
- [36] Martínez A. and Santos D. S. (2012). Hydrogen absorption/Desorption
-

---

Properties in the TiCrV Based Alloys. *Materials Research*, 15(5), 809-812.

- [37] Dornheim M., Doppiu S., Barkhordarian G., Boesenberg U., Klassen T., Gutfleisch O., Bormann R., (2007) Hydrogen storage in magnesium-based hydrides and hydride composites, *Scripta Materialia*, 56 841-846.
- [38] Huot J., (2012) Nanocrystalline Metal Hydrides Obtained by Severe Plastic Deformations, *Metals*, 2 22.
- [39] Danaie M, Mauer C, Mitlin D, Huot J. (2011) Hydrogen storage in bulk Mg-Ti and Mg-stainless steel multilayer composites synthesized via accumulative roll-bonding (ARB). *International Journal of Hydrogen Energy*, 36 3022-36.
- [40] Hu Y. Q., Zhang H. F., Yan C., Ye L., Ding B. Z. and Hu Z. Q. (2004). Preparation and hydrogenation of body-centered-cubic TiCr<sub>2</sub> alloy. *Materials Letters*, 58(5), 783-786.
- [41] Cho S.-W., Yoo J.-H., Chang H.-K., Kim W.-B., Kil D.-S. and Ahn J.-G.. (2011). Changes in the microstructure and hydrogen storage properties of Ti–Cr–V alloys by ball milling and heat treatment. *Journal of Alloys and Compounds*, 509(18), 5545-5550.
- [42] Yu X.B., Wu Z., Xia B.J., Xu N.X., (2004) Hydrogen absorption performance of Ti–V-based alloys surface modified by carbon nanotubes, *Physics Letters A*, 333 468-472.
- [43] Yu X.B., Wu Z., Xia B.J., Xu N.X., (2005) Improvement of activation performance of the quenched Ti–V-based BCC phase alloys, *Journal of Alloys and Compounds*, 386, 258-260.
- [44] Couillaud, S., Enoki, H., Amira, S., Bobet, J. L., Akiba, E., & Huot, J. (2009). Effect of ball milling and cold rolling on hydrogen storage properties of nanocrystalline TiV<sub>1.6</sub>Mn<sub>0.4</sub> alloy. *Journal of Alloys and Compounds*, 484(1–2), 154-158.
- [45] Singh BK, Shim G, Cho S-W. (2007) Effects of mechanical milling on hydrogen storage properties of alloy. *International Journal of Hydrogen Energy*, 32, 4961-5.

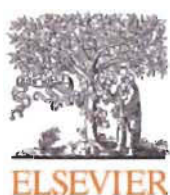
- 
- [46] Bobet J.-L., Chevalier B., (2004) Hydrogen storage properties of Mg-based mixtures elaborated by reactive mechanical grinding, *Journal of Materials Science*, 39 5243-4246.
- [47] Varin RA, Czujko T, Wronski Z. (2006) Particle size, grain size and  $\gamma$ -MgH<sub>2</sub> effects on the desorption properties of nanocrystalline commercial magnesium hydride processed by controlled mechanical milling. *Nanotechnology*; 17, 3856.
- [48] Young K., Ouchi T., Nei J., and Wang L. (2016) Annealing effects on Laves phase-related body-centered-cubic solid solution metal hydride alloys. *Journal of Alloys and Compounds* 654, 216-225.
- [49] Cho, S.-W., Shim, G., Good-Sun, C., Park, C., Yoo, J.-H., & Choi, J. (2007). Hydrogen absorption-desorption properties of Ti<sub>0.32</sub>Cr<sub>0.43</sub>V<sub>0.25</sub> alloy *Journal of Alloys and Compounds*, 430, 136-141.
- [50] Cho, S.-W., Enoki, H., & Akiba, E. (2000). Effect of Fe addition on hydrogen storage characteristics of Ti<sub>0.16</sub>Zr<sub>0.05</sub>Cr<sub>0.22</sub>V<sub>0.57</sub> alloy. *Journal of Alloys and Compounds*, 307(1), 304-310.
- [51] Mohammed Abdul, J., Hearth Chown, L., Kolawole Odusote, J., Nei, J., Young, K.-H., & Taiye Olayinka, W. (2017). Hydrogen Storage Characteristics and Corrosion Behaviour of Ti<sub>24</sub>V<sub>40</sub>Cr<sub>34</sub>Fe<sub>2</sub> Alloy. *Batteries*, 3(2), 19.
- [52] Rong M., Wang F., Wang J., Wang Z., Zhou H., (2017) Effect of heat treatment on hydrogen storage properties and thermal stability of V<sub>68</sub>Ti<sub>20</sub>Cr<sub>12</sub> alloy, *Progress in Natural Science: Materials International*, 27, 543-549, ISSN 1002-0071.
- [53] Liu X., Jiang L., Li Z., Huang Z. and Wang S. (2009). Improve plateau property of Ti<sub>32</sub>Cr<sub>46</sub>V<sub>22</sub> BCC alloy with heat treatment and Ce additive. *Journal of Alloys and Compounds*, 471(1-2), L36-L38.
- [54] Zhang L.T., Ito K., Vasudevan V.K., Yamaguchi M., (2001) Hydrogen absorption and desorption in a B2 single-phase Ti-22Al-27Nb alloy before and after deformation, *Acta Materialia*, 49, 751-758, ISSN 1359-6454,
- [55] Lee S. M. and Perng T. P. (1994). Effect of the second phase on the initiation of
-

- 
- hydrogenation of  $\text{TiFe}_{1-x}\text{M}_x$  ( $\text{M} = \text{Cr, Mn}$ ) alloys. *International Journal of Hydrogen Energy*, 19(3), 259-263.
- [56] Shirasaki K., Tamura T., Kuriwa T., Goto T., Kamegawa A., Takamura H. and Okada M. (2002). Cyclic properties of protium absorption-desorption in Ti-V-Cr alloys. *Material Transactions*, 43(5), 1115-1119.  
<https://www.jim.or.jp/journal/e/pdf3/43/05/1115.pdf>
- [57] Banerjee S., Kumar A., Ruz P., Sengupta P., Influence of Laves phase on microstructure and hydrogen storage properties of Ti-Cr-V based alloy, *International Journal of Hydrogen Energy*, 41 (2016) 18130-18140.
- [58] Enomoto M. (1992). The Cr-Ti-V system (Chromium-Titanium-Vanadium). *Journal of Phase Equilibria*, 13(2), 195-199.  
<https://link.springer.com/content/pdf/10.1007/BF02667488.pdf>
- [59] Murray J. L., "The Ti-V System Phase Diagrams of Binary Titanium Alloys", J.L. Murray, Ed., ASM International, Metals Park, OH, 319-327 (1987). ISBN 0871702487
- [60] Samsonova N. N., Budberg P. B., Kornilov I. I., and Asanov U. A., (1966), "Interaction of the  $\text{TiCr}_2$  Intermetallic with V" *Izv. Akad. Nauk SSSR, Neorg. Mater.*, 2, 1882.
- [61] Mohammed Abdul J., (2016), Development of Titanium Alloys for Hydrogen Storage. PhD Thesis, University of the Witwatersrand, Johannesburg.  
<http://hdl.handle.net/10539/21151>
- [62] Young W., Yongqing Z., Weidong Z., Hongliang H. and Yaoqi W. (2010). Behaviour of Hydrogen Absorption/Desorption of Ti600, TC21 and Ti40 Alloys. *Rare Metal Materials and Engineering*, 39(9), 1509-1512.
- [63] <http://www.rsc.org/periodic-table/element/22/titanium> Last accessed on 22 May 2018.
- [64] <http://www.rsc.org/periodic-table/element/23/vanadium> Last accessed on 22 May 2018.
- [65] <http://www.rsc.org/periodic-table/element/24/chromium> Last accessed on 22
-

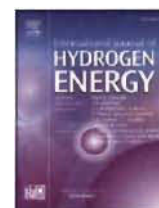
- 
- May 2018.
- [66] <http://www.rsc.org/periodic-table/element/40/zirconium> Last accessed on 22 May 2018.
- [67] <http://www.rsc.org/periodic-table/element/28/nickel> Last accessed on 22 May 2018.
- [68] [https://www.spexsampleprep.com/equipment-and-accessories/accessory\\_product/8007](https://www.spexsampleprep.com/equipment-and-accessories/accessory_product/8007) Last accessed on 22 May 2018.
- [69] Cho H., Kwon J., Kim K., Mun M. (2013) Optimum choice of the make-up ball sizes for maximum throughput in tumbling ball mills, *Powder Technology*, 246 625-634.
- [70] Bruker AXS, TOPAS V4, in: General Profile and Structure Analysis Software for Powder Diffraction Data, Karlsruhe, Germany, 2008. [https://www.bruker.com/fileadmin/user\\_upload/8-PDF-Docs/X-rayDiffraction/ElementalAnalysis/XRD/Flyers/TOPAS\\_Flyer\\_DOC-H88-EXS013\\_V2\\_en\\_high.pdf](https://www.bruker.com/fileadmin/user_upload/8-PDF-Docs/X-rayDiffraction/ElementalAnalysis/XRD/Flyers/TOPAS_Flyer_DOC-H88-EXS013_V2_en_high.pdf) Last accessed on 22 May 2018.
- [71] Coelho A. A. Topas-Academic. A Computer Programme for Rietveld Analysis. 2004. <http://www.topas-academic.net/> Last accessed on 22 May 2018.
- [72] <http://www.crystallography.net/> Last accessed on 22 May 2018.
- [73] <http://www.rzuser.uni-heidelberg.de/~hb6/labor/rem/REM-kurzes-Skriptum.pdf> accessed on 22 May 2018.
- [74] Collins T. (2007) ImageJ for Microscopy. *BioTechniques*, 43. S25-S30.
- [75] Abramoff M D, Magalhães P J, Ram S J. (2004) Image processing with ImageJ. *Biophotonics international*. 11(7), 36-42. <https://imagescience.org/meijering/publications/download/bio2004.pdf> Last accessed on 22 May 2018.



1. Kamble, A., Sharma, P., & Huot, J. (2017). Effect of doping and particle size on hydrogen absorption properties of BCC solid solution 52Ti-12V-36Cr. *International Journal of Hydrogen Energy*, 42(16), 11523-11527. doi: <https://doi.org/10.1016/j.ijhydene.2017.02.137>
2. Kamble, A., Sharma, P., & Huot, J. Effect of addition of Zr, Ni, and Zr-Ni alloy on the hydrogen absorption of Body Centred Cubic 52Ti-12V-36Cr alloy. *International Journal of Hydrogen Energy*. doi:<https://doi.org/10.1016/j.ijhydene.2018.02.106>
3. Kamble, A., Sharma, P., & Huot, J. Effect of heat treatment on crystal structure, microstructure and hydrogen absorption of Body Centred Cubic 52Ti-12V-36Cr alloy with additives 4wt%Zr<sub>7</sub>Ni<sub>10</sub>, 4wt%Zr, 2.2wt%Zr, and 4wt%Ni. submitted at Progress in Natural Science: Materials International
4. Effect of heat treatment on crystal structure, microstructure and hydrogen absorption of Body Centred Cubic 52Ti-12V-36Cr alloy – To be submitted
5. Mechanically addition of Zr to Body Centred Cubic 52Ti-12V-36Cr alloy – To be submitted

Available online at [www.sciencedirect.com](http://www.sciencedirect.com)

ScienceDirect

journal homepage: [www.elsevier.com/locate/ijhydene](http://www.elsevier.com/locate/ijhydene)

## Short Communication

# Effect of doping and particle size on hydrogen absorption properties of BCC solid solution 52Ti-12V-36Cr

Amol Kamble<sup>a,b,c,\*</sup>, Pratibha Sharma<sup>b</sup>, Jacques Huot<sup>a,\*\*</sup><sup>a</sup> IRH, UQTR, Trois-Rivières, Quebec, G9A5H7, Canada<sup>b</sup> Department of Energy Science & Engineering, IIT Bombay, Mumbai, Maharashtra, 400076, India<sup>c</sup> Department of Automobile Engineering, PHCET, Rasayani, Maharashtra, 410207, India

## ARTICLE INFO

## Article history:

Received 24 December 2016

Received in revised form

2 February 2017

Accepted 17 February 2017

Available online 18 March 2017

## Keywords:

Hydrogen storage

BCC solid solutions

Metal hydrides

First hydrogenation

## ABSTRACT

The effect of chemical composition and particle size on the first hydrogenation of BCC alloy 52Ti-12V-36Cr were investigated. The alloy was studied in the undoped state and doped with 4%Zr. Three particle size ranges were selected: less than 0.5 mm, between 0.5 mm and 1 mm, and bigger than 1 mm. It was found that doping reduced the incubation time by more than two orders of magnitudes. Smaller particle size also reduces incubation time but only by a factor of three. The intrinsic hydrogenation kinetics were also significantly enhanced by doping. Moreover, there is some synergetic effect between doping and reduction of particle size. It was also found that incubation time depends on the average particle size and not on the distribution of particle sizes.

© 2017 Hydrogen Energy Publications LLC. Published by Elsevier Ltd. All rights reserved.

## Introduction

Ti-V-Cr BCC solid solutions are attractive solid state hydrogen storage alloys due to their ability to absorb hydrogen at room temperature and under relatively low hydrogen pressure [1–5]. BCC solid solution attracted more attention in 1998 when Iba and Akiba introduced the concept of Laves phases related BCC solid solution in Ti-V-Mn and Ti-V-Cr systems which can have reversible hydrogen capacity higher than 2 wt% [6]. Nevertheless, Ti-V-Cr BCC alloys usually

display resistance to hydrogenation when they are first exposed to hydrogen, the so-called activation step [1]. Typically, activation process shows an incubation time followed by a relatively rapid hydrogenation. Subsequent hydrogenation does not display such incubation time and hydrogenation proceed with relatively fast kinetics. Therefore, the main detrimental feature of activation is the incubation time.

Usually, the only way to have rapid activation is to perform the hydrogenation at high temperature and pressure. The reasons for activation resistance are still not well understood but the presence of surface oxide certainly plays a role. The

\* Corresponding author. IRH, UQTR, Trois-Rivières, Quebec, G9A5H7, Canada.

\*\* Corresponding author.

E-mail addresses: [amol.kamble@gmail.com](mailto:amol.kamble@gmail.com) (A. Kamble), [Jacques.Huot@uqtr.ca](mailto:Jacques.Huot@uqtr.ca) (J. Huot).<http://dx.doi.org/10.1016/j.ijhydene.2017.02.137>

0360-3199/© 2017 Hydrogen Energy Publications LLC. Published by Elsevier Ltd. All rights reserved.

incubation time can be reduced by a pre-activation/degassing heat treatment at 350°C–700°C step which dissolves the oxide layer into the bulk volume of material and produce clean metal/alloy surface for immediate hydrogenation [3,5,7]. But this is a time-consuming process that adds additional cost to the metal hydride synthesis [1].

Nucleation formation and growth of metal hydride phase occurs along strain fields induced by hard secondary phase, high density of defects (dislocations/twins) and cracks. Therefore, increasing the number of heterogeneous sites could improve activation kinetics [8].

The respective effect of particle size and nanocrystallinity on hydrogen sorption kinetics of metal hydrides has been investigated by many researchers. For example, Domheim et al. showed improved kinetics with reduced particle size by reactive ball milling for  $\text{MgH}_2$  [9]. Bobet et al. have shown that reduction in particle size increases specific surface area which gives rise to surface reactions and accelerate hydrogen absorption [10]. Effect of particle size of ball milled  $\text{MgH}_2$  has also been investigated by Varin et al. [11]. They distinguished the respective contribution to reduce particle size and the presence of a metastable phase ( $\gamma\text{-MgH}_2$ ) on the dehydrogenation kinetics. However, reduction of particle size and nanocrystallinity could have a detrimental effect on hydrogen sorption properties as shown for BCC solid solution alloys [12,13].

Other ways to improve activation kinetics are addition of catalysts and addition of dopants. In a recent work, Miraglia et al. showed that a dramatic improvement of activation kinetics could be achieved by casting 4wt%  $\text{Zr}_7\text{Ni}_{10}$  to previously cast BCC 33Ti–30V–37Cr alloy [2].

In a previous investigation, it was found that melting BCC alloy 52Ti–12V–36Cr with 4wt%  $\text{Zr}_7\text{Ni}_{10}$  resulted in a fast activation at room temperature and low hydrogen pressure [1]. In order to understand the activation mechanism and the relative importance of particle size and addition of a dopant, it is suitable to study a simpler system. In this paper, we report the activation behaviour of the BCC solid solution alloy 52Ti–12V–36Cr undoped and doped with 4wt%Zr.

## Materials and methods

The raw materials Titanium (sponge, 3–19 mm, 99.95%), Vanadium (granules, 1–3 mm, 99.7%), Chromium (pieces, irregular, 99%) and Zirconium (sponge, 0.8–25.4 mm, 99.5%) were purchased from Alfa Aesar and used without further purification. Two types of samples of nominal composition 52Ti–12V–36Cr were synthesized: undoped and doped with 4wt% of zirconium. Chunks of all raw elements were mixed in the proper stoichiometry and melted using an arc melting apparatus (Centorr Associates Inc, USA). In order to get homogeneous samples, each composition was melted three times with samples flipped over after each melting.

To avoid oxidation, the sample pellets were crushed using a mortar and pestle in an argon-filled glovebox. Ball milling was not used to reduce particle size because it may have a detrimental effect of hydrogen storage properties by inducing a BCC  $\rightarrow$  FCC phase change and also reducing the crystallite size to nanometer scale. Sample powder was sieved inside the

glove box, using sieves of size 0.5 mm and 1.0 mm to collect sorted samples in three different particle size ranges: diameters of less than 0.5 mm, diameters between 0.5 and 1.0 mm and diameters bigger than 1 mm. Scanning Electron Microscopy was performed using JEOL scanning electron microscope JSM-5500 and micrographs analyzed with ImageJ 1.50i software. Particle size was defined as the mean Equivalent Circle Diameter (ECD) as determined with ImageJ.

First hydrogenation was performed at 298 K under 20 bar hydrogen pressure using a homemade hydrogen titration system.

## Results and discussion

### Particle size analysis

Fig. 1 shows a typical particle size distribution of the as-cast alloy 52Ti–12V–36Cr + 4wt%Zr after being crushed in a mortar and pestle. Undoped sample had similar size distribution.

Based on this distribution, we decided to split the powder in three populations: particles of less than 0.5 mm, particles between 0.5 mm and 1 mm, and particles of sizes bigger than 1 mm. Fig. 2 shows, for the alloy 52Ti–12V–36Cr + 4wt%Zr, the micrographs of these three distributions as well as the powder before sieving.

The as-crushed image shows that the particles have irregular shape with sharp edges. This indicates that the hand crushing only broke the particles and had limited wear on the particle's surface. Fig. 2a–c confirms the sieving process.

From SEM micrographs, the particle size of each population was determined and is shown in Table 1.

### First hydrogenation

First hydrogenation (activation) kinetics of as-crushed powder and the three sieved samples for the 52Ti–12V–36Cr + 4wt%Zr alloy are shown on Fig. 3. We see that all curves have the same general shape showing an incubation time followed by a very fast kinetics reaching the full hydrogen capacity of the alloy.

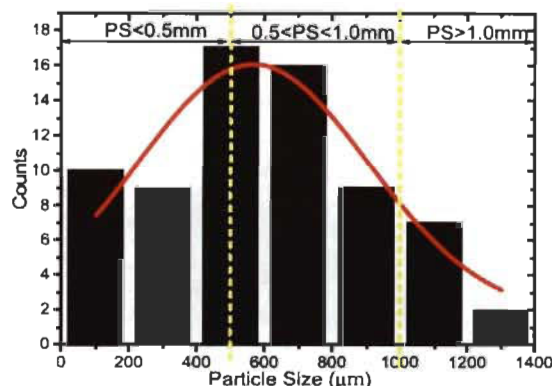


Fig. 1 – Particle size distribution of 52Ti–12V–36Cr + 4wt% Zr powder.



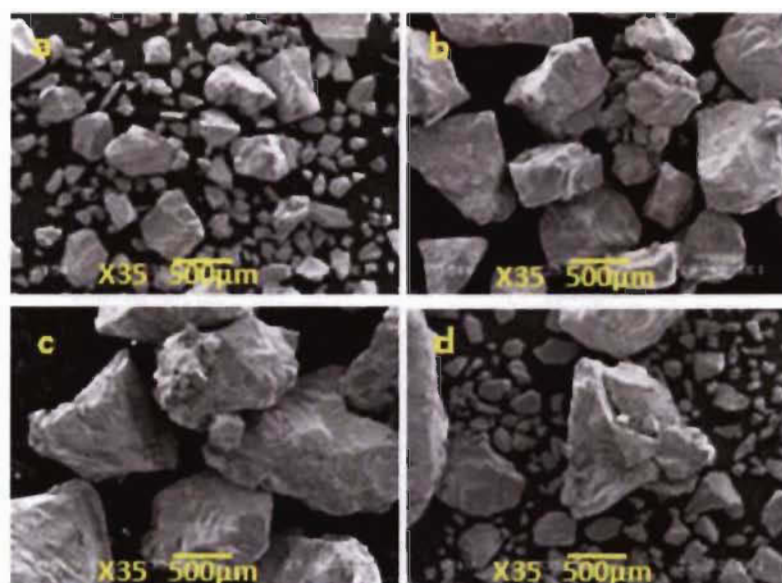


Fig. 2 – Secondary Electron Images of 52Ti-12V-36Cr + 4wt%Zr alloy. PS < 0.5 mm(a), 0.5 < PS < 1.0 mm(b), PS > 1.0 mm(c) and as-crushed (d).

It is clear that the main difference between the curves is the incubation time. These incubation times are listed in Table 2. As could be anticipated, incubation time is shorter for smaller particles. A smaller particle size means a higher specific surface area and thus greater area for metal–hydrogen interaction. Therefore, it may be expected that the reduction of particle size would have an effect on the hydrogenation kinetics as well. But, as seen in Fig. 3, the intrinsic kinetics (hydrogenation rate after incubation time) is very fast for all samples. There is something that is not expected if the kinetics is a function of the exposed surface. As the 52Ti-12V-36Cr + 4wt%Zr is a two-phase material, one possibility is that, upon crushing, some phase segregation may occur, resulting in the smaller particles having a higher proportion of the secondary phase and therefore exhibiting a shorter incubation time. But this means that the intrinsic kinetics would be noticeably faster for the smaller particles which is not what is seen. Moreover, as different particle size shows different incubation time, we expect that the as-crushed sample will show various activation steps coming from the different particle size of this particular sample. However, this is not what is seen. This behaviour is difficult to explain. Therefore, in order to distinguish between the effect of doping agent and particle

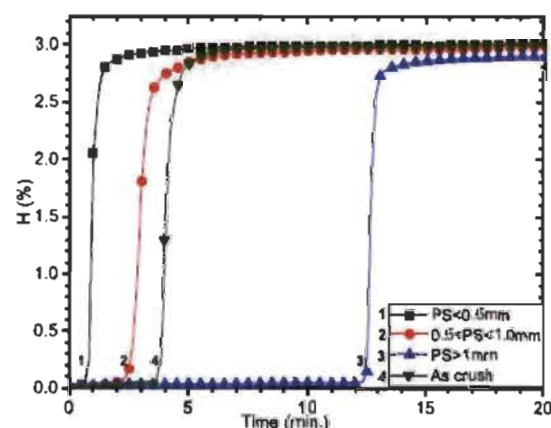


Fig. 3 – First hydrogenation curves of 52Ti-12V-36Cr doped with 4%Zr for different particle size and for the as-crushed sample.

Table 1 – Particle Size of sample powder ( $\mu\text{m}$ ) for the alloy 52Ti-12V-36Cr + 4wt%Zr.

Sample	ECD ( $\mu\text{m}$ )
As crushed	560 $\pm$ 400
PS < 0.5 mm	150 $\pm$ 60
0.5 < PS < 1.0 mm	770 $\pm$ 10
PS > 1.0 mm	1120 $\pm$ 70

Table 2 – Incubation of doped ( $t_D$ ) and undoped ( $t_{UD}$ ) samples.

Sample Description	Incubation (min.)	
	( $t_D$ )	( $t_{UD}$ )
As crushed	4	1340
PS < 0.5 mm ( $t_{0.5}$ )	0.3	434
0.5 < PS < 1.0 mm ( $t_{0.5-1.0}$ )	2	1280
PS > 1.0 mm ( $t_{1.0}$ )	12	1520

size, we performed the same type of investigation with the undoped 52Ti-12V-36Cr alloy.

Fig. 4 shows the activation kinetics of first hydrogenation of 52Ti-12V-36Cr alloy for the as-crushed sample and for sieved powders. From Figs. 3 and 4, we see that the effect of particle size is qualitatively the same for the undoped and doped alloys.

As shown in Table 2, main difference is that the incubation time for the doped alloy is much reduced compared to the undoped ones. Table 3 shows the ratio of these incubation time for each size of particles.

It is clear that the effect of doping is more important for the small particles than for the big ones. Nevertheless, doping reduces the incubation time by at least two orders of magnitude. It is known from previous investigation that these alloys have a microstructure made up of a main BCC phase and a zirconium rich secondary phase [14]. Therefore, chemical composition and/or presence of a secondary phase play a more important role in the reduction of incubation time than the reduction of particle size.

Even if the effect of particle size is much smaller than doping, it is still worthy to understand the effect of particle size. In this perspective, we calculated the ratio of incubation times over the small particles' incubation time. These ratios are shown in Table 4. For the undoped sample, incubation time is only reduced by a factor 3.5 when small particles are used. On the other hand, small particles of the doped sample are 36.5 times faster than the big particles. These results indicate that particle size reduction is beneficial for reduction of incubation time but there is a synergetic effect between

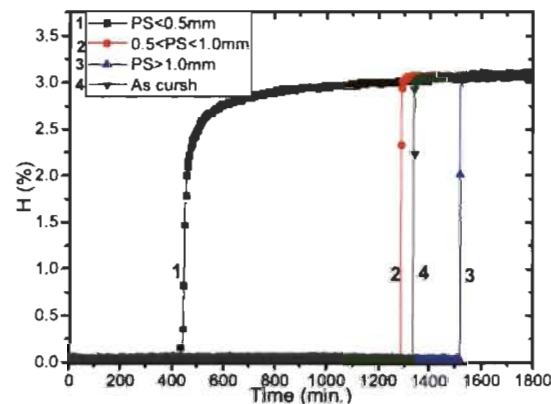


Fig. 4 – First hydrogenation curves of undoped 52Ti-12V-36Cr for different particle size and for the as-crushed sample.

Table 3 – Ratio of incubation time of doped and undoped samples with the same particle size.

Sample Description	$\frac{t_{\text{inc}}}{t_{\text{ref}}}$
As-crushed	335
PS < 0.5 mm	1447
0.5 < PS < 1.0 mm	640
PS > 1.0 mm	127

Table 4 – Effect of particle size on incubation.

Sample's ratio	Incubation (min.)	
	Doped	Undoped
$\frac{t_{\text{inc}}}{t_{\text{ref}}}$	6.7	2.9
$\frac{t_{\text{inc}}}{t_{\text{ref}}}$	40	3.5

doping and particle size deduction. Moreover, synergy between particle size and doping is more important for smaller particle size.

For both doped and undoped samples the hydrogenation kinetics is very fast after incubation time. The intrinsic kinetics were compared by taking the slope of each curve at half capacity (i.e. 1.5 wt.%). Results are listed in Table 5. The intrinsic kinetics of the doped samples are faster than their undoped counterparts. For the undoped particles, the intrinsic kinetics decreases with decreasing particle size with an almost tenfold decreases between the bigger particle and smaller ones. Such a trend is not seen for the doped samples. Actually the intrinsic kinetics of the intermediate size particles is smaller than the kinetics shown by bigger and smaller particles. But the main fact is that there is only a small variation of intrinsic kinetics amongst the doped samples. This shows that intrinsic kinetics is mainly due to the presence of doping element and particle size plays a negligible role.

From these results, it is clear that the most important factor for reducing incubation time is the chemical nature of the alloys and to a much lesser extent the particle size. The reduction of incubation time with decreases of particle size could be explained, in part, by the increases of specific surface area when average particle size is smaller. However, the reduction of incubation time with particle size is too important to be explained just by this fact. One possible explanation could be that small particles have a higher proportion of surface defects per unit area than the big particles. A higher number of defects means that there are more sites available for nucleation of a new phase, in the present case the hydride phase, which will result in a decrease of incubation time.

Another interesting fact shown by undoped and doped samples is that the as-crushed sample act as a monolithic sample. From the results of the sieved samples, one could expect that the as crushed samples will show three different activation steps, corresponding to each population. On the contrary, the as-crushed sample showed a single activation time which is close to the weighted average of the individual activation times. Therefore, this is a proof that there is a strong synergy between particles during the activation process and that the powder always act collectively no matter what is the size distribution.

Table 5 – Intrinsic kinetics of doped and undoped samples.

Sample Description	Intrinsic kinetics (%H/min.)	
	Doped	Undoped
As crush	5.55	0.42
PS < 0.5 mm	2.97	0.11
0.5 < PS < 1.0 mm	3.85	0.81
PS > 1.0 mm	6.80	0.98



## Conclusion

From this investigation, we were able to find the relative importance of particle size and chemical composition on the first hydrogenation (activation) of a Ti-V-Cr BCC solid solution alloy. We found that the chemical composition and presence of a second phase has a much bigger impact on decrease of incubation time than reduction of particle size. Thus, the most efficient ways to reduce activation time is to modify the chemical composition of the alloy. Moreover, doping has strong effect of the intrinsic kinetics of activation.

Reduction of particle size leads to a decrease of activation time but it could not be explained by increases of specific area alone. We also found that activation is a monolithic process where a mixture of different particle size will have an incubation time proportional to the average particle size.

## Acknowledgements

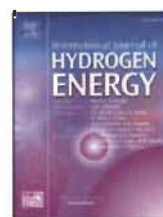
We would like to acknowledge the help of A. Lejeune for SEM micrographs. AK would like to thank Queen Elizabeth II Diamond Jubilee Scholarship for PhD fellowship. AK is grateful to Dr. K. M. Vasudevan Pillai, Chairman & CEO of Mahatma Education Society, Maharashtra, India for granting study leave at UQTR.

## REFERENCES

- [1] Bibienne T, Bobet J-L, Huot J. Crystal structure and hydrogen storage properties of body centered cubic 52Ti–12V–36Cr alloy doped with Zr<sub>7</sub>Ni<sub>10</sub>. *J Alloys Compd* 2014;607:251–7.
- [2] Miraglia S, de Rango P, Rivoirard S, Fruchart D, Charbonnier J, Skryabina N. Hydrogen sorption properties of compounds based on BCC Ti<sub>1-x</sub>V<sub>1-y</sub>Cr<sub>1+x+y</sub> alloys. *J Alloys Compd* 2012;536:1–6.
- [3] Lin HC, Lin KM, Wu KC, Hsiung HH, Tsai HK. Cyclic hydrogen absorption-desorption characteristics of TiCrV and alloys. *Int J Hydrogen Energy* 2007;32:4966–72.
- [4] Iba H, Akiba E. Hydrogen absorption and modulated structure in Ti–V–Mn alloys. *J Alloys Compd* 1997;253–254:21–4.
- [5] Cho S-W, Akiba E, Nakamura Y, Enoki H. Hydrogen isotope effects in Ti<sub>1.0</sub>Mn<sub>0.9</sub>V<sub>1.1</sub> and Ti<sub>1.0</sub>Cr<sub>1.5</sub>V<sub>1.5</sub> alloys. *J Alloys Compd* 2000;297:253–60.
- [6] Akiba E, Iba H. Hydrogen absorption by Laves phase related BCC solid solution. *Intermetallics* 1998;6:461–70.
- [7] Towata S-I, Noritake T, Itoh A, Aoki M, Miwa K. Effect of partial niobium and iron substitution on short-term cycle durability of hydrogen storage Ti–Cr–V alloys. *Int J Hydrogen Energy* 2013;38:3024–9.
- [8] Danaie M, Mauer C, Mitlin D, Huot J. Hydrogen storage in bulk Mg–Ti and Mg–stainless steel multilayer composites synthesized via accumulative roll-bonding (ARB). *Int J Hydrogen Energy* 2011;36:3022–36.
- [9] Dornheim M, Doppiu S, Barkhordarian G, Boesenberg U, Klassen T, Gutfleisch O, et al. Hydrogen storage in magnesium-based hydrides and hydride composites. *Scr Mater* 2007;56:841–6.
- [10] Bobet JL, Chevalier B, Song MY, Darriet B, Etourneau J. Hydrogen sorption of Mg-based mixtures elaborated by reactive mechanical grinding. *J Alloys Compd* 2002;336:292–6.
- [11] Varin RA, Czujko T, Wronski Z. Particle size, grain size and  $\gamma$ -MgH<sub>2</sub> effects on the desorption properties of nanocrystalline commercial magnesium hydride processed by controlled mechanical milling. *Nanotechnology* 2006;17:3856.
- [12] Huot J, Enoki H, Akiba E. Synthesis, phase transformation, and hydrogen storage properties of ball-milled TiV<sub>0.9</sub>Mn<sub>1.1</sub>. *J Alloys Compd* 2008;453:203–9.
- [13] Singh BK, Shim G, Cho S-W. Effects of mechanical milling on hydrogen storage properties of alloy. *Int J Hydrogen Energy* 2007;32:4961–5.
- [14] Bibienne T, Razafindramanana V, Bobet J-L, Huot J. Synthesis, characterization and hydrogen sorption properties of a Body Centered Cubic 42Ti–21V–37Cr alloy doped with Zr<sub>7</sub>Ni<sub>10</sub>. *J Alloys Compd* 2015;620:101–8.

Available online at [www.sciencedirect.com](http://www.sciencedirect.com)

ScienceDirect

journal homepage: [www.elsevier.com/locate/ijhe](http://www.elsevier.com/locate/ijhe)

## Effect of addition of Zr, Ni, and Zr-Ni alloy on the hydrogen absorption of Body Centred Cubic 52Ti-12V-36Cr alloy

Amol Kamble<sup>a,b,c</sup>, Pratibha Sharma<sup>b</sup>, Jacques Huot<sup>a,\*</sup><sup>a</sup> IRH, Université Du Québec à Trois-Rivières, Trois-Rivières, Quebec-G9A5H7, Canada<sup>b</sup> Department of Energy Science & Engineering, IIT Bombay, Mumbai, Maharashtra-400076, India<sup>c</sup> Department of Automobile Engineering, PHCET, Rasayani, Maharashtra-410207, India

### ARTICLE INFO

#### Article history:

Received 23 October 2017

Received in revised form

15 February 2018

Accepted 17 February 2018

Available online 19 March 2018

#### Keywords:

Metal hydrides

BCC alloys

Hydrogen storage

Secondary phase

### ABSTRACT

The effects of addition of Zr, Ni and  $Zr_7Ni_{10}$  on the crystal structure, microstructure and hydrogen absorption of Body Centred Cubic (BCC) 52Ti-12V-36Cr were investigated. We found that addition of Zr and/or Ni led to the formation of a Ni/Zr rich secondary phase. This secondary phase is responsible for the much faster first hydrogenation of the alloys with additives compared to the bare BCC alloy. Zirconium addition had positive influence on incubation time and intrinsic hydrogenation kinetics while nickel addition improved the hydrogen capacity. Among the additives tested,  $Zr_7Ni_{10}$  is the best for optimized hydrogenation kinetics and capacity.

© 2018 Hydrogen Energy Publications LLC. Published by Elsevier Ltd. All rights reserved.

### Introduction

Ti-V-Cr Body Centred Cubic (BCC) solid solutions can form hydrides of relatively high capacity which store hydrogen at room temperature under low hydrogen pressure [1–3]. The hydrogen capacity of these alloys has been reported to be 2–3 times more than traditional solid state hydrogen storage intermetallic alloys [1]. Usually, the first hydrogenation, the so-called activation, of BCC alloys is a lengthy and difficult process [2,4,5]. The reasons are still not well understood but presence of surface oxide could play a role. The traditional way to improve activation is heating/degassing at 300 °C–600 °C under dynamic vacuum before hydrogenation [6,7]. The step of heat treatment may be unwanted for industrial applications as it adds additional cost to the process.

The Ti-V-Cr BCC alloys attracted more attention in 1998, when Iba and Akiba reported 2.2wt% reversible hydrogen capacity at room temperature and atmospheric pressure [2,8]. It is frequently communicated that presence of a secondary phase is helping hydrogen absorption and induces notable improvement in hydrogen absorption kinetics [2,4,5,9,10]. This secondary phase may act as gateways for diffusion of hydrogen into the bulk of alloys. For example, Banerjee et al. have reported that improvement in hydrogen sorption of annealed  $Ti_2VCr + 5\% ZrFe_{1.5}V_{0.2}$  was due to induced Laves phases [11]. Miraglia et al. have shown that when cast 33Ti-30V-37Cr was remelted with addition of 4wt%  $Zr_7Ni_{10}$  the resulting alloy presented a shorten incubation time during the first hydrogenation without the need of any pre-hydrogenation treatment [5,12]. Later, Bibienne et al. reported negligible incubation time

\* Corresponding author.

E-mail addresses: [amol.kamble@gmail.com](mailto:amol.kamble@gmail.com) (A. Kamble), [jacques.huot@uqtr.ca](mailto:jacques.huot@uqtr.ca) (J. Huot).<https://doi.org/10.1016/j.ijhydene.2018.02.106>

0360-3199/© 2018 Hydrogen Energy Publications LLC. Published by Elsevier Ltd. All rights reserved.

in the activation of BCC 52Ti-12V-36Cr to which 4wt%Zr, Ni<sub>10</sub> was added and melted together [4].

In our previous work, we reported drastic reduction in incubation time and increase in intrinsic kinetics due to addition of 4wt%Zr to BCC 52Ti-12V-36Cr [10]. These results showed that the enhancement of activation kinetics is due to the presence of a secondary phase rich in zirconium and nickel. In order to understand the activation mechanism and relative effect of concentrations of Zr and Ni in additive, we studied the activation behaviour of BCC solid solution alloy 52Ti-12V-36Cr with addition of 4wt% Zr, Ni<sub>10</sub>, 4wt%Zr, 2.2wt% Zr and 4wt%Ni.

## Experimental

### Material synthesis

The raw materials Ti (sponge, 3–19 mm, 99.95%), V (granules, 1–3 mm, 99.7%), Cr (irregular pieces, 99%), Ni (wire, diameter 2 mm, 99.95%) and Zr (sponge, 0.8–25.4 mm, 99.5%) were

purchased from Alfa Aesar. Chunks of all raw elements were mixed according to the nominal composition and arc-melted. In order to get homogeneous samples, the cast pellets were turned over and remelted two more times. To avoid oxidation, the sample pellets were crushed into powder using a mortar and pestle in an argon-filled glovebox.

### Material characterization

X-ray diffraction (XRD) patterns of each sample powder before and after first hydrogenation was recorded on D8 Focus Bruker X-ray powder diffractometer with Cu K<sub>α</sub> radiation. The XRD patterns were further analyzed with Topas software [13,14] in order to determine crystal structure, lattice parameters and crystallite size.

Scanning Electron Microscopy was performed using JEOL scanning electron microscope JSM-5500 for back scattered electron (BSE) images. The elemental mapping distribution was captured by electron probe micro analysis coupled with Energy Dispersive Spectroscopy (EDS) for phase distribution and phase composition. The EDS apparatus from Oxford

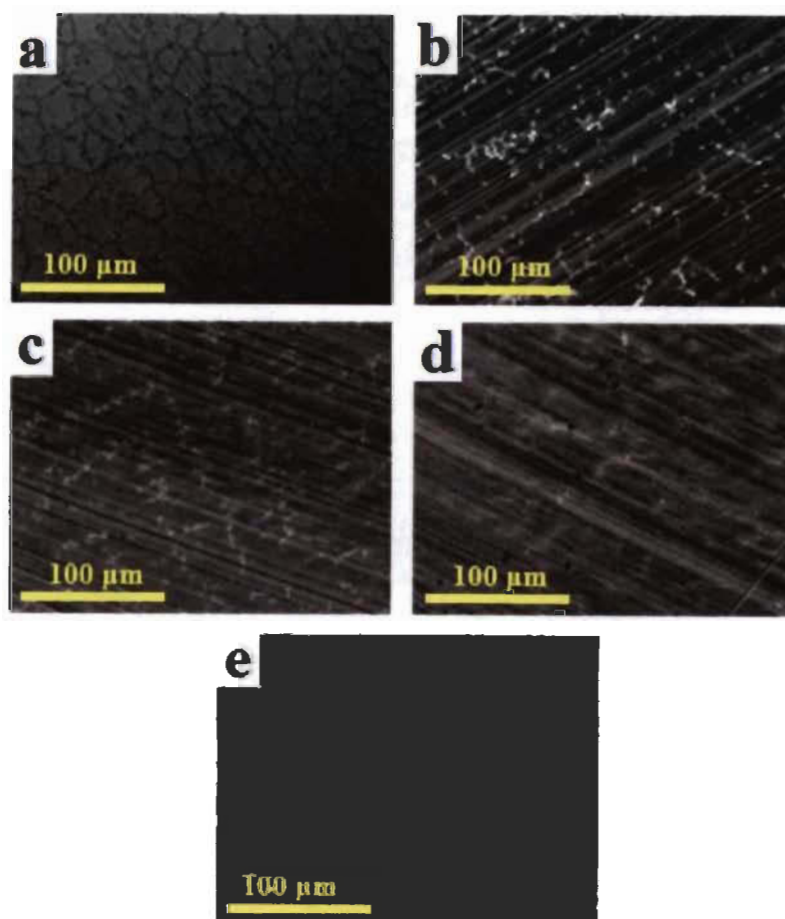


Fig. 1 – Backscattering electrons (BSE) SEM micrographs of as cast 52Ti-12V-36Cr without additive (a) and with 4wt% Zr, Ni<sub>10</sub> (b), 4wt%Zr (c), 2.2wt%Zr (d) and 4wt%Ni (e) additives.



Instrument was calibrated at the installation but no further calibration was performed prior to the present measurement. For this reason, the uncertainty on element abundance determined by EDS has been evaluated to be  $\pm 1$  at%. For each micrograph, the fractions of the surface occupied by each phase were determined by using ImageJ software [15,16]. First hydrogenation was measured at 298 K under 20 bar hydrogen pressure using a homemade hydrogen titration system.

## Results and discussion

### Microstructural study

#### Scanning Electron Microscopy

The alloy's microstructure presented in Fig. 1(a) shows that as-cast BCC 52Ti-12V-36Cr is essentially single phase with only a small amount of black intergranular precipitation. When this alloy is cast together with Zr/Ni based additives, a multi-phase system is produced as shown in Fig. 1(b–e). All compositions have a similar microstructure which is made of a dark matrix phase, a bright secondary phase and less abundant black precipitates. Analogous microstructure has been reported in the literature [4,5]. The black phase is seen only for nickel containing additive. In fact, the biggest proportion of black phase is seen for the alloy with 4wt% Ni addition.

The fractions of areas occupied by each phase are presented in Table 1. These numbers were determined by the analysis of one micrograph but, as the magnification of the micrographs was relatively small, each micrograph represent a large area and the statistic is relatively good. It shows that alloys with additives had a lower dark phase abundance. As expected, the alloy with only 2.2 wt% of Zr has a smaller

amount of bright phase. Addition of pure nickel increases the amount of black phase while addition of pure zirconium had the opposite effect.

#### Energy Dispersive X-ray spectroscopy

Different additives gave different abundance of secondary phase but the chemical composition should also be different. Bulk chemical composition was measured using Energy Dispersive X-ray Spectroscopy (EDS). The results are presented in Table 2. For all alloys, the measured nominal bulk compositions agree with nominal compositions.

The composition of each phase was also measured. Fig. 2 shows the localization of each measurement for all alloys. The grooves seen on a few micrographs are due to the roughness of the polishing. Except for the bare alloy, multiple measurements were taken on each individual phase. For all phases, individual measurements agree amongst themselves. Here, we report the chemical composition of the three spots corresponding to the dark phase, black phase, and bright phase.

The phase compositions for dark phase of each sample are reported in Table 3. We see that, for most of the alloys, the dark phase has composition very close to 52Ti-12V-36Cr. Only the alloys having Ni-containing additive shows a noticeable deviation from this stoichiometry. In this case, the Ti content is lower than the nominal one. Dark phases have low concentration of elements Zr and/or Ni. Only when pure nickel is added than the concentration of nickel in the dark phase is high. From this table, we see that the dark BCC phase could not accommodate the Zr and/or Ni atoms from the additive thus, forcing the formation of the secondary phase.

The atomic compositions of black phase in each sample are reported in Table 4. It is clear that the black phase has a high concentration of titanium, being essentially pure titanium for Ni-containing additive. For pure zirconium additive, the titanium content is much less. In these cases, chromium and vanadium content of black phase are also more important. It is interesting to note that, even if nickel favoured the formation of black phase, nickel is absent of that phase.

The phase compositions for bright phases are reported in Table 5. There is no bright phase in the sample without additive. For the alloys with additives, the bright phase is mainly constituted by titanium and chromium. Concentration of chromium is reduced when the additive contains nickel. In fact, it seems that nickel substitute with chromium in that

**Table 1** – Fraction of area (in %) occupied by each phase in as cast 52Ti-12V-36Cr alloys with and without additives. Calculation was performed on a randomly chosen single view.

Additive	Dark	Bright	Black
Without	97	–	3
4wt%Zr-Ni <sub>10</sub>	84	14	2
4wt%Zr	90	10	<1
2.2wt%Zr	94	5	1
4wt%Ni	85	9	6

**Table 2** – Element abundances as measured from EDS for bulk compositions of as cast 52Ti-12V-36Cr alloys with and without additives. Calculation was performed on a randomly chosen single view.

Additive		Ti	V	Cr	Zr	Ni
Without	Nominal composition	52	12	36	–	–
	Bulk measured composition	53	12	36	–	–
4wt%Zr-Ni <sub>10</sub>	Nominal composition	50.6	11.7	35.0	1.2	1.6
	Bulk measured composition	51	11	34	1	2
4wt%Zr	Nominal composition	50.9	11.7	35.2	2.2	–
	Bulk measured composition	52	11	34	2	–
2.2wt%Zr	Nominal composition	51.4	11.9	35.6	1.2	–
	Bulk measured composition	52	11	35	1	–
4wt%Ni	Nominal composition	50.3	11.6	34.8	–	3.3
	Bulk measured composition	50	14	33	–	3

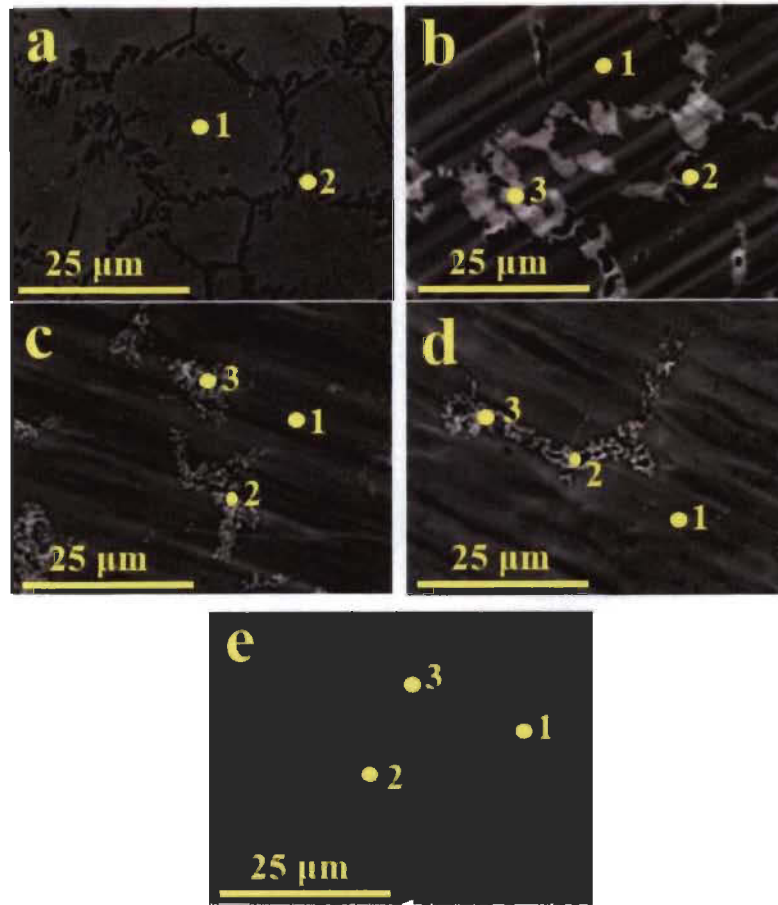


Fig. 2 – Point mapping of dark phase(1), black phase(2) and bright phase(3) on micrographs of as-cast BCC 52Ti-12V-36Cr without additive (a) and with 4wt% Zr<sub>7</sub>Ni<sub>10</sub> (b), 4wt%Zr (c), 2.2wt%Zr (d) and 4wt%Ni (e) additives.

phase. Considering the relative proportion of each phase, we could conclude that most of the zirconium/nickel is inside the bright phase. Similar situation has been reported in literature [4,5].

#### X-ray diffraction before hydrogenation

The X-ray diffraction (XRD) patterns for as-cast BCC 52Ti-12V-36Cr with and without additive are as shown in Fig. 3. In

the as-cast state, all alloys have the BCC crystal structure (S.G. Im-3m). Because of the relatively small abundance of secondary phases, the Bragg peaks of these phases are not noticeable in the patterns. Rietveld refinement was performed on all these patterns and the results are reported in Table 6. From this table it seems that addition of zirconium had for effect of reducing the crystallite size of the BCC phase even if this element is almost absent in BCC. On the other hand, adding nickel does not drastically change the

Table 3 – Chemical composition of dark phases in as cast 52Ti-12V-36Cr alloys with and without additives. Uncertainties are  $\pm 1$  at. %.

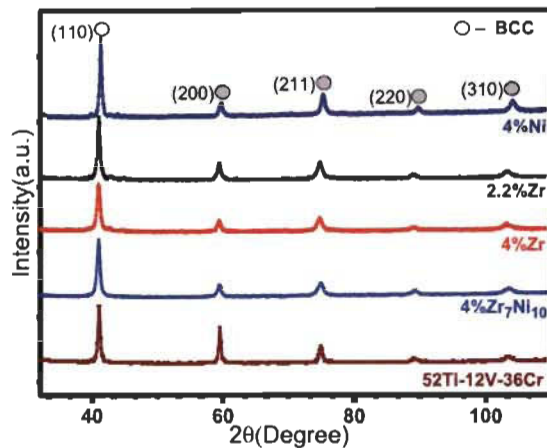
Additive	Ti	V	Cr	Zr	Ni
Without	53	12	35	–	–
4wt%Zr <sub>7</sub> Ni <sub>10</sub>	50	12	36	1	1
4wt%Zr	52	12	34	1	–
2.2wt%Zr	53	10	36	11	–
4wt%Ni	49	12	34	–	4

Table 4 – Chemical composition of black phases in as cast 52Ti-12V-36Cr alloys with and without additives. Uncertainties are  $\pm 1$  at. %.

Additive	Ti	V	Cr	Zr	Ni
Without	75	8	18	–	–
4wt%Zr <sub>7</sub> Ni <sub>10</sub>	91	1	2	5	0
4wt%Zr	60	12	26	2	–
2.2wt%Zr	55	9	29	6	–
4wt%Ni	97	2	1	–	0

**Table 5 – Chemical composition of bright phases in as cast 52Ti–12V–36Cr alloys with and without additives. Uncertainties are  $\pm 1$  at.%.**

Additive	Ti	V	Cr	Zr	Ni
Without	–	–	–	–	–
4wt%Zr <sub>7</sub> Ni <sub>10</sub>	40	7	38	8	7
4wt%Zr	42	9	40	9	–
2.2wt%Zr	43	8	42	7	–
4wt%Ni	44	8	36	–	12



**Fig. 3 – XRD patterns of as cast 52Ti–12V–36Cr alloys with and without additives.**

crystallite size even if the amount of nickel in the BCC phase is relatively high.

#### First hydrogenation

The first hydrogenation curves of BCC 52Ti–12V–36Cr alloys with and without additive are shown in Fig. 4. All curves show similar behaviour. There is some incubation time followed by a quick absorption. Clearly, the incubation time is strongly dependent on the nature of the additive but all additive studied reduced the incubation time by at least one order of magnitude. Therefore, we could conclude that multiphase have a positive effect on incubation time. Table 7 list the incubation time, full capacity, and slope at mid-capacity for all samples.

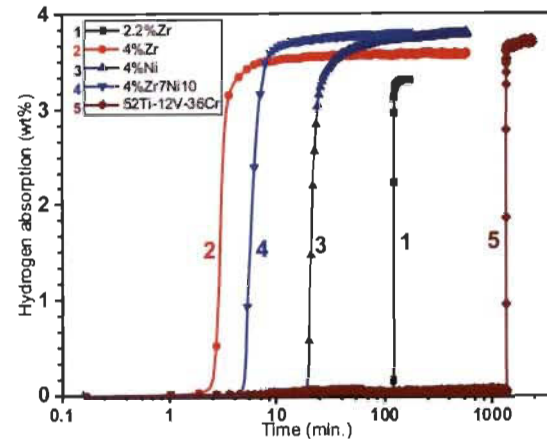


**Fig. 4 – First hydrogenation of as cast 52Ti–12V–36Cr alloys with and without additives.**

**Table 7 – Hydrogenation characteristics of 52Ti–12V–36Cr alloys with and without additive.**

Additive	Incubation time (min)	Hydrogen Capacity (wt.%)	Intrinsic kinetics (wt.%/min)
Without	1340	3.69	0.984
4wt% Zr <sub>7</sub> Ni <sub>10</sub>	4	3.76	1.7
4wt%Zr	2	3.62	6.66
2.2wt%Zr	120	3.31	2.55
4wt%Ni	19	3.78	0.91

From Fig. 4 and Table 7, it is clear that the main effect of additives is to reduce incubation time. The alloys with additives showed a reduction of incubation time of at least one order of magnitude up to more than two orders of magnitudes. The effect on capacity and intrinsic kinetics was much weaker. The intrinsic kinetics was faster by a factor of 7 for the best case. We see that zirconium is most effective to reduce incubation time but just 2.2 wt% of zirconium is not sufficient for getting a high capacity. Also, incubation time and intrinsic kinetics seem to be correlated. Shorter incubation time means gives faster intrinsic kinetics. In the case of nickel, its effect on incubation time is not as efficient as zirconium but it makes the capacity much higher. Therefore, the best compromise in

**Table 6 – Crystal structure parameters as determined by Rietveld refinement of 52Ti–12V–36Cr with and without additive. The number in parentheses is the error on the last significant digit.**

Additive	As-cast-BCC(Im-3m)		Hydrogenated-FCC(Fm-3m)		
	a(Å)	Crystallite Size(nm)	a(Å)	Crystallite Size(nm)	Microstrain(%)
Without	3.1066(5)	19.8(8)			
4wt%Zr <sub>7</sub> Ni <sub>10</sub>	3.1110(7)	11.3(2)	4.334(1)	12.0(6)	1.00(6)
4wt%Zr	3.1116(7)	10.3(2)	4.3444(9)	11.6(4)	1.10(4)
2.2wt%Zr	3.1091(6)	13.1(3)	4.341(2)	9.6(4)	0.5(1)
4wt%Ni	3.0933(4)	17.1(3)	4.330(1)	10.8(4)	1.06(5)



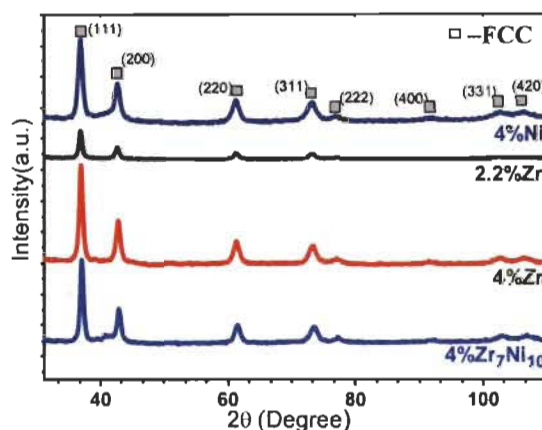


Fig. 5 – XRD patterns of hydrogenated 52Ti-12V-36Cr alloy with and without additives.

terms of high capacity and short incubation time is given by the additive  $Zr_7Ni_{10}$ . For this additive, the capacity reached is quite close to the theoretical full capacity of 4.08 wt%.

#### X-ray diffraction after hydrogenation

All alloys with and without additive absorbed hydrogen and, as expected, their patterns are a FCC (Face Centred Cubic) crystal structure (Space group Fm-3m) as shown in Fig. 5.

All patterns were analyzed by Rietveld refinement and the results are presented in Table 6. The lattice parameters of all hydrogenated alloys are practically the same, as well as their crystallite size. The hydrogenated alloys also presented a small amount of microstrain due to expansion of the unit cell upon hydrogenation.

#### Conclusions

The investigation of crystal structure, microstructure and hydrogen absorption properties of BCC 52Ti-12V-36Cr without and with additives 4wt%  $Zr_7Ni_{10}$ , 4wt%Zr, 2.2wt%Zr and 4wt% Ni was carried out. All as-cast alloys have a main BCC phase but the ones with additives present a microstructure made up of at least one secondary phase.

Without additive, the first hydrogenation of 52Ti-12V-36Cr is very lengthy. Adding Zr and/or Ni drastically reduced the incubation time of hydrogenation.

The sample with additive 4wt%Zr exhibited the smallest incubation and fastest intrinsic kinetic. It seems that the presence of zirconium influences the incubation time and kinetics. In the case of nickel addition, it favoured an increase of capacity. Thus, due to synergetic effect, the additive 4wt%  $Zr_7Ni_{10}$  stands as most effective additive with low incubation time and high hydrogen capacity.

#### Acknowledgements

We would like to acknowledge the help of C. Gosselin and Marie-Eve Marchand Lamarche for laboratory work. AK would like to thank Queen Elizabeth II Diamond Jubilee Scholarship for PhD fellowship. AK is appreciative to his wife, Anjali for her moral support.

#### REFERENCES

- [1] Sakintuna B, Lamari-Darkrim F, Hirscher M. Metal hydride materials for solid hydrogen storage: a review. *Int J Hydrogen Energy* 2007;32:1121–40.
- [2] Akiba E, Iba H. Hydrogen absorption by Laves phase related BCC solid solution. *Intermetallics* 1998;6:461–70.
- [3] Kabutomori T, Takeda H, Wakisaka Y, Ohnishi K. Hydrogen absorption properties of TiCrA (A = V, Mo or other transition metal) B.C.C. solid solution alloys. *J Alloy Comp* 1995;231:528–32.
- [4] Bibienne T, Bobet J-L, Huot J. Crystal structure and hydrogen storage properties of body centered cubic 52Ti-12V-36Cr alloy doped with  $Zr_7Ni_{10}$ . *J Alloy Comp* 2014;607:251–7.
- [5] Miraglia S, de Rango P, Rivoirard S, Fruchart D, Charbonnier J, Skryabina N. Hydrogen sorption properties of compounds based on BCC Ti1-xV1-yCr1+x+y alloys. *J Alloy Comp* 2012;536:1–6.
- [6] Yoo J-H, Shim G, Park C-N, Kim W-B, Cho S-W. Influence of Mn or Mn plus Fe on the hydrogen storage properties of the Ti-Cr-V alloy. *Int J Hydrogen Energy* 2009;34:9116–21.
- [7] Lin HC, Lin KM, Wu KC, Hsiung HH, Tsai HK. Cyclic hydrogen absorption-desorption characteristics of TiCrV and alloys. *Int J Hydrogen Energy* 2007;32:4966–72.
- [8] Iba H, Akiba E. Hydrogen absorption and modulated structure in Ti-V-Mn alloys. *J Alloy Comp* 1997;253–254:21–4.
- [9] Cho S-W, Akiba E, Nakamura Y, Enoki H. Hydrogen isotope effects in Ti1.0Mn0.9V1.1 and Ti1.0Cr1.5V1.7 alloys. *J Alloy Comp* 2000;297:253–60.
- [10] Kamble A, Sharma P, Huot J. Effect of doping and particle size on hydrogen absorption properties of BCC solid solution 52Ti-12V-36Cr. *Int J Hydrogen Energy* 2017;42:11523–7.
- [11] Banerjee S, Kumar A, Ruz P, Sengupta P. Influence of Laves phase on microstructure and hydrogen storage properties of Ti-Cr-V based alloy. *Int J Hydrogen Energy* 2016;41:18130–40.
- [12] Charbonnier J, De RP, Fruchart D, Miraglia S, Rivoirard S, Skryabina N. Pulverulent intermetallic materials for the reversible storage of hydrogen. Google Patents; 2007.
- [13] [https://www.bruker.com/fileadmin/user\\_upload/8-PDF-Docs/X-rayDiffraction\\_ElementalAnalysis/XRD/Flyers/TOFAS\\_Flyer\\_DOC-H88-EXS013\\_V2\\_en\\_high.pdf](https://www.bruker.com/fileadmin/user_upload/8-PDF-Docs/X-rayDiffraction_ElementalAnalysis/XRD/Flyers/TOFAS_Flyer_DOC-H88-EXS013_V2_en_high.pdf) [Accessed on 15 September 2017].
- [14] Cheary RW, Coelho AA, Cline JP. Fundamental parameters line profile fitting in laboratory diffractometers. *J Res Natl Inst Stand Technol* 2004;109:1–25.
- [15] Collins T. ImageJ for microscopy. *BioTechniques* 2007;43:S25–30. <http://dx.doi.org/10.1001/1071.12517>.
- [16] Abramoff MD, Magalhães PJ, Ram SJ. Image processing with ImageJ. *Biophot Int* 2004;11(7):36–42.

## Manuscript Details

Manuscript number	PNSMI_2018_808
Title	Effect of annealing on crystal structure, microstructure and hydrogenation behaviour of BCC 52Ti-12V-36Cr alloys with Zr, Ni and Zr-Ni additives.
Article type	Full Length Article

### Abstract

The effect of heat treatment at 1273K for 1 week on the first hydrogenation of Body Centred Cubic (BCC) 52Ti-12V-36Cr alloys with zirconium and/or nickel additives was investigated. The BCC crystal structure turned into a complex pattern after heat treatment, containing mainly three phases BCC, C15- type Laves phase and  $\alpha$ -Ti. The network of minor secondary C15 phase was completely broken. The phase abundance of BCC phase was drastically reduced with increased abundance of C15 and  $\alpha$ -Ti phases. This resulted in the elimination of incubation time and faster first hydrogenation kinetics but also an important reduction of hydrogen capacity.

Keywords	Hydrogen storage; annealing; Ti-based metal hydrides; Laves phase; Ti-V-Cr BCC alloy
Taxonomy	Materials Characterization, Alloys, Energy Storage Materials, Materials Processing
Corresponding Author	Amol Kamble
Corresponding Author's Institution	D Y Patil School of Engineering Academy, Ambli
Order of Authors	Amol Kamble, Pratibha Sharma, Jacques Huot
Suggested reviewers	Pio Aguiar, Martin Sahlgren, Suwarno Suwarno

## Submission Files Included in this PDF

### File Name [File Type]

Cover letter.docx [Cover Letter]

Highlights-Heat Treatment.docx [Highlights]

Graphical Abstract-Heat Treatment.docx [Graphical Abstract]

Title Page-Heat treatment.docx [Title Page (with Author Details)]

Manuscript-Heat Treatment.docx [Manuscript (without Author Details)]

Figures-Heat Treatment.docx [Figure]

Tables-Heat Treatment.docx [Table]

To view all the submission files, including those not included in the PDF, click on the manuscript title on your EVISE Homepage, then click 'Download zip file'.

## Research Data Related to this Submission

There are no linked research data sets for this submission. The following reason is given:  
Data will be made available on request



**Institut de Recherche sur l'Hydrogène**  
Université du Québec à Trois-Rivières  
C.P. 500, Trois-Rivières (Québec) Canada G9A 5H7

November 24, 2018

Dr. Y. Han  
Editor-in-Chief,  
Chinese Materials Research Society,  
China

**Subject:** Manuscript- *Effect of annealing on crystal structure, microstructure and hydrogen absorption properties of BCC 52Ti12V-36Cr alloys with additives 4wt%Zr<sub>7</sub>Ni<sub>10</sub>, 4wt%Zr, 2.2wt%Zr, and 4wt%Ni.*

Dear Dr. Y. Han

On behalf of all authors I would like to submit our paper entitled Effect of heat treatment on crystal structure, microstructure and hydrogen absorption properties of BCC 52Ti12V-36Cr alloys with additives 4wt%Zr<sub>7</sub>Ni<sub>10</sub>, 4wt%Zr, 2.2wt%Zr, and 4wt%Ni for publication in **Progress in Natural Science; Materials International**. This paper is in fact a continuation of our work on doping BCC alloy which was published in IJHE (Kamble, A., P. Sharma, and J. Huot, Effect of addition of Zr, Ni, and Zr-Ni alloy on the hydrogen absorption of Body Centred Cubic 52Ti-12V-36Cr alloy. International Journal of Hydrogen Energy, 2018. 43(15): p. 7424-7429). In the present paper, the effect of heat treatment on the first hydrogenation of 52Ti-12V-36Cr alloy with zirconium and/or nickel additives is reported. It was found that heat treatment resulted in the elimination of incubation time and faster first hydrogenation kinetics but also an important reduction of hydrogen capacity.

We will gladly answer all questions and comments of the referees assigned to our paper.

Sincerely,

Jacques Huot

Professor, Chemistry, Biochemistry and Physics department  
Université du Québec à Trois-Rivières and Hydrogen Research Institute  
3351 des Forges, CP 500, Trois-Rivières (Qc) G9A 5H7, Canada  
Tel: 1-819-376-5011 ext.3576  
Fax: 1-819-376-5164,

e-mail: [jacques.huot@uqtr.ca](mailto:jacques.huot@uqtr.ca)

## Effect of annealing on crystal structure, microstructure and hydrogenation behaviour of BCC 52Ti-12V-36Cr alloys with Zr, Ni and Zr-Ni additives.

### Abstract-

The effect of heat treatment at 1273K for 1 week on the first hydrogenation of Body Centred Cubic (BCC) 52Ti-12V-36Cr alloys with zirconium and/or nickel additives was investigated. The BCC crystal structure turned into a complex pattern after heat treatment, containing mainly three phases BCC, C15- type Laves phase and  $\alpha$ -Ti. The network of minor secondary C15 phase was completely broken. The phase abundance of BCC phase was drastically reduced with increased abundance of C15 and  $\alpha$ -Ti phases. This resulted in the elimination of incubation time and faster first hydrogenation kinetics but also an important reduction of hydrogen capacity.

**Keywords-** Hydrogen storage, annealing, Ti-based metal hydrides, Laves phase, Ti-V-Cr BCC alloy.

### 1. Introduction-

Titanium-based solid solution body centred cubic (BCC) alloys are considered to be interesting candidates for hydrogen storage, because of their high hydrogen capacity (around 3.5wt%) at room temperature under low hydrogen pressure (less than 2 MPa) [1-4]. However, the reversible capacity of these alloys is usually around 2 wt.% due to the very stable plateau pressure of the monohydride [2]. Heat treatment is one of the efficient ways to change crystal structure, phase distribution and phase compositions [5]. The respective effect of additive and heat treatment has been investigated by many researchers. For example, Liu et al. presented an effective improvement in flatness of the plateau after heat treatment due to homogenization of the microstructure of  $\text{Ti}_{32}\text{Cr}_{46}\text{V}_{22}$  [6]. They also showed that the flatness of the plateau improved further for heat treated  $\text{Ti}_{32}\text{Cr}_{46}\text{V}_{22} + 4\text{at}\% \text{Ce}$ . This amelioration in hydrogen capacity was due to reduction of oxygen concentration and homogenization of microstructure. Hang et al. reported the presence of C14-type Laves phase and BCC phase, before and after annealing of  $\text{Ti}_{10}\text{V}_{77}\text{Cr}_6\text{Fe}_6\text{Zr}$  [7]. The BCC phase abundance increased after annealing and the hydrogenation plateau pressure was flattened. The total hydrogen capacity was reduced but the reversible capacity increased. Zhou et al. mentioned the presence of C14-type Laves phase after annealing in a previously single-phase BCC  $\text{V}_{35}\text{Ti}_{20}\text{Cr}_{45}$  alloy [4]. The first hydrogenation (activation) performance and kinetic properties were improved greatly after annealing due to the presence of C14-type Laves phase. Young et. al. reported that, in  $\text{Ti}_{15.6}\text{Zr}_{2.1}\text{V}_{40.0}\text{Cr}_{11.2}\text{Mn}_{6.9}\text{Co}_{1.4}\text{Ni}_{22.5}\text{Al}_{0.3}$  alloy, C14-type Laves phase and TiNi are present in the as-cast alloy while  $\text{Ti}_2\text{Ni}$  and  $\sigma$ -VNi phases are seen after annealing [8]. They optimized annealing temperature and holding time on the basis of abundance of hydrogen absorbing BCC phase. They reported that annealing at 1173 K for 12 hours resulted in an alloy with high phase abundance of BCC phase. Banerjee et al. also mentioned the appearance of the C15-type Laves phase when  $\text{Ti}_2\text{CrV}$  alloy with additive  $\text{ZrFe}_{1.8}\text{V}_{0.2}$  was annealed at 1173K for 2 days. The coexistence of C15-type Laves phase with BCC  $\text{Ti}_2\text{CrV}$  led to quick hydrogenation. They also pointed out reduction of hydrogen capacity with increased concentration of additive [9].



The addition of Zr-Ni-based intermetallic has been used for the improvement of hydrogen storage properties of Ti-V-Cr alloys [10-14]. Miraglia et al. first showed that the addition of 4wt%  $Zr_7Ni_{10}$  to BCC alloy greatly improves the first hydrogenation kinetics [10]. Later, Bibienne et al. studied different BCC compositions as well as different synthesis processes and confirmed that first hydrogenation improvement is due to presence of Zr-Ni rich secondary phase [11-12]. In a previous investigation on 52Ti-12V-36Cr alloy melted together with Zr and/or Ni, we found that the additive has significant impact over first hydrogenation in terms of shortened incubation time and faster hydrogen absorption [13]. Addition of Zr had a stronger influence on kinetics while addition of Ni tends to increase capacity. From another investigation of the same composition, it was concluded that, for this system, the chemical composition has a greater impact on activation behaviour than reduction of particle size [14].

In these previous investigations, alloys were characterized in their as-cast state. However, multiphase alloys may be metastable and therefore, the hydrogen sorption properties found may be dependent on this metastability. In a recent paper, we have shown that first hydrogenation of 52Ti-12V-36Cr alloy without additive is extremely lengthy [14]. In a subsequent paper, we reported the first hydrogenation of 52Ti-12V-36Cr alloy with the additives 4wt%  $Zr_7Ni_{10}$ , 4wt%Zr, 2.2wt%Zr, and 4wt%Ni [13]. In the present paper, we report the investigation on the effect of heat treatment on crystal structure, microstructure and hydrogen storage properties of the BCC 52Ti-12V-36Cr alloy with additives.

## 2. Materials & methods

The raw materials Ti (sponge, 3-19 mm, 99.95%), V (granules, 1-3 mm, 99.7%), Cr (pieces, irregular, 99%) Ni (wire, diameter 2 mm, 99.95%) and Zr (sponge, 0.8-25.4 mm, 99.5%) were purchased from Alfa Aesar. Raw elements were mixed in the proper stoichiometry of nominal composition 52Ti-12V-36Cr with additives 4wt% $Zr_7Ni_{10}$ , 4wt%Zr, 2.2wt%Zr, and 4wt%Ni. The raw mixtures were arc melted under argon using a Centorr Associates Inc arc melting apparatus. In order to get homogeneous samples, the ingots were remelted three times with turning over after each melting. As cast samples were further annealed under argon at 1273K [8-9, 15] for one week in a Branstead Thermolyne type tubular furnace. To avoid oxidation of hot annealed pellets, pellets were cooled to room temperature inside the furnace under continuous flow of argon. As the surface of heat-treated pellets was still partially oxidized due to residual oxygen in the argon flow, the oxide was removed using sand paper and acetone.

The sample pellets were crushed into powder using a mortar and pestle inside an argon-filled glovebox. X-ray diffraction (XRD) patterns of each sample before and after first hydrogenation were obtained using a D8 Focus Bruker X-ray diffractometer with Cu  $K_\alpha$  radiation. The XRD patterns were further analyzed using the Rietveld method with Topas software to determine crystal structure, lattice parameters, microstrain and crystallite size [16-17].

Scanning Electron Microscopy (SEM) was performed using a JEOL scanning electron microscope JSM-5500. The micrographs were analyzed with ImageJ software [18-19] for phase abundance. The elemental mapping distribution was captured by electron probe micro analysis (EPMA) coupled with Energy Dispersive Spectroscopy (EDS) to measure bulk and



individual phase compositions. First hydrogenation was measured at 298K under 2 MPa hydrogen pressure using a homemade hydrogen titration system.

### 3. Results & Discussions

#### 3.1 Microstructural study

The SEM micrographs of BCC 52Ti-12V-36Cr alloys with additive in as-cast and annealed states are shown in Fig. 1. The parallel lines seen in some micrographs are due to grinding media.

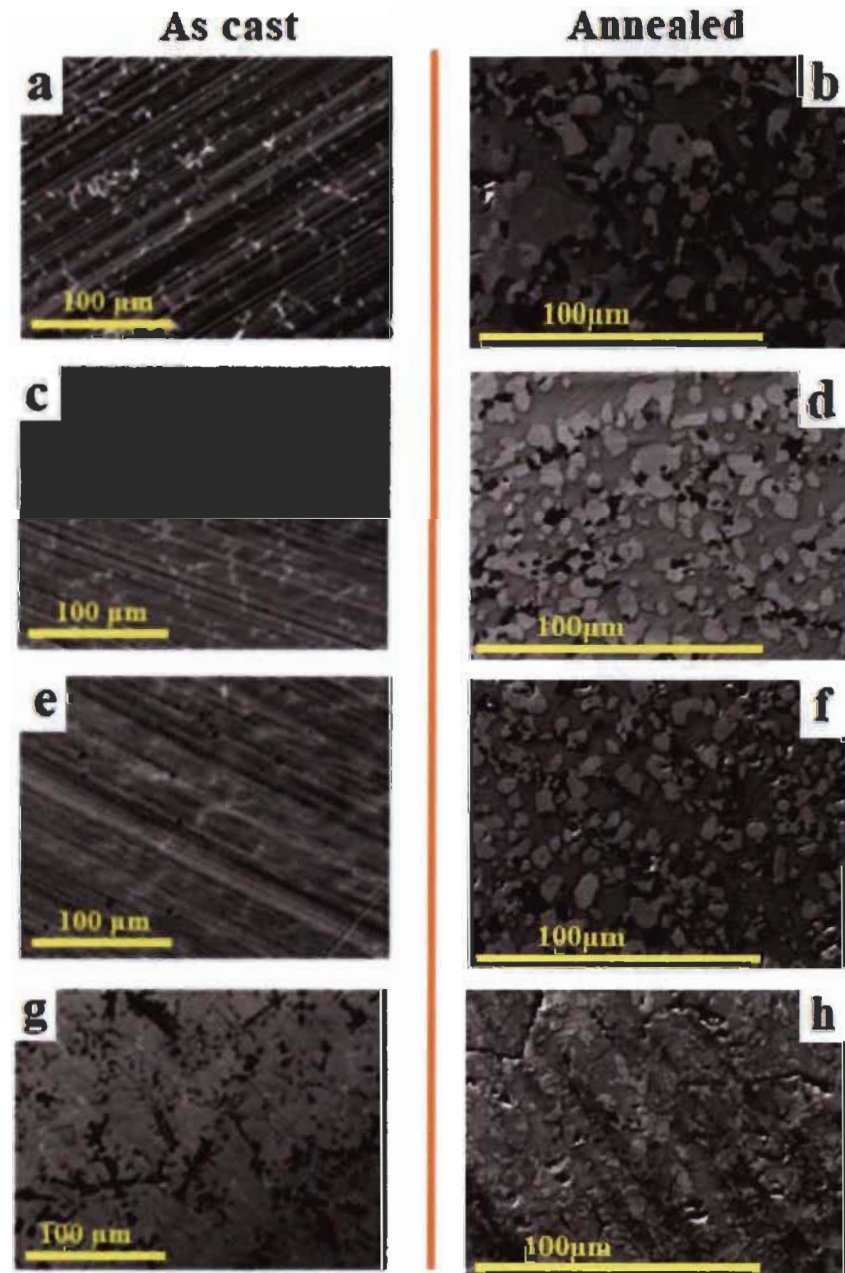


Fig. 1. Backscattering electrons (BSE) SEM micrographs of the as cast (Left) and annealed (Right) BCC 52Ti-12V-36Cr alloy with 4wt%  $Zr_7Ni_{10}$  (a, b), 4wt%Zr (c, d), 2.2wt%Zr (e, f) and 4wt%Ni (g, h) additives.

The as cast samples with additive showed similarity among themselves. They all have a main dark phase with a network of minor bright phase and some black precipitates. The micrographs of annealed samples show that the microstructure drastically change upon heat treatment. The network of minor bright phase seen in the as-cast alloy is completely broken after heat treatment. The fractional area occupied by each phase was measured using ImageJ and is reported in Table 1.

**Table 1. Fraction area (in %) occupied by each phase in as-cast and annealed BCC 52Ti-12V-36Cr with additives. Uncertainty on each measurement is  $\pm 1\%$ .**

Additive	As-cast			Annealed		
	Dark	Bright	Black	Dark	Bright	Black
4wt%Zr <sub>7</sub> Ni <sub>10</sub>	84	14	2	34	52	14
4wt%Zr	90	10	<1	30	56	14
2.2wt%Zr	94	5	1	29	52	19
4wt%Ni	85	9	6	36	56	8

From Table 1, we could see that the black precipitate abundance greatly increased upon heat treatment except with the 4wt%Ni additive. For all alloys, the abundance of dark phase significantly decreases while the bright phase abundance increases. It could be noticed that the black phase usually precipitates alongside or within the bright phase.

In order to understand more about phases and their compositions, Energy Dispersive Spectroscopy (EDS) was performed. The EDS measurements for bulk composition are presented in Table 2. For all samples, the bulk measured composition agreed with the nominal one.

**Table 2. Element abundances as measured from EDS for bulk compositions of annealed 52Ti-12V-36Cr alloys with additives. Uncertainties on measured composition are  $\pm 1$  at%.**

Additive		Ti	V	Cr	Ni	Zr
4wt%Zr <sub>7</sub> Ni <sub>10</sub>	Nominal	50.55	11.67	34.99	1.15	1.64
	Bulk Measured	54	11	32	1	2
4wt%Zr	Nominal	50.85	11.73	35.2	2.22	-
	Bulk Measured	52	12	34	2	-
2.2wt%Zr	Nominal	51.36	11.85	35.56	1.22	-
	Bulk Measured	53	11	35	1	-
4wt%Ni	Nominal	50.28	11.61	34.81	-	3.3
	Bulk Measured	51	12	33	-	4

The EDS point mapping was carried out to measure the chemical compositions of each individual phase. The measurements were taken at multiple locations on micrographs. Fig. 2 shows the localization of each point. For each phase in each alloy, measurements on different localization agree among themselves within experimental error. The phase compositions for dark phases and bright phases before and after heat treatment are reported in Table 3 and Table 4 respectively.

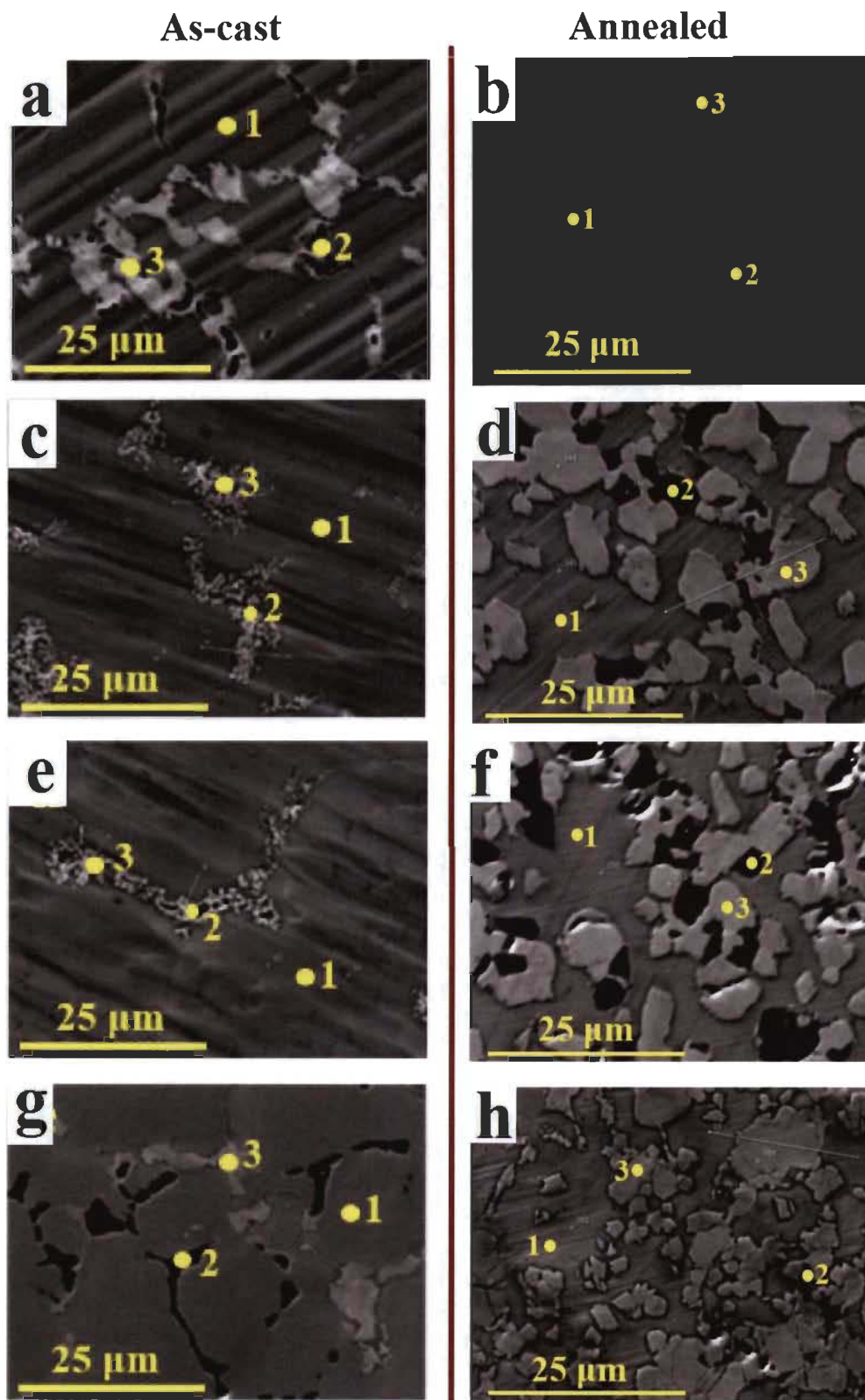


Fig. 2. Point mapping of dark phase (1), black phase (2) and bright phase (3) on micrographs of as cast (left) and annealed (right) BCC 52Ti-12V-36Cr with 4wt%  $Zr_7Ni_{10}$  (a, b), 4wt%Zr (c, d), 2.2wt%Zr (e, f) and 4wt%Ni (g, h) additives.

**Table 3. Chemical composition of dark phases in 52Ti-12V-36Cr alloys with additives. Uncertainties on measured composition are  $\pm 1$  at%.**

Additive	As-cast (at%)					Annealed (at%)				
	Ti	V	Cr	Zr	Ni	Ti	V	Cr	Zr	Ni
4wt%Zr <sub>7</sub> Ni <sub>10</sub>	50	12	36	1	1	59	7	29	2	3
4wt%Zr	52	12	34	1	-	61	15	23	<1	-
2.2wt%Zr	53	10	36	1	-	56	15	28	1	-
4wt%Ni	49	12	34	-	4	53	16	29	-	2

For as-cast samples, the dark phase has chemical composition near the bulk nominal composition for all additives. It should be pointed out that nickel seems to be much easier to enter the dark phase than zirconium. It also seems that nickel replace titanium in the dark phase.

For heat treated samples, the dark phase chemical composition change depending on the type of additive. The titanium abundance in the dark phase increases with the amount of zirconium in additive and the chromium abundance decreases in the same proportions except for 2.2 wt.% Zr additives. When both zirconium and nickel are added, the main effect is an important reduction of vanadium content compared to the annealed samples with other additives.

From Fig. 1 and Fig. 2, it could be seen that a minor bright secondary phase co-exists with dark primary phase. The composition of this bright phase before and after heat treatment is shown in Table 4. In the as-cast alloys, the composition of the bright phase does not change much with the proportion or nature of additive. However, it seems that nickel has a tendency to substitute for chromium.

**Table 4. Chemical composition of bright phases in 52Ti-12V-36Cr alloys with additives. Uncertainties on measured composition are  $\pm 1$  at%.**

Additive	As-cast (at%)					Annealed (at%)				
	Ti	V	Cr	Zr	Ni	Ti	V	Cr	Zr	Ni
4wt%Zr <sub>7</sub> Ni <sub>10</sub>	40	7	38	8	7	33	10	54	3	<1
4wt%Zr	42	9	40	9	-	32	9	55	4	-
2.2wt%Zr	43	8	42	7	-	31	9	56	4	-
4wt%Ni	44	8	36	-	12	62	4	14	-	20

After heat treatment, the chemical composition of the bright phase drastically changed. The most important change was seen for the 4 wt.% Ni additive. The proportion of titanium increased, and nickel is the second most abundant element in that phase. The other alloys have very similar chemical composition. In fact, the stoichiometry is near TiCr<sub>2</sub>.

The phase composition for black precipitates was measured to be basically titanium precipitates and is shown in Table 5. For as-cast samples, the precipitation of titanium in black phase was more abundant in the case of Ni additive even though no nickel was present in that phase. In case of pure Zr additives, titanium proportion was more than 70% and chromium was the second most abundant element.



**Table 5.** Chemical composition of black phases in 52Ti-12V-36Cr alloys with additives. Uncertainties on measured composition are  $\pm 1$  at%.

Additive	As-cast (at%)					Annealed (at%)				
	Ti	V	Cr	Zr	Ni	Ti	V	Cr	Zr	Ni
4wt%Zr <sub>7</sub> Ni <sub>10</sub>	92	1	2	5	-	87	3	8	1	<1
4wt%Zr	74	6	16	4	-	94	1	1	4	-
2.2wt%Zr	72	6	21	1	-	95	1	1	3	-
4wt%Ni	94	3	3	-	-	76	6	14	-	4

Upon heat treatment, precipitation of practically pure titanium took place. The black phase of the alloy with 4wt%Zr<sub>7</sub>Ni<sub>10</sub> additive did not significantly change composition. In the case of Ni additive, the titanium proportion decreased compared to as-cast state and the chromium content increased. A small amount of nickel entered the black phase.

### 3.2 X-ray diffraction (XRD) before hydrogenation-

The X-ray diffraction patterns of the as-cast alloys have been shown in a previous paper [13]. For all alloys a BCC phase was detected. The lattice parameters for different alloys were around 3.1 Å and changing slightly with the amount and nature of additive. For all as-cast alloys, the amount of secondary (bright and black phases) were too small to be detected by X-ray diffraction.

The XRD patterns for heat treated BCC 52Ti-12V-36Cr with additive are shown in Fig. 3. These patterns are quite similar to each other and clearly indicate multi-phase alloys. Rietveld refinement was performed on all patterns and the results are reported in Table 6.

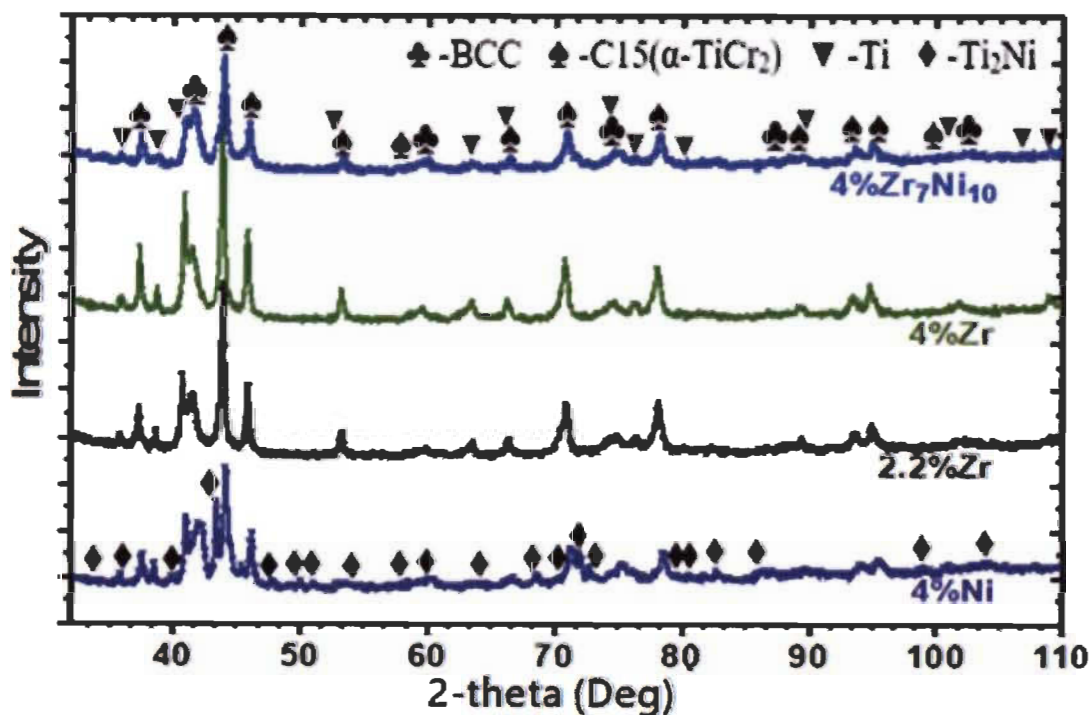


**Fig. 3.** XRD patterns of BCC 52Ti-12V-36Cr alloys with additive after heat treatment.

**Table 6.** Crystal structure parameters as determined by Rietveld's refinement of heat treated 52Ti-12V-36Cr with additive. The number in parentheses is the error on the last significant digit.

Additive	Crystal structure	Phase Abundance (%)	Lattice Parameter(Å)	Cell Volume(Å <sup>3</sup> )	Crystallite Size(nm)
4wt%Zr <sub>7</sub> Ni <sub>10</sub>	BCC	31	a = 3.148(1)	31.19(3)	6.6(3)
	α-TiCr <sub>2</sub>	55	a = 6.989(2)	341.4(3)	12.6(3)
	Ti	13	a = 2.968(1), c = 4.779(4)	36.45(4)	16(2)
4wt%Zr	BCC	30	a = 3.1579(9)	31.49(3)	5.8(2)
	α-TiCr <sub>2</sub>	55	a = 7.0002(7)	343.0(1)	24.1(6)
	Ti	15	a = 2.9736(4), c = 4.7774(8)	36.58(1)	63.662
2.2wt%Zr	BCC	28	a = 3.1463(8)	31.15(2)	6.3(3)
	α-TiCr <sub>2</sub>	53	a = 6.9922(9)	341.9(1)	21.9(5)
	Ti	19	a = 2.9717(6), c = 4.778(2)	36.54(2)	22(2)
4wt%Ni	BCC	38	a = 3.123(2)	30.47(5)	4.7(3)
	α-TiCr <sub>2</sub>	45	a = 6.961(2)	337.3(3)	12.5(5)
	Ti	12	a = 2.947(1), c = 4.802(4)	36.11(4)	47(15)
	Ti <sub>2</sub> Ni	6	a = 11.087(3)	1363(1)	140(60)

The XRD patterns of heat treated alloys revealed three main phases: BCC [Space Group (S.G.) Im-3m], C15-type Laves phase (α-TiCr<sub>2</sub>) [S.G. Fd-3m] and Ti [S.G. P6<sub>3</sub>/mmc]. In the case of 4wt%Ni additive, there were additional peaks of minor phase of Ti<sub>2</sub>Ni [S.G. Fd-3m]. Compared to the as-cast samples that were essentially 100% BCC, the abundance of the BCC phase of heat treated alloys was greatly reduced to about 30% with an increase of lattice parameters up to 3.15 Å. The change in the lattice parameter is most likely due to change in chemical composition of the BCC phase upon heat treatment [11]. The crystallite size also reduced from the range 10-20 nm before heat treatment to the range 4.5-6.5 nm after heat treatment. Usually, heat treatment result in increasing crystallite size contrary to what is observed here. However, in the present case, heat treatment transformed an alloy that was essentially single-phase BCC to a multiphase alloy. Also, the chemical composition of the BCC changed with heat treatment. These may be the reasons why crystallite size decreased upon heat treatment.

The C15 (α-TiCr<sub>2</sub>) phase in heat treated samples has an abundance near 45-55% as shown in Table 6. The bright phase of all samples has reported abundance of 52-56% in Table 1 and ratio of concentrations of Ti/Cr near to 2 as shown in Table 4. It indicates that C15 could be considered as the bright phase. In a similar way, Ti phase seen in the diffraction patterns could be associated with the black phase. Rietveld refinement revealed no microstrain. This is consistent with the process of heat treatment which is well known to relieve stresses.

### 3.3 First hydrogenation (Activation)

The first hydrogenation behaviour of the as-cast alloys has been reported before [13]. It was found that the as cast alloy without additive was very hard to activate with an incubation time of 22 hours. Alloys with additives presented a much shorter incubation time, varying from 2 to 20 minutes. The presence of zirconium in additive has an impact on the kinetics of hydrogen absorption while presence of nickel has influence on hydrogen capacity. The

additive 4wt%Zr<sub>7</sub>Ni<sub>10</sub> has been found to be the most effective, giving an incubation time of 4 min, a hydrogen capacity of 3.76% and a fast intrinsic kinetics.

The first hydrogenation curves for heat treated samples compared to as-cast ones are shown in Fig. 4. The heat treatment essentially eliminates incubation time. This is probably due to change in phase composition and refined microstructure with reduced crystallite size. After the incubation time, all as-cast samples showed very fast hydrogen absorption kinetics and the same hydrogen capacity. Unfortunately, the hydrogen capacity of all samples was reduced by 40 % after heat treatment. This diminution of capacity is most probably due to the reduction of the BCC phase upon heat treatment as shown in the diffraction patterns.

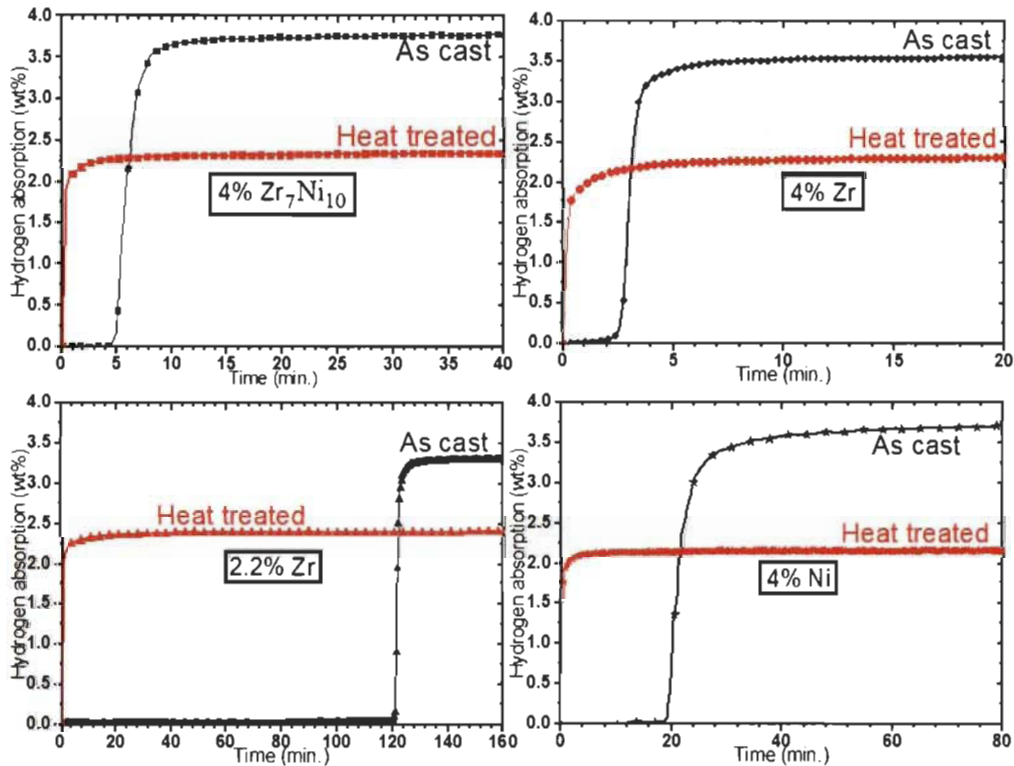


Fig. 4. First hydrogenation curves of heat treated BCC 52Ti-12V-36Cr with additive.

### 3.4 X-ray diffraction after hydrogenation

The XRD patterns of heat treated samples after hydrogenation are shown in Fig. 5. The complex patterns indicate multi-phase systems. Rietveld refinement was performed on the patterns to determine change in lattice parameters, crystallite size and phase abundance after hydrogenation. The results are presented in Table 7.

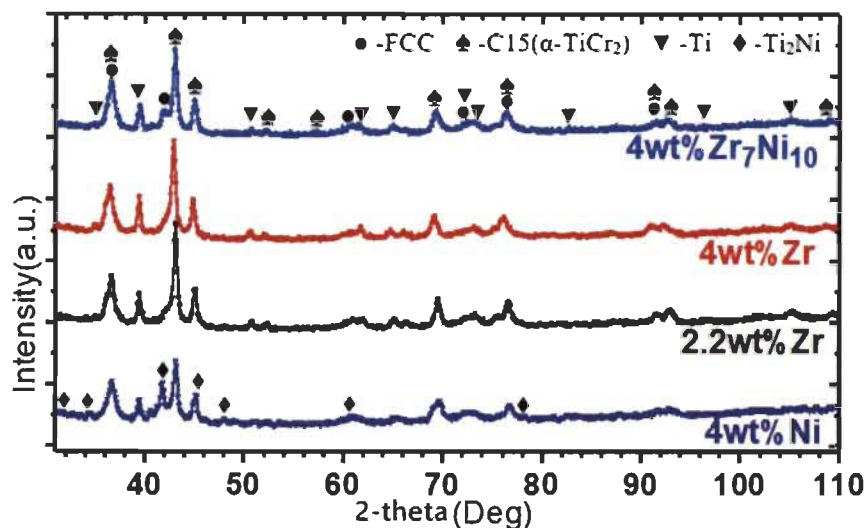


Fig. 5. XRD patterns of hydrogenated annealed BCC 52Ti-12V-36Cr with additive.

Table 7. Rietveld's refinement of annealed BCC 52Ti-12V-36Cr with additive after hydrogenation.

Additive	Crystal structure	Phase Abundance %	Lattice Parameter a, c Å	Cell Volume (Å <sup>3</sup> )	Crystallite Size (nm)	Microstrain (%)
4wt%Zr <sub>7</sub> Ni <sub>10</sub>	FCC	36(2)	a = 4.37(2)	83.5(1)	50(70)	0.85(3)
	α-TiCr <sub>2</sub>	58(2)	a = 7.13(2)	362.1(3)	12.7(4)	
	Ti	6(5)	a = 3.05(2), c = 5.07(2)	40.8(1)	11(10)	
4wt%Zr	FCC	25(1)	a = 4.37(2)	83.4(1)	7.3(2)	0.52(2)
	α-TiCr <sub>2</sub>	46(2)	a = 7.15(2)	364.8(2)	13.0(3)	
	Ti	30(2)	a = 3.04(3), c = 5.11(3)	40.9(2)	15.8(9)	
2.2wt%Zr	FCC	33(1)	a = 4.37(2)	83.2(1)	6.0(5)	0.41(2)
	α-TiCr <sub>2</sub>	52(1)	a = 7.12(2)	360.1(2)	15.4(3)	
	Ti	16(7)	a = 3.04(3), c = 5.10(1)	40.8(2)	14.8(9)	
4wt%Ni	FCC	30(2)	a = 4.36(3)	83.1(1)	15(8)	0.63(3)
	α-TiCr <sub>2</sub>	47(3)	a = 7.12(2)	360.7(4)	12.4(6)	
	Ti	9.3(1)	a = 3.03(3), c = 5.14(3)	40.9(1)	12(3)	
	Ti <sub>2</sub> Ni	14(2)	a = 11.53(3)	1534(2)		

For all alloys, three phases were identified: an FCC phase, a C15-type Laves phase and α-Ti. In the case of 4wt%Ni, additional Ti<sub>2</sub>Ni phase was also present. The abundance of the FCC phase could be seen to be close to the BCC phase abundance after heat treatment. This confirms that the BCC phase was fully hydrogenated and transformed into an FCC phase (γ-dihydride phase). However, the fully hydride phase has a theoretical capacity of 4 wt.%. Considering that the proportion of the FCC phase is between 25 and 36% then, the hydrogen capacity should be between 1 wt.% and 1.4 wt.%. This clearly does not match the measured capacity. That means there should be some more phases which are absorbing hydrogen. Thus, we measured the unit cell expansion after hydrogenation of the other phases present in



the diffraction patterns. The change in unit cell volume of each phase for all samples is reported in Table 8. By dividing the change of unit cell volume by the number of formula units per unit cell, the volume expansion per formula unit could be estimated. Number of formula units per unit cell for C15-type Laves phase, hexagonal  $\alpha$ -Ti, and  $\text{Ti}_2\text{Ni}$  are respectively 4, 2 and 32. Using the criterion that a hydrogen atom produces a volume expansion between 2 and 3  $\text{\AA}^3$  it was possible to estimate number of hydrogen atoms per formula unit. These results are reported in Table 8. It shows that C15-type Laves phase and  $\alpha$ -Ti seem to be mono-hydrided and additional the  $\text{Ti}_2\text{Ni}$ -like phase in the 4wt%Ni additive may be dihydride.

**Table 8. Change in unit cell volume of phases other than BCC due to hydrogenation of BCC 52Ti-12V-36Cr with additive.**

Additive	Phase	Expansion of unit Cell Volume, ( $\text{\AA}^3$ )	Expansion per formula unit ( $\text{\AA}^3$ )	Number of H atoms per formula unit
4wt% $\text{Zr}_7\text{Ni}_{10}$	Laves C15	20.7	2.58	1
	Ti	4.33	2.16	1
4wt%Zr	Laves C15	21.77	2.72	1
	Ti	4.34	2.17	1
2.2wt%Zr	Laves C15	18.24	2.28	1
	Ti	4.26	2.13	1
4wt%Ni	Laves C15	23.4	2.93	1
	Ti	4.34	2.17	1
	$\text{Ti}_2\text{Ni}$	171.2	5.3	2

The heat-treated samples with additive are multi-phase systems, containing BCC, Laves phase C15 and  $\alpha$ -Ti. However, even if these alloys are multiphase and more than one phase absorbs hydrogen, the kinetics of hydrogenation showed curves without obvious change of slope and/or kinks. Thus, the curves look like absorption of a single-phase alloy. This is consistent with the gateway mechanism proposed in previous papers where the secondary phase is acting as a gateway for hydrogen to enter the main phase and thus making the activation easier [10-11].

#### 4. Conclusions

The effect of heat treatment on microstructures, crystal structures and hydrogen absorption properties of BCC 52Ti-12V-36Cr alloy with additives 4wt% $\text{Zr}_7\text{Ni}_{10}$ , 4wt%Zr, 2.2wt%Zr and 4wt%Ni were investigated.

The BCC phase found in the as-cast alloys turned to a complex multi-phase structure upon heat treatment. For all compositions, similar multi-phase microstructures with BCC, C15 and Ti precipitates were observed after heat treatment. There was a drastic change in phase composition and distribution compared to the as-cast alloys.

The first hydrogenation (activation) of heat-treated alloys was studied. The elimination of incubation time by annealing is probably caused by the synergy of absorption of the different phases present in the heat-treated alloy before hydrogenation, change in phase compositions and homogenization of microstructure. However, the heat treatment had greatly reduced hydrogen capacity by 40%. The reduction in hydrogen capacity is probably due to the reduction of BCC phase abundance. The C15-type Laves phase and Ti-precipitates were

formed during heat treatment but, upon hydrogenation they seem to have turned into monohydrides. The hydrogenation showed single slope hydrogen absorption like single phase alloys even after containing more than one phase. It indicates synergy among the phases for hydrogen absorption and indicates a gateway mechanism.

### Acknowledgements-

We would like to acknowledge the help of A. Lejeune for SEM micrographs. AK would like to thank Queen Elizabeth II Diamond Jubilee Scholarship for PhD fellowship. AK is appreciative to D Y Patil School of Engineering Academy, Ambi, MH, India for its continuous support.

### Data availability Statement-

The raw/processed data required to reproduce these findings cannot be shared at this time due to legal or ethical reasons and also it is part of an ongoing study.

### References-

- [1] B. Sakintuna, F. Lamari-Darkrim, M. Hirscher, Metal hydride materials for solid hydrogen storage: A review, *International Journal of Hydrogen Energy*, 32 (2007) 1121-1140.
- [2] E. Akiba, H. Iba, Hydrogen absorption by Laves phase related BCC solid solution, *Intermetallics*, 6 (1998) 461-470.
- [3] T. Kabutomori, H. Takeda, Y. Wakisaka, K. Ohnishi, Hydrogen absorption properties of TiCrA ( $A \equiv V$ , Mo or other transition metal) B.C.C. solid solution alloys, *Journal of Alloys and Compounds*, 231 (1995) 528-532.
- [4] H.Y. Zhou, F. Wang, J. Wang, Z.M. Wang, Q.R. Yao, J.Q. Deng, C.Y. Tang, G.H. Rao, Hydrogen storage properties and thermal stability of V35Ti20Cr45 alloy by heat treatment, *International Journal of Hydrogen Energy*, 39 (2014) 14887-14895.
- [5] H.C. Lin, K.M. Lin, K.C. Wu, H.H. Hsiung, H.K. Tsai, Cyclic hydrogen absorption-desorption characteristics of TiCrV and alloys, *International Journal of Hydrogen Energy*, 32 (2007) 4966-4972.
- [6] X. Liu, L. Jiang, Z. Li, Z. Huang, S. Wang, Improve plateau property of Ti32Cr46V22 BCC alloy with heat treatment and Ce additive, *Journal of Alloys and Compounds*, 471 (2009) L36-L38.
- [7] Z. Hang, X. Xiao, S. Li, H. Ge, C. Chen, L. Chen, Influence of heat treatment on the microstructure and hydrogen storage properties of Ti<sub>10</sub>V<sub>77</sub>Cr<sub>6</sub>Fe<sub>6</sub>Zr alloy, *Journal of Alloys and Compounds*, 529 (2012) 128-133.
- [8] K. Young, T. Ouchi, J. Nei, L. Wang, Annealing effects on Laves phase-related body-centred-cubic solid solution metal hydride alloys, *Journal of Alloys and Compounds*, 654 (2016) 216-225.
- [9] S. Banerjee, A. Kumar, P. Ruz, P. Sengupta, Influence of Laves phase on microstructure and hydrogen storage properties of Ti-Cr-V based alloy, *International Journal of Hydrogen Energy*, 41 (2016) 18130-18140.
- [10] S. Miraglia, P. de Rango, S. Rivoirard, D. Fruchart, J. Charbonnier, N. Skryabina, Hydrogen sorption properties of compounds based on BCC Ti1-xV1-yCr1+x+y alloys, *Journal of Alloys & Compounds*, 536 (2012) 1-6.
- [11] T. Bibienne, J.-L. Bobet, J. Huot, Crystal structure and hydrogen storage properties of body centred cubic 52Ti-12V-36Cr alloy doped with Zr7Ni10, *Journal of Alloys & Compounds*, 607 (2014) 251-257.
- [12] T. Bibienne, V. Razafindramanana, J.-L. Bobet, J. Huot, Synthesis, characterization and hydrogen sorption properties of a Body Centred Cubic 42Ti-21V-37Cr alloy doped with Zr7Ni10, *Journal of Alloys & Compounds*, 620 (2015) 101-108.
- [13] A. Kamble, P. Sharma, J. Huot, Effect of addition of Zr, Ni, and Zr-Ni alloy on the hydrogen absorption of Body Centred Cubic 52Ti-12V-36Cr alloy, *International Journal of Hydrogen Energy*, 43 (2018) 7424-7429.
- [14] A. Kamble, P. Sharma, J. Huot, Effect of doping and particle size on hydrogen absorption properties of BCC solid solution 52Ti-12V-36Cr, *International Journal of Hydrogen Energy*, 42 (2017) 11523-11527.
- [15] M. Enomoto, The Cr-Ti-V system (Chromium-Titanium-Vanadium), *Journal of Phase Equilibria*, 13(2) (1992) 195-199.

- [16] [https://www.bruker.com/fileadmin/user\\_upload/8-PDF-Docs/X-rayDiffraction\\_ElementalAnalysis/XRD/Flyers/TOPAS\\_Flyer\\_DOC-H88-EXS013\\_V2\\_en\\_high.pdf](https://www.bruker.com/fileadmin/user_upload/8-PDF-Docs/X-rayDiffraction_ElementalAnalysis/XRD/Flyers/TOPAS_Flyer_DOC-H88-EXS013_V2_en_high.pdf)  
(Accessed on 15 September 2017).
- [17] Cheary R W, Coelho A, Cline J P. Fundamental Parameters Line Profile Fitting in Laboratory Diffractometers. Journal of research of the National Institute of Standards and Technology. 2004;109:1-25.
- [18] T. Collins, ImageJ for Microscopy, BioTechniques, 43 (2007) S25-S30. <http://dx.doi.org/10.2144/000112517>. 2007
- [19] M.D. Abràmoff, P.J. Magalhães, S.J. Ram, Image processing with ImageJ, Biophotonics international, 11(7) (2004) 36-42.